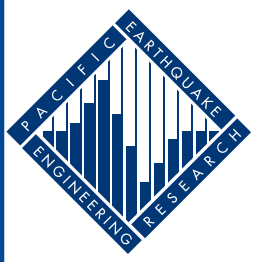

PACIFIC EARTHQUAKE ENGINEERING
RESEARCH CENTER

Rocking Response of Equipment Anchored to a Base Foundation

Nicos Makris

Cameron J. Black
Department of Civil and Environmental Engineering
University of California, Berkeley

Final report to PG&E on research conducted under grant PG&E-UCB-00956

PEER 2001/14
SEPTEMBER 2001

Rocking Response of Equipment Anchored to a Base Foundation

Nicos Makris
Professor
Department of Civil and Environmental Engineering
University of California, Berkeley

and

Cameron J. Black
Graduate Student Researcher
Department of Civil and Environmental Engineering
University of California, Berkeley

Final Report to PG&E on research conducted
under grant PG&E-UCB-00956

Abstract

This study concentrates on the rocking response of rigid equipment supported on a foundation base. In most cases heavy electrical equipment is anchored on a concrete base with plan dimensions that are larger than the footprint of the equipment. In the event that the strength of the restrainers, F_u, is sufficiently large and the ground acceleration is sufficiently strong, the equipment will engage its foundation in rocking motion. On the other hand, if the restrainers are too fragile they will fracture and eventually the equipment will rock atop its foundation base. Accordingly, equipment anchored to a base foundation exhibits two distinct rocking capacities: (a) the equipment engages the base foundation in rocking motion and (b) the restrainers fracture and the equipment subsequently rocks as a freestanding block atop its foundation base. The aim of this study is to compare these two capacities for practical values of the foundation footprint and the restrainer strength. The study examines intensity levels of ground shaking that will exceed serviceability levels (6 in. uplift at edge), and intensity levels that will result in overturning.

The study shows that for specific equipment/base configurations the high-strength restrainers used by PG&E are sufficient to engage the foundation base in rocking motion for a wide family of recorded earthquake motions. It was shown that the minimum strength capacity of the restrainer needed to avoid fracture is closely related to peak ground acceleration and that only the Cape Mendocino record is capable of fracturing the high-strength restrainers. It was found that the strength capacity of the restrainer should be as high as $F_u = W$ to engage the base foundation in rocking motion. The study reveals that for earthquakes with long distinguishable pulses ($T_p > 2.5\,\text{sec}$), the margin between exceeding the serviceability level of uplift and achieving overturning is minimal.

Nevertheless, none of the strong motions used in this study is capable of overturning the freestanding configurations examined. Two records, the Rinaldi Receiving Station record (1994 Northridge earthquake) and the Takatori record (1995 Kobe earthquake), are capable of uplifting the two transformers of interest beyond the serviceability level; however, it is found that small fractions of the foundation protrusion, *d*, to the half-width of the equipment, *b*, reduce the uplift appreciably. Occasional exceptions to this conclusion have been identified and explained.

Acknowledgments

This work is supported by the Pacific Gas and Electric Company under Grant PG&E-UCB-00956 to the Pacific Earthquake Engineering Research Center. The assistance of Mr. Dimitrios Konstantinidis in computing the data of Figure 5.3, and the valuable comments of Mr. Eric Fujisaki and Mr. Henry Ho. are greatly appreciated.

This project was sponsored by the Pacific Earthquake Engineering Research Center's Program of Applied Earthquake Engineering Research of Lifeline Systems supported by the California Energy Commission, the California Department of Transportation, and the Pacific Gas & Electric Company.

This work made use of Pacific Earthquake Engineering Research Center Shared Facilities supported by the Earthquake Engineering Research Centers Program of the National Science Foundation under award number EEC-9701568.

Contents

List of Figures

List of Tables

List of Symbols

A	area of equipment or equipment/foundation system [m^2]
A_p	acceleration amplitude of pulse [$m/\sec^2$]
b	half width of equipment m
d	length of protrusion of foundation base [m]
e	$= d/b$, ratio of foundation length to equipment
$f(t)$	time derivative of state vector
$f(\theta)$	restrainer fracture function
F	horizontal force in foundation [N]
F_u	ultimate restrainer strength [N]
g	acceleration of gravity [$m/\sec^2$]
h	half height of equipment [m]
h_c	height of center of gravity [m]
I_o	moment of inertia of equipment/base system
dJ	momentum vector of infinitessimal mass dm [$kg\ \ m/\sec$]
K	pre-yield stiffness [N/m]
m_e	mass of equipment [kg]
m_f	mass of foundation [kg]
M	total mass of equipment/foundation system [kg]
M_w	seismic moment magnitude of an earthquake
n	dimensionless parameter used in Bouc-Wen model
N	vertical reaction force on foundation [N]
p	$= \sqrt{(3g)/(4R)}$, frequency parameter of rocking block [$rad/\sec$]
$P(t)$	force in restrainer [N]
r	square of coefficient of restitution
r_{max}	square of maximum coefficient of restitution

R distance from pivot point of equipment to center of gravity [m]

R_o radius of gyration of equipment [m]

s half thickness of foundation slab [m]

t time [sec]

T_p period of pulse [sec]

$u(t)$ extension of restrainer [m]

u_f extension of restrainer at failure [m]

u_y extension of restrainer at yield [m]

$\ddot{u}_g$ ground acceleration [$m/\sec^2$]

V_p velocity of pulse approximation

W weight of equipment or equipment/foundation system [N]

x displacement variable [m]

$y(t)$ state vector

z vertical displacement variable [m]

$Z(t)$ dimensionless hysteretic parameter used in Bouc-Wen model

α slenderness angle [rad]

β dimensionless parameter used in Bouc-Wen model

γ dimensionless parameter used in Bouc-Wen model

δ lever arm of momentum vector of infinitesimal mass, dm [m]

ε post- to pre-yield stiffness of restrainer

ζ viscous damping ratio

η $= \sqrt{r}$, coefficient of restitution

$\theta(t)$ rotation of equipment or equipment/base [rad]

θ_f rotation of equipment at restrainer failure [rad]

θ_y rotation of equipment at restrainer yield [rad]

Λ moment of momentum [$kg\ m^2/\sec$]

μ ductility

ρ uniform mass density [kg/m^3]

ρ_e uniform mass density of equipment [kg/m^3]

ρ_f uniform mass density of foundation [kg/m^3]

τ time variable [sec]

φ phase [rad]

ω_p circular frequency of excitation pulse [$rad/$sec]

1 Introduction

1.1 Problem Statement

Past studies supported by PG&E have investigated separately the rocking response of freestanding blocks to earthquake loading (Makris and Roussos 1998, 2000) and the seismic rocking response of anchored blocks (Makris and Zhang 1999, 2001). These studies uncovered the many complexities involved with the rocking response of a rigid block and proposed various parameters related to the kinematic characteristic of the ground motions and the geometric characteristics of the rocking block in order to identify some order in the computed response.

In this study we build on past knowledge in order to examine the response of electrical equipment, accounting for geometric details of their in situ configurations. In most cases, heavy electrical equipment rest on concrete foundations with plan dimensions that are larger than the footprint of the equipment. The protrusion of the base foundation from the sides of the equipment varies, since in practice the same base may support different equipment at different times. In most cases, electrical equipment are anchored to their base foundations with restrainers that have limited strength, F_u ($0.4 \le F_u / mg \le 1.0$), where m = mass of equipment anchored to the base foundation.

Equipment that is anchored to a base foundation exhibits two distinct capacities to resist uplift and eventual overturning: (a) the restrainers are strong enough and the equipment engages the base foundation in rocking motion or (b) the restrainers fracture and the equipment subsequently rocks as a freestanding block atop its foundation base. In some instances the ground motion is strong enough to fracture the restrainers and overturn the resulting freestanding equipment as illustrated in Figure 1.1, a photo taken after the 1971 San Fernando, California, earthquake.

Figure 1.1. Overturned electrical equipment at Sylmar Converter Station damaged during the 1971 San Fernando earthquake (top), and a detail showing the failed back-left restrainer (bottom). Photos taken from the Steinbrugge collection, NISEE, University of California, Berkeley.

1.2 Response Analysis

Owing to the large number of parameters involved in this problem, the scope of the investigation is limited to the seismic response of two typical slender equipment configurations used by PG&E — a 60 kip and a 230 kip transformer supported on a base foundation.

This study examines the response of the equipment to 14 strong ground motions, most of which were recorded near the causative fault of major earthquakes. The study revisits the coherent acceleration and velocity pulses that are distinguishable in most of these strong motion records in an effort to correlate the rocking potential of ground motion with the kinematic characteristics of simple trigonometric pulses that best approximate the main shaking of the ground.

The analysis presented here considers the two capacities of the equipment-foundation system to resist uplift and overturning separately. First, the response of equipment anchored to a base foundation with restrainers that are sufficiently strong to engage the base is investigated and the levels of shaking needed to reach prescribed uplift levels are established. Subsequently, the response of equipment anchored to a monolithic base with restrainers that have finite strength is analyzed.

The study concludes with the level of ground shaking needed to exceed serviceability limits and to achieve overturning in association with the practical values of restrainer strength used by PG&E.

2 Equipment Rocking with Its Foundation Base

We consider the rectangular block shown in Figure 2.1 (top) which is rigidly connected to a rectangular base. It is assumed that the anchorages of the block to its base are strong enough so that when rocking occurs, the block with its base oscillates about the centers of rotation 0 and 0'. Depending on the level and form of the ground excitation, the block with its base may translate with the ground, slide, rock or rock-slide. In most cases the foundation slab (base) of the block is partially embedded in the ground — a situation that is not favorable for sliding or rocking-sliding.

2.1 Problem Definition

With reference to Figure 2.1, we consider that the mass of the equipment, $m_e = 4\rho_e bh$ and that the mass of the foundation base $m_f = 4\rho_f s(b+d)$; where ρ_e and ρ_f are the uniform mass densities (mass per area) of the equipment and the foundation base, respectively. In general $\rho_e \neq \rho_f$ — for the 60 kip transformer $\rho_e/\rho_f = 0.4$ and for the 230 kip transformer $\rho_e/\rho_f = 0.6$. For this study, in the interest of simplicity, it is assumed that $\rho_e = \rho_f = \rho$. This is a conservative assumption since in reality the center of gravity of the equipment/base structure is slightly lower. With this assumption the total mass, $M = m_e + m_f$, of the equipment/base structure is given by

$$M = 4\rho(bh + bs + ds), \tag{1}$$

and the location of the center of gravity is

$$h_c = \frac{h^2 + 2hs + s^2(1+e)}{h + s(1+e)}, \tag{2}$$

where $e = \frac{d}{b} < 1$.

The distance to the center of gravity of the entire structure from the pivot points 0 and 0' is $R = \sqrt{h_c^2 + (b+d)^2}$, and with the help of equation (2) one obtains

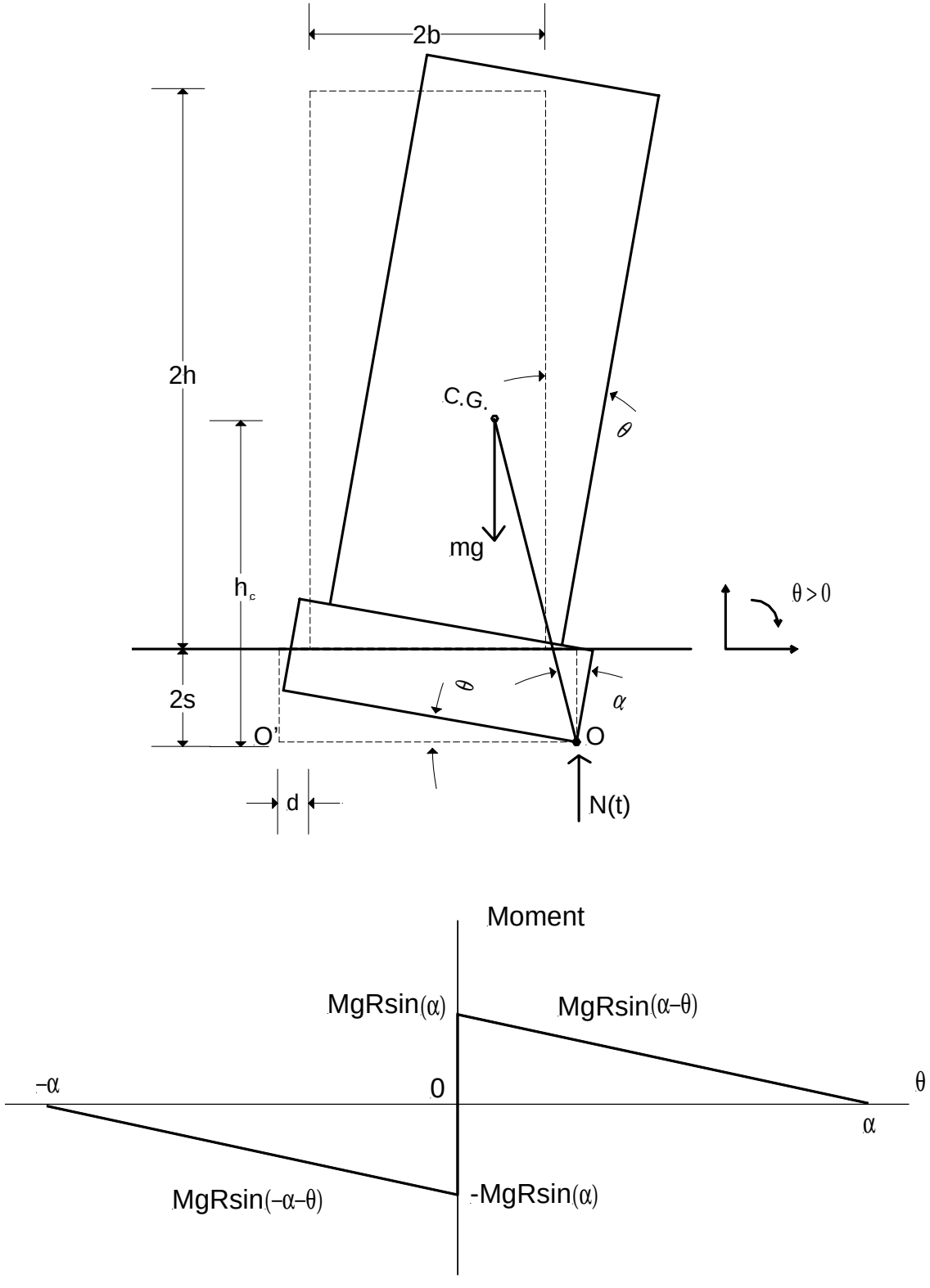

Figure 2.1. Schematic of a rigid block and its foundation in rocking motion (top) and its moment-rotation diagram (bottom).

$$R^2 = \left[\frac{h^2 + 2hs + s^2(1+e)}{h + s(1+e)}\right]^2 + b^2(1+e)^2 . \tag{3}$$

The moment of inertia, I_0, of the equipment/base structure about the pivot point 0 or 0' is

$$I_0 = m_f\left[\frac{4}{3}((b+d)^2 + s^2)\right] + m_e\left[\frac{1}{3}(b^2 + h^2)\right] + m_e[(h+2s)^2 + (b+d)^2] . \tag{4}$$

With the assumption that $\rho_e = \rho_f = \rho$, Equation (4) takes the form

$$I_0 = 4\rho\left[\frac{4}{3}s(b+d)[(b+d)^2 + s^2] + \frac{1}{3}bh(b^2 + h^2) + bh[(h+2s)^2 + (b+d)^2]\right]. \tag{5}$$

The radius of gyration, $R_0 = \sqrt{I_0/M}$, of this configuration is

$$R_0^2 = \frac{I_0}{M} = \frac{\frac{4}{3}s(1+e)[(b+d)^2 + s^2] + \frac{1}{3}h(b^2 + h^2) + h[(h+2s)^2 + (b+d)^2]}{h + s + es} . \tag{6}$$

2.2 Governing Equations under Rocking Motion

Under a positive horizontal ground acceleration and assuming that the base does not slide, the structure will initially rotate with a negative rotation $\theta < 0$, and if it does not overturn, it will eventually assume a positive rotation and so forth. Figure 2.1 (top) portrays the equipment/base system under a positive rotation. The equations that govern the rocking motion about points 0 and 0' under horizontal ground acceleration, $\ddot{u}_g(t)$ are

$$I_0\ddot{\theta}(t) + MgR\sin(-\alpha - \theta) = -M\ddot{u}_g(t)R\cos(-\alpha - \theta), \qquad \theta < 0 \tag{7}$$

and

$$I_0\ddot{\theta}(t) + MgR\sin(\alpha - \theta) = -M\ddot{u}_g(t)R\cos(\alpha - \theta) . \qquad \theta > 0 \tag{8}$$

Equations (7) and (8) are well known in the literature (Yim et al. 1980) and are valid for arbitrary values of the angle $\alpha = \text{atan}\left(\frac{b+d}{h_c}\right)$. Equations (7) and (8) can be expressed in the compact form

$$\ddot{\theta}(t) = -p^2\left\{\sin[\alpha\,\mathrm{sgn}[\theta(t)] - \theta(t)] + \frac{\ddot{u}_g}{g}\cos[\alpha\,\mathrm{sgn}[\theta(t)] - \theta(t)]\right\} \tag{9}$$

where $p = \sqrt{\frac{gR}{R_0^2}}$ with R and R_0 given by equations (3) and (6). For the configurations of interest

1.5 rad/sec < p < 2 rad/sec.

Figure 2.1 (bottom) shows the moment-rotation relation during the rocking motion of a freestanding structure. The system has infinite stiffness until the magnitude of the applied moment reaches $mgR\sin\alpha$. Once the structure is rocking its stiffness decreases monotonically, reaching zero when $\theta = \alpha$. During the oscillatory rocking motion, the moment-rotation path follows this curve without enclosing any area. Energy is lost only during impact when the angle of rotation reverses. In order for a rigid structure to sustain rocking motion a minimum amount of energy loss is needed during every impact. This minimum amount of energy loss is a function of the geometry of the structure alone and is computed by applying the conservation of moment of momentum.

The rocking response of a freestanding structure subjected to horizontal ground excitation is computed numerically via a state-space formulation that can accommodate the nonlinear nature of the problem (Makris and Roussos 1998, 2000; Makris and Zhang 1999, 2000). The state vector of the system is

$$\{y(t)\} = \begin{Bmatrix} \theta(t) \\ \dot{\theta}(t) \end{Bmatrix} \tag{10}$$

and the time-derivative vector is $f(t)$ is

$$\{f(t)\} = \{\dot{y}(t)\} = \begin{Bmatrix} \dot{\theta}(t) \\ -p^2\left\{\sin[\alpha\,\mathrm{sgn}[\theta(t)] - \theta(t)] + \frac{\ddot{u}_g}{g}\cos[\alpha\,\mathrm{sgn}[\theta(t)] - \theta(t)]\right\} \end{Bmatrix}. \tag{11}$$

The numerical integration of (11) is performed with standard ODE solvers available in MATLAB (1992). The fidelity of the numerical algorithms has been validated elsewhere (Makris and Roussos 1998). As the integration proceeds in time and a reversal of the rotation is detected, the angu-

lar velocity after the impact is set equal to the angular velocity before the impact multiplied by the coefficient of restitution. The maximum value of the coefficient of restitution that allows for rocking motion is computed in the following section.

2.3 Conservation of Moment of Momentum When Rotation Reverses

When the angle of rotation reverses, it is assumed that the rotation continues smoothly from point 0 to $0'$. Figure 2.2 shows the rocking structure that is about to transfer its pivot point from 0 to $0'$. The momentum of a mass element dm, at a distance r from point 0 is

$$dJ = r\dot{\theta}_1 dm, \tag{12}$$

and the moment of momentum, $d\Lambda$ of that elementary mass about point $0'$ before impact is

$$d\Lambda = dJ \cdot \delta = \rho r\dot{\theta}_1 \delta dxdy \tag{13}$$

where $\delta = r - \frac{x}{r}2(b+d)$ is the lever arm of the element momentum vector dJ about point $0'$. Accordingly in terms of Cartesian coordinates (x, y), the total moment of momentum of the rocking structure about point $0'$ before impact is given by

$$\Lambda = \rho\dot{\theta}_1\left[\int_A (x^2+y^2)dxdy - 2(b+d)\int_A xdxdy\right] \tag{14}$$

where A is the total area of the rocking structure and $\dot{\theta}_1$ is the angular velocity before impact. Equation (14) can be written as

$$\Lambda = I_0\dot{\theta}_1 - \rho\dot{\theta}_1 2(b+d)\left[\int_0^{2s} dy \int_0^{2b+2d} xdx + \int_{2s}^{2h+2s} dy \int_d^{d+2b} xdx\right], \tag{15}$$

which after integrating yields

$$\Lambda = I_0\dot{\theta}_1 - M\dot{\theta}_1 2(b+d)^2. \tag{16}$$

The moment of momentum about point $0'$ after the impact is

$$\Lambda = I_0\dot{\theta}_2 \tag{17}$$

where $\dot{\theta}_2$ is the angular velocity after impact. Conservation of the moment of momentum before and after the impact gives

$$I_0\dot{\theta}_1 - M\dot{\theta}_1 2R^2\sin^2\alpha = I_0\dot{\theta}_2 \tag{18}$$

The ratio of the kinetic energy after and before the impact is

$$r = \frac{\dot{\theta}_2^2}{\dot{\theta}_1^2} < 1\,. \tag{19}$$

Substitution of (19) into (18) gives

$$r = \left[1 - \frac{2R^2}{R_0^2}\sin^2\alpha\right]^2. \tag{20}$$

In the special case of a rectangular block without the base $R_0^2 = \frac{4}{3}R^2$ and equation (20) simplifies to $r = \left[1 - \frac{3}{2}\sin^2\alpha\right]^2$. The value of the coefficient of restitution given by (20) is the maximum value of r under which a structure with slenderness, α, will undergo rocking motion. Consequently, in order to observe rocking motion the impact has to be inelastic ([angular velocity after impact] $= \sqrt{r}\times$ [angular velocity before impact]). As the slenderness of a structure decreases the more inelastic the impact becomes (i.e., as α increases r increases).

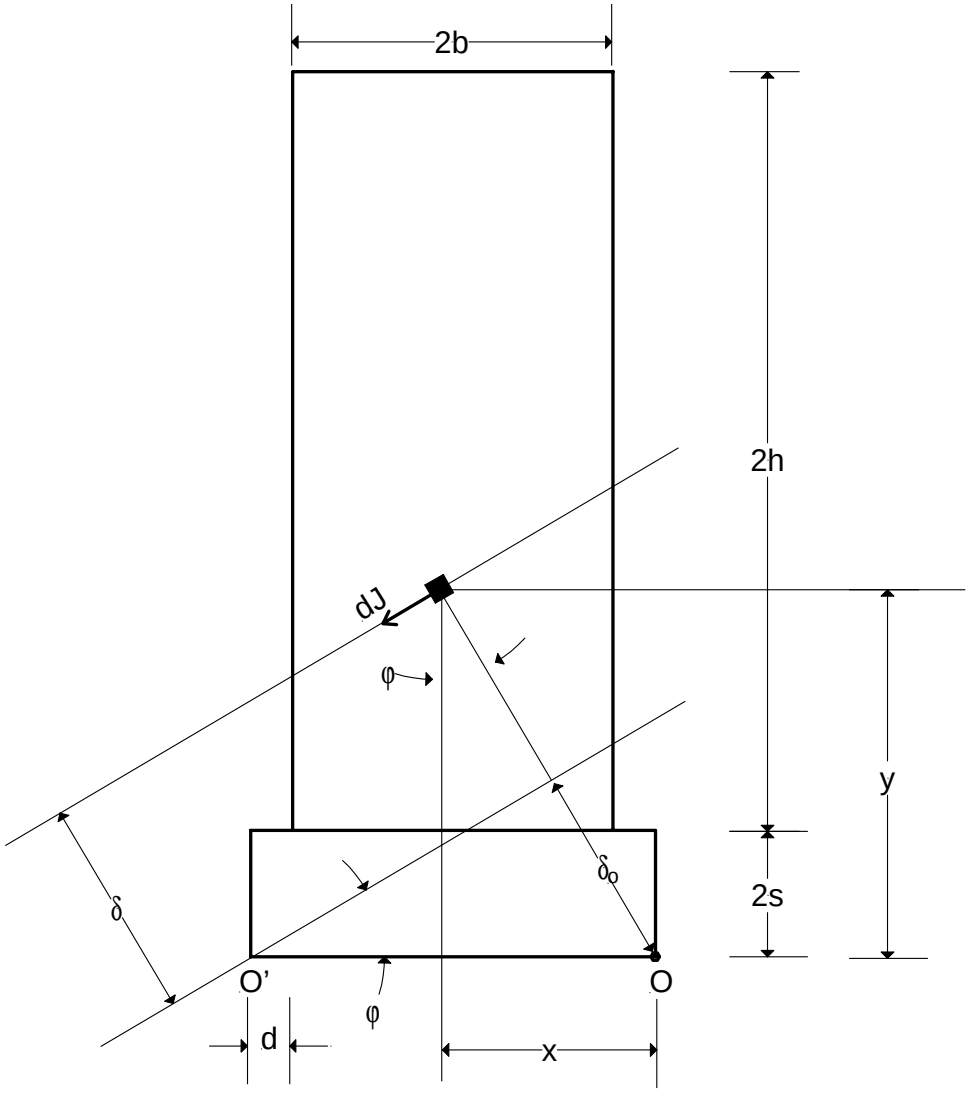

Figure 2.2. Schematic of the momentum vector dJ of an elementary portion of the rocking structure just before impact at point 0'.

3 Rocking Response of Anchored Equipment

In the foregoing analysis it was assumed that the anchorages of the equipment to its foundation slab are strong enough to engage the foundation slab in rocking motion. The anchorages (hold-downs) have a finite strength, F_u, that in most cases is a function of the weight of the equipment, W, ($0.25 \le F_u/W \le 1.0$). In this study it is assumed that the restrainers behave linearly until the ultimate strength, F_u, is reached and that subsequently they deform plastically until the fracture displacement, u_f, is reached. Beyond that point the restrainers fracture and the block continues to rock without experiencing any restoring or dissipative force.

In this study we are interested in comparing the overturning capacity of equipment that rocks with its foundation base against the overturning capacity of equipment that is anchored with the same restrainers to a monolithic foundation. Figure 3.1 shows a schematic of anchored equipment in rocking motion. The restoring elements on each side of the block represent the combined restrainers that are present at the edge of the block that uplifts.

3.1 Ductile Behavior

Figure 3.2 illustrates the force-displacement relation of restrainers with ductile behavior. In general the restrainers can exhibit a post-yielding stiffness and maintain their strength until they reach a fracture displacement, u_f. A measure of their ductile behavior is the ductility coefficient, $\mu = u_f/u_y$. A suitable model to approximate such nonlinear hysteretic behavior is given by

$$P(t) = \varepsilon K u(t) + (1-\varepsilon) K u_y Z(t) \tag{21}$$

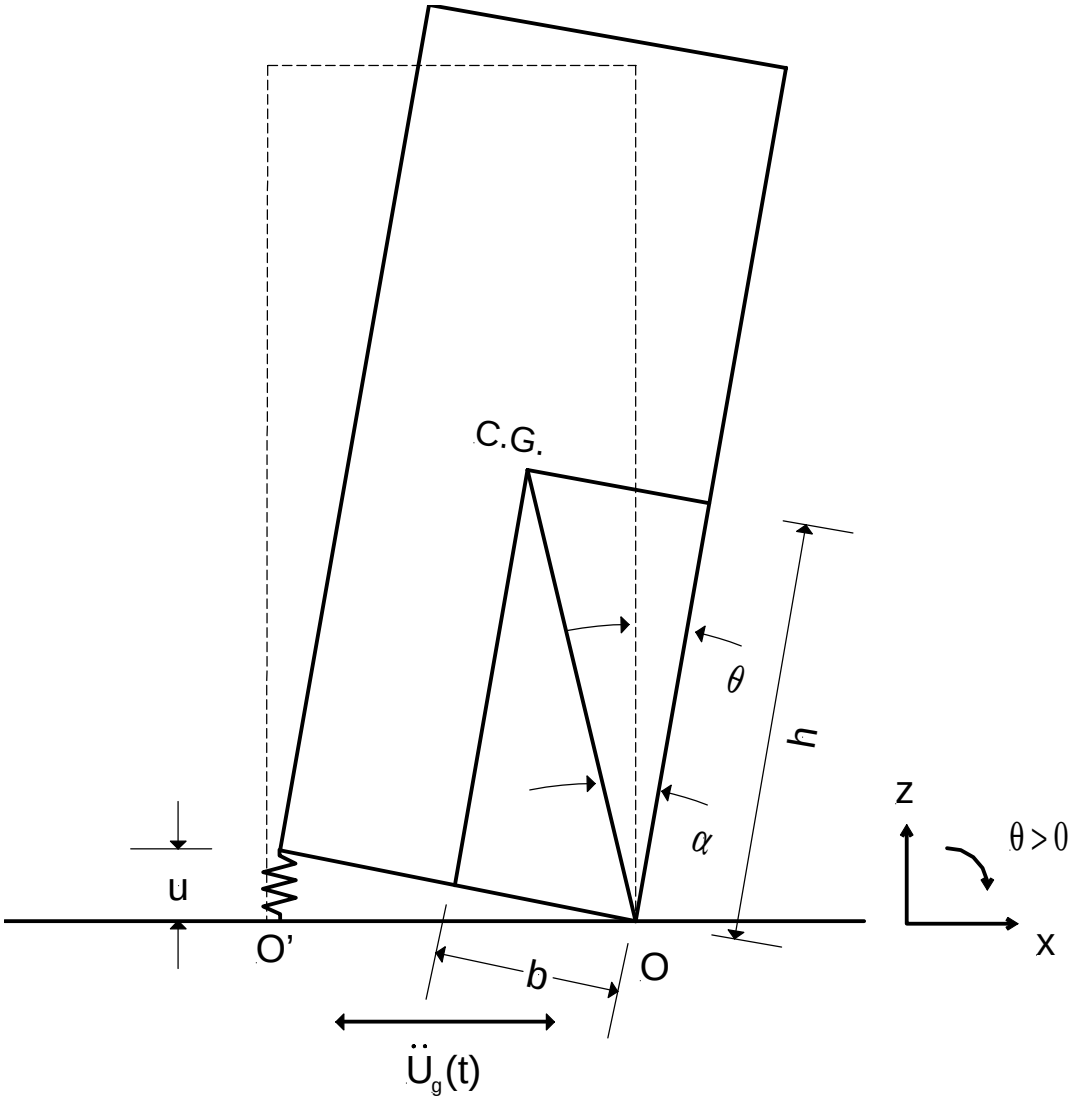

Figure 3.1. Schematic of an anchored block in rocking motion.

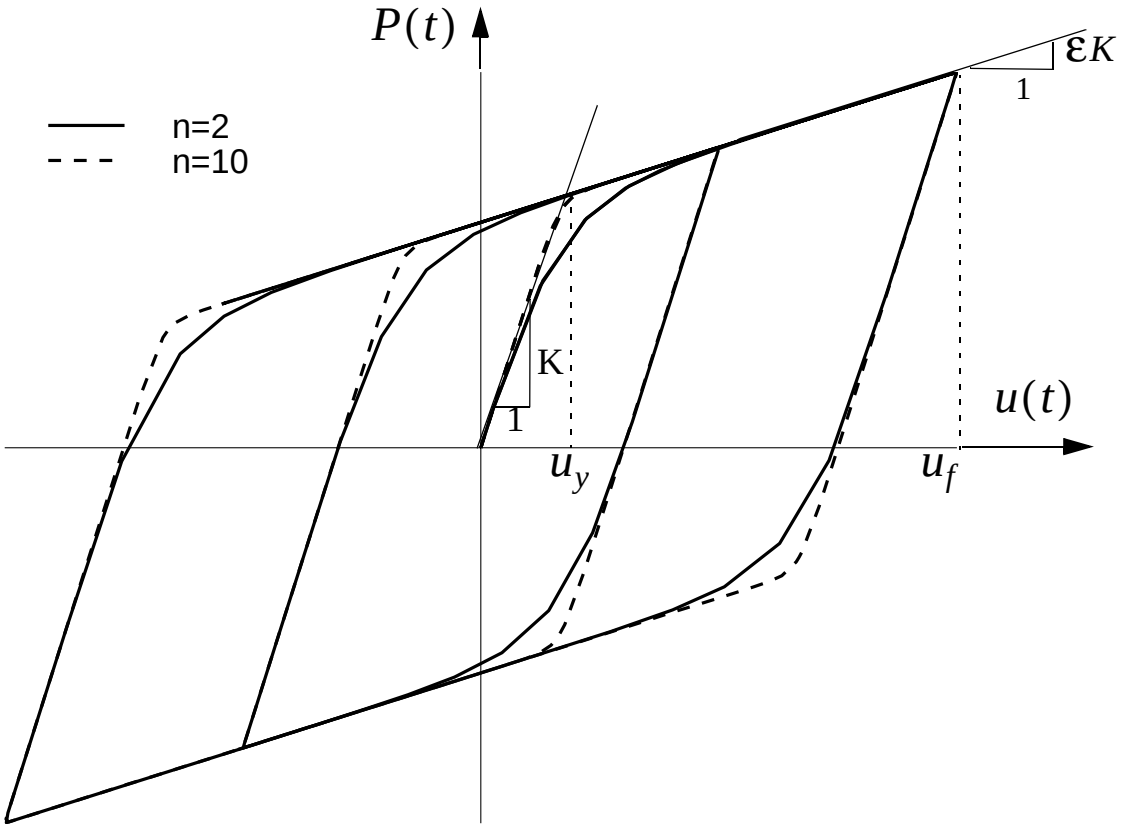

Figure 3.2. Force-displacement curve of an element with bilinear behavior.

where $u(t)$ is the extension of the restrainer, K is the pre-yielding stiffness, ε is the ratio of the post- to pre-yielding stiffness, u_y is the yield displacement, and $Z(t)$ is a hysteretic dimensionless quantity that is governed by the equation:

$$u_y \dot{Z}(t) + \gamma |\dot{u}(t)| Z(t) |Z(t)|^{n-1} + \beta \dot{u}(t) |Z(t)|^n - \dot{u}(t) = 0 . \qquad (22)$$

In the above equation β, γ, and n are dimensionless quantities that control the shape of the hysteretic loop. The hysteretic model, expressed by (21) and (22), was originally proposed by Bouc (1971) for *n=1*, subsequently extended by Wen (1975, 1976), and used in random vibration studies of inelastic systems.

In this study the special case of elasto-plastic behavior is considered by setting the post-yielding stiffness equal to zero ($\varepsilon = 0$). However, the developed formulation can easily be extended to account for situations with $\varepsilon \neq 0$.

Figure 3.3 (center) illustrates the moment-rotation relation that results from the presence of restrainers with elasto-plastic behavior, while Figure 3.3 (top) illustrates again the moment-rotation relation of a freestanding block. Under these two restoring mechanisms, the equations that govern the rocking motion of an anchored block with mass, m, and moment of inertia, I_0 (about pivot point 0 or 0') are

$$I_0 \ddot{\theta}(t) + M \ddot{u}_g R \cos(-\alpha - \theta) = -MgR \sin(-\alpha - \theta) - P(t) 2b \cos\left(\frac{\theta}{2}\right), \quad \theta < 0 \qquad (23)$$

and

$$I_0 \ddot{\theta}(t) + M \ddot{u}_g R \cos(\alpha - \theta) = -MgR \sin(\alpha - \theta) - P(t) 2b \cos\left(\frac{\theta}{2}\right), \quad \theta > 0 \qquad (24)$$

where $P(t)$ is the force originating from the restrainers that for the general case is given by (21), and the special elasto-plastic case ($\varepsilon = 0$) reduces to

$$P(t) = K u_y Z(t) . \qquad (25)$$

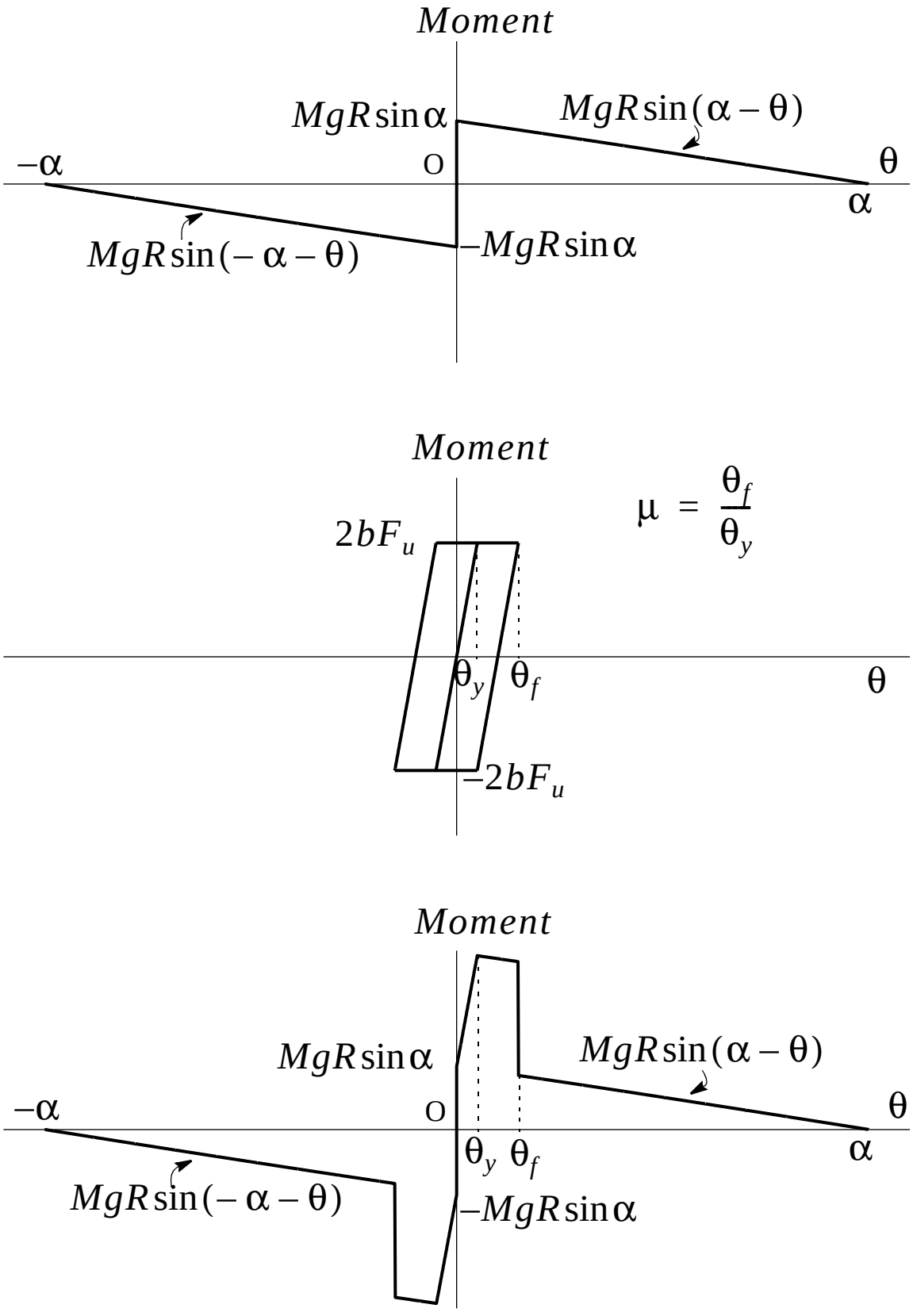

Figure 3.3. Moment-rotation curves of freestanding block (top), elastic-plastic anchorages (center), and anchored block with elastic-plastic restrainers (bottom).

With reference to Figure 3.1, $u_y = 2b\theta_y$, and equation (25) gives

$$P(t) = 2Kb\theta_y Z(t). \tag{26}$$

Substitution of (26) into (23) and (24) gives

$$I_0\ddot{\theta}(t) + MgR\sin(-\alpha-\theta) + 4Kb^2\theta_y Z(t)\cos\left(\frac{\theta}{2}\right) = -M\ddot{u}_g(t)R\cos(-\alpha-\theta), \quad \theta < 0 \tag{27}$$

and

$$I_0\ddot{\theta}(t) + MgR\sin(\alpha-\theta) + 4Kb^2\theta_y Z(t)\cos\left(\frac{\theta}{2}\right) = -M\ddot{u}_g(t)R\cos(\alpha-\theta), \qquad \theta > 0. \tag{28}$$

Using that for a rectangular block, $I_0 = \frac{4}{3}MR^2$, equation (27) and (28) can be expressed in the compact form

$$\ddot{\theta}(t) = -p^2\left\{\sin[\alpha\,\mathrm{sgn}\,\theta(t) - \theta(t)] + \frac{\ddot{u}_g(t)}{g}\cos[\alpha\,\mathrm{sgn}\,\theta(t) - \theta(t)] + \frac{3F_u\sin^2\alpha}{Mu_y p^2}\theta_y Z(t)\cos\left(\frac{\theta}{2}\right)\right\} \tag{29}$$

where $p = \sqrt{(3g)/(4R)}$, and $Z(t)$ is the solution of (22) which in terms of rotation takes the form

$$\theta_y\dot{Z}(t) + \gamma|\dot{\theta}(t)|Z(t)|Z(t)|^{n-1} + \beta\dot{\theta}(t)|Z(t)|^n - \dot{\theta}(t) = 0. \tag{30}$$

Equation (29) is valid so long as the restrainers hold. Once their fracture displacement, $u_f = 2b\sin\theta_f$, is reached, they do not provide any resistance, and equation (29) reduces to the equation of motion of the freestanding block given by (9). Figure 3.3 (bottom) shows the moment-rotation relation during rocking motion of an anchored block with restrainers that exhibit elastoplastic behavior. For rotation angles $|\theta(t)| \le \theta_y$, energy is lost only during the reversal of motion due to impact. Once θ_y is exceeded, the restrainers along the uplifted side yield. In the case that the motion reverses before the rotation reaches θ_f, additional energy is dissipated equal to the area of the flag-shaped regions. This dissipation mechanism will be repeated so long as the maximum rotation does not reach the fracture rotation, θ_f. If θ_f is exceeded, the restrainers fracture and the moment-curvature curve reduces to that of the freestanding block.

The transition from equation (29) to (9) is conducted with the fracture function $f(\theta)$ defined as

$$f(\theta) = 1 \text{ when } |\theta(t)| \le \theta_f \tag{31}$$

and

$$f(\theta) = 0 \text{ when } |\theta(t)| \ge \theta_f \tag{32}$$

where $\theta_f = \mu\theta_y$ and θ_y is given by $\theta_y = F_u/(2Kb)$.

With the help of the fracture function, the pre-fracture and post-fracture equation of rocking motion can be expressed as

$$\ddot{\theta}(t) = -p^2\left\{\sin[\alpha\,\mathrm{sgn}\,\theta(t) - \theta(t)] + \frac{\ddot{u}_g(t)}{g}\cos[\alpha\,\mathrm{sgn}\,\theta(t) - \theta(t)] + \frac{3\sigma\sin^2\alpha}{q}\theta_y Z(t)\cos\left(\frac{\theta(t)}{2}\right)f(\theta)\right\}. \tag{33}$$

The integration of (33) requires the simultaneous integration of (30). In this case the state vector of the system is

$$\{y(t)\} = \begin{Bmatrix} \theta(t) \\ \dot{\theta}(t) \\ Z(t) \end{Bmatrix} \tag{34}$$

and the time-derivative vector $f(t)$ is

$$\{f(t)\} = \begin{bmatrix} \dot{\theta}(t) \\ -p^2\left\{\sin[\alpha\,\mathrm{sgn}\,\theta(t) - \theta(t)] + \frac{\ddot{u}_g(t)}{g}\cos[\alpha\,\mathrm{sgn}\,\theta(t) - \theta(t)] + \frac{3F_u\sin^2\alpha}{Mu_y p^2}\theta_y Z(t)\cos\left(\frac{\theta(t)}{2}\right)f(\theta)\right\} \\ \frac{1}{\theta_y}[\dot{\theta}(t) - \gamma|\dot{\theta}(t)|Z(t)|Z(t)|^{n-1} - \beta\dot{\theta}(t)|Z(t)|^n] \end{bmatrix} \tag{35}$$

3.2 Reaction Forces at the Pivot Points

With reference to Figure 3.1, let F and N be the horizontal and vertical reactions at the pivot points 0 and 0'. Under a horizontal ground acceleration, $\ddot{u}_g(t)$, the dynamic equilibrium of the rocking structure along the horizontal and vertical directions gives

$$M(\ddot{u}_g(t) + \ddot{x}(t)) = F(t) - P(t)\sin\left(\frac{\theta(t)}{2}\right) \tag{36}$$

$$M\ddot{z}(t) = N(t) - Mg - P(t)\cos\left(\frac{\theta(t)}{2}\right) \tag{37}$$

where $x(t)$ and $z(t)$ are the horizontal and vertical displacements of the center of mass of the rocking structure and $P(t)$ is the force originating from the restrainer. In the case of a freestanding structure as shown in Figure 2.1, $P(t) = 0$. Equations (36) and (37) together with equation (33) (or (9) for the freestanding case) represent the three equations of dynamic equilibrium in the rocking plane.

The kinematics of the rocking motion yield that

$$\ddot{x}(t) = R\ddot{\theta}(t)\cos[\alpha\,\mathrm{sgn}\,\theta(t) - \theta(t)] + R\dot{\theta}^2(t)\sin[\alpha\,\mathrm{sgn}\,\theta(t) - \theta(t)] \tag{38}$$

and

$$\ddot{z}(t) = R\ddot{\theta}(t)\sin[\alpha\,\mathrm{sgn}\,\theta(t) - \theta(t)] - R\dot{\theta}^2(t)\cos[\alpha\,\mathrm{sgn}\,\theta(t) - \theta(t)]\,. \tag{39}$$

The expressions given by (38) and (39) substituted into equations (36) and (37) yield

$$F(t) = M\{\ddot{u}_g(t) + R\ddot{\theta}(t)\cos[\alpha\,\mathrm{sgn}\,\theta(t) - \theta(t)] + R\dot{\theta}^2(t)\sin[\alpha\,\mathrm{sgn}\,\theta(t) - \theta(t)]\} + P(t)\sin\left(\frac{\theta(t)}{2}\right) \tag{40}$$

and

$$N(t) = M\{g + R\ddot{\theta}(t)\sin[\alpha\,\mathrm{sgn}\,\theta(t) - \theta(t)] - R\dot{\theta}^2(t)\cos[\alpha\,\mathrm{sgn}\,\theta(t) - \theta(t)]\} + P(t)\cos\left(\frac{\theta(t)}{2}\right) \tag{41}$$

The reactions, $F(t)$ and $N(t)$, are computed from the elements of the state vector (Equation (34)) with $\ddot{\theta}(t)$ provided by (33) and $P(t)$ provided by (26). For the simpler case of a freestanding structure ($P(t) = 0$), the reaction forces at the pivot points are explicit expressions of the state variables $\theta(t)$ and $\dot{\theta}(t)$ and are given by

$$\frac{F(t)}{Mg} = \frac{\ddot{u}_g(t)}{g}\left(1-\frac{1}{2}\frac{R^2}{R_o^2}\right)+\frac{1}{2}\frac{R^2}{R_o^2}\left(-\sin(2[\alpha\,\mathrm{sgn}\,\theta(t)-\theta(t)])-\frac{\ddot{u}_g(t)}{g}\cos(2[\alpha\,\mathrm{sgn}\,\theta(t)-\theta(t)])\right) \tag{42}$$
$$+2\frac{(\dot{\theta}(t))^2}{p^2}\sin[\alpha\,\mathrm{sgn}\,\theta(t)-\theta(t)]$$

and

$$\frac{N(t)}{Mg} = \left(1-\frac{1}{2}\frac{R^2}{R_o^2}\right)+\frac{1}{2}\frac{R^2}{R_o^2}\left(\cos(2[\alpha\,\mathrm{sgn}\,\theta(t)-\theta(t)])-\frac{\ddot{u}_g(t)}{g}\sin(2[\alpha\,\mathrm{sgn}\,\theta(t)-\theta(t)])\right) \tag{43}$$
$$-2\frac{(\dot{\theta}(t))^2}{p^2}\cos[\alpha\,\mathrm{sgn}\,\theta(t)-\theta(t)]$$

4 Ground Motions and Trigonometric Pulses

The ground motions of interest in this study are listed in Table 1 in historic order. They are strong ground motions, most of them recorded less than 5 mi (8 km) from the earthquake fault. The fifth column of Table 1 indicates velocity amplitudes and periods of simple trigonometric pulses that can approximate some of the kinematic characteristics of the recorded motions (Makris and Roussos 2000; Makris and Chang 2000). The sixth and seventh columns list the level of the earthquake which causes the free standing 60 kip equipment (discussed in the next section) to reach the serviceability limit state and the ultimate limit state, respectively. The serviceability limit has been established from experience (Fujisaki 2001) as an uplift of 6 in. whereas the ultimate limit state corresponds to overturning of the equipment. A complete discussion of the limit state response of the equipment is presented in the following section.

Figure 4.1 (left) shows the acceleration, velocity, and displacement time histories recorded at the Pacoima Dam during the 1971 San Fernando earthquake. The ground displacement exhibits one main long-period cycle. This long-period pulse is also distinguishable in the ground velocity history along with high-frequency spikes. Near-fault ground motions, where the displacement history exhibits one or more long-duration cycles are approximated with type C pulses (Makris and Roussos 2000; Makris and Chang 2000). An *n*-cycle ground displacement is approximated with a type C_n pulse that is defined as

$$\ddot{u}_g(\tau) = \omega_p V_p \sin(\omega_p \tau + \varphi), \qquad 0 \le \tau \le \left(n + \frac{1}{2} - \frac{\varphi}{\pi}\right) T_p \tag{44}$$

$$\dot{u}_g(\tau) = V_p \cos(\omega_p \tau + \varphi) - V_p \sin(\varphi), \qquad 0 \le \tau \le \left(n + \frac{1}{2} - \frac{\varphi}{\pi}\right) T_p \tag{45}$$

$$u_g(\tau) = -\frac{V_p}{\omega_p} \cos(\omega_p \tau + \varphi) - V_p \tau \sin(\varphi) + \frac{V_p}{\omega_p} \cos(\varphi), \qquad 0 \le \tau \le \left(n + \frac{1}{2} - \frac{\varphi}{\pi}\right) T_p \tag{46}$$

Table 1: List of recorded ground motions used in this study.

Earthquake	Record	Magnitude M_w	Distance (km)	Trigonometric Approximation	Level of earthquake needed to uplift the 60 kip equipment by 6 in.	Level of earthquake needed to overturn the 60 kip equipment
San Fernando 02/09/71	Pacoima Dam, 164	6.7	5	C_1: T_p = 1.3s, V_p = 0.85m/s	123	286
Tabas 9/16/78	Tabas, TR	7.4	3	C_1: T_p = 5.0s, V_p = 0.95m/s	176	188
Imperial Valley 10/15/79	El Centro Array #5, 230	6.6	27.7	B: T_p = 3.2s, V_p = 0.7m/s	159	215
Loma Prieta 10/18/89	Los Gatos (LGPC, 000)	6.9	6.1	C_1: T_p = 3.0s, V_p = 0.75m/s	105	201
Erzikan 3/13/92	Erzikan, N-S	6.7	2	C_1: T_p = 1.8s, V_p = 0.70m/s	139	171
Cape Mendocino 4/25/92	Cape Mendocino, 000	7.1	8.5	A: T_p = 0.55s, V_p = 1.35m/s C_1: T_p = 4.40s, V_p = 0.40m/s	213	303
Northridge 1/17/94	Rinaldi Receiving Station, 228	6.7	7.1	A: T_p = 0.8s, V_p = 1.75m/s B: T_p = 1.3s, V_p = 1.3m/s	81	136
Northridge 1/17/94	Sylmar Converter Station (FN)	6.7	7.1	C_2: T_p = 2.3s, V_p = 0.60m/s	138	180
Kobe 1/16/95	Takatori, 000	6.9	4.3	NA	90	163
Kobe 1/16/95	Takatori, 090	6.9	4.3	NA	80	223
Taiwan 9/20/99	TCU068, E-W	7.6	36.0	A: T_p = 6.5s, V_p = 2.40m/s	118	120
Taiwan 9/20/99	TCU068, N-S	7.6	36.0	A: T_p = 6.5s, V_p = 2.40m/s B: T_p = 9.5s, V_p = 1.90m/s	171	171
Taiwan 9/20/99	TCU052, E-W	7.6	33.3	C_1: T_p = 5.5s, V_p = 1.00m/s	143	148
Taiwan 9/20/99	TCU052, N-S	7.6	33.3	A: T_p = 6.5s, V_p = 2.00m/s	131	139

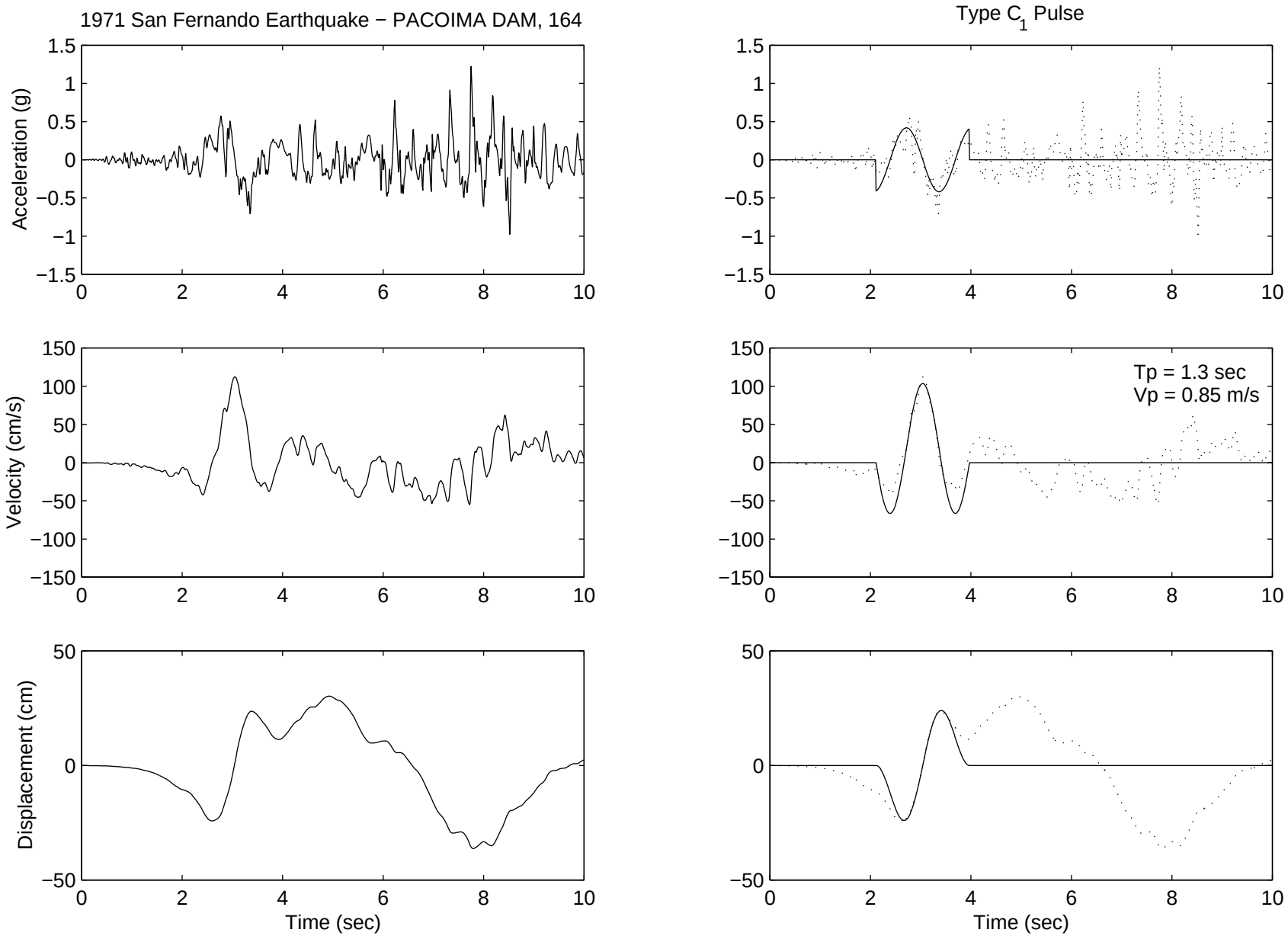

Figure 4.1. Fault-normal components of the acceleration, velocity, and displacement time histories recorded at Pacoima Dam during the February 9, 1971, San Fernando earthquake (left), and a cycloidal type C_1 pulse (right).

In deriving these expressions, it was required that the displacement and velocity be differentiable signals. The value of, φ, is determined by requiring that the ground displacement at the end of the pulse be equal to a prescribed permanent displacement. In most cases the ground displacement at the end of the pulse is zero. A type C_n pulse with frequency $\omega_p = 2\pi/T_p$ has a duration $T = \left(n + \frac{1}{2}\right)T_p - \frac{2\varphi}{\omega_p} = \left(n + \frac{1}{2} - \frac{\varphi}{\pi}\right)T_p$. In order to have a zero ground displacement at the end of a type C_n pulse:

$$\int_0^{(n + 1/2 - \varphi/\pi)T_p} \dot{u}_g(\tau)d\tau = 0. \tag{47}$$

Evaluating the integral in Equation (47) we obtain

$$\cos[(2n + 1)\pi - \varphi] + [(2n + 1)\pi - 2\varphi]\sin\varphi - \cos\varphi = 0. \tag{48}$$

The solution of the transcendental equation given by (48) gives the values of the phase φ. As an example, for a type C_1 pulse ($n = 1$), $\varphi = 0.0697\pi$, whereas for a type C_2 pulse ($n = 2$), $\varphi = 0.0410\pi$. Figure 4.1 (right) shows the kinematic characteristics of a 1.3 sec type C_1 pulse with amplitude $V_p = 0.85m/\sec$. Figure 4.2 plots the true acceleration, true velocity, and displacement response spectra due to the Pacoima Dam record and the associated trigonometric pulse. The UBC 1997 acceleration design spectrum for $\zeta = 5\%$ and the type *D* soil profile are also provided for comparison.

Figure 4.3 (left) shows the acceleration, velocity, and displacement time histories recorded during the September 16, 1978, Tabas, Iran, earthquake, while Figure 4.3 (right) shows a type C_1 cycloidal pulse with $T_p = 5\sec$ and $V_p = 0.95m/\sec$. Figure 4.4 plots the true response spectra due to the Tabas record and the associated trigonometric pulse. Note that while the acceleration spectra are drastically different, the displacement spectra are very similar.

In comparing Figures 4.2 and 4.4 one can recognize the information that trigonometric approximations offer. Figure 4.2 (center-left) shows that the peak spectral velocity occurs at a period of

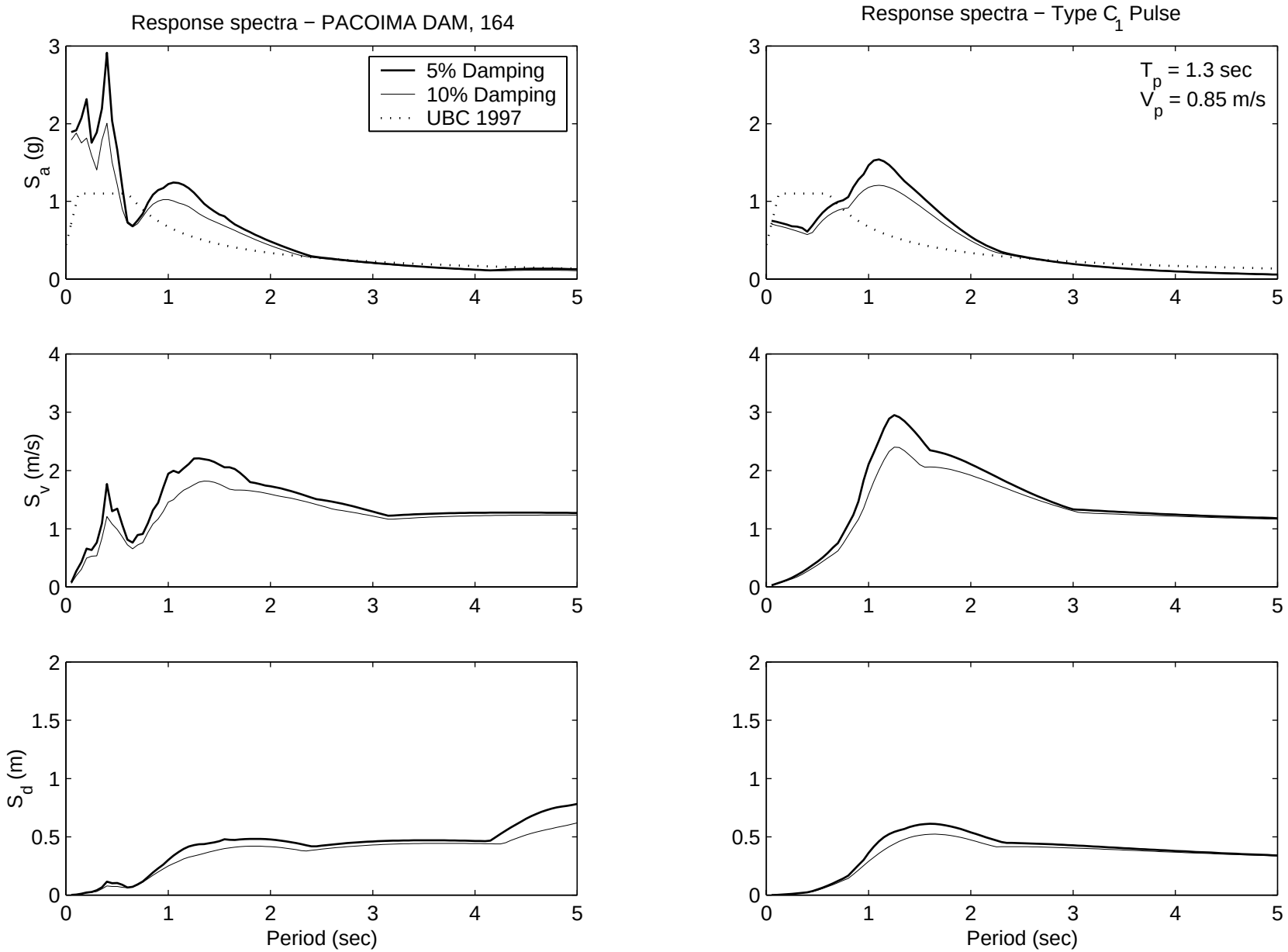

Figure 4.2. Acceleration, velocity, and displacement response spectra calculated due to the Pacoima Dam record (left), and the associated cycloidal type C_1 pulse (right).

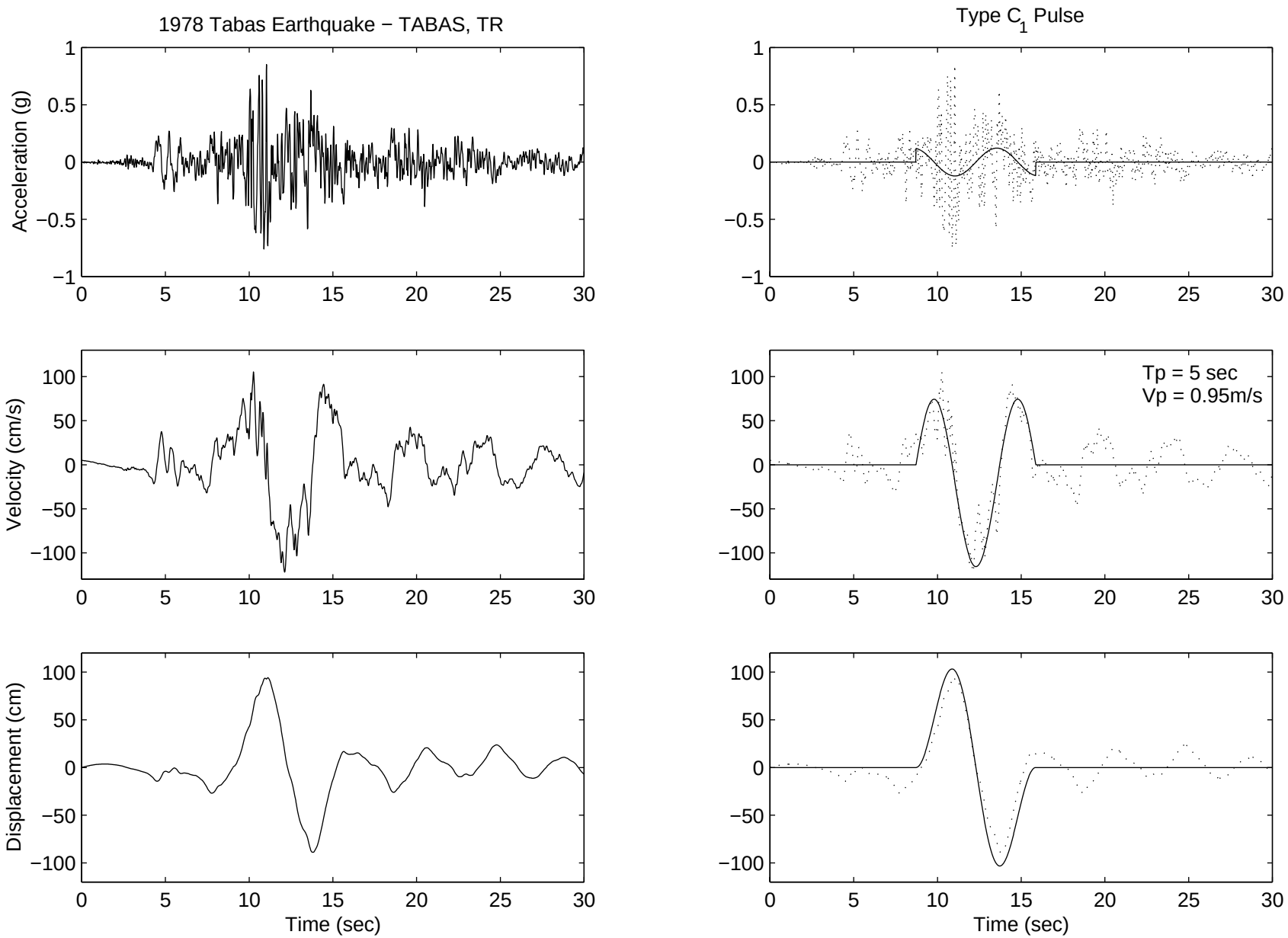

Figure 4.3. Fault-normal components of the acceleration, velocity, and displacement time-histories recorded during the September 16, 1978, Tabas, Iran, earthquake (left), and a cycloidal type C_1 pulse (right).

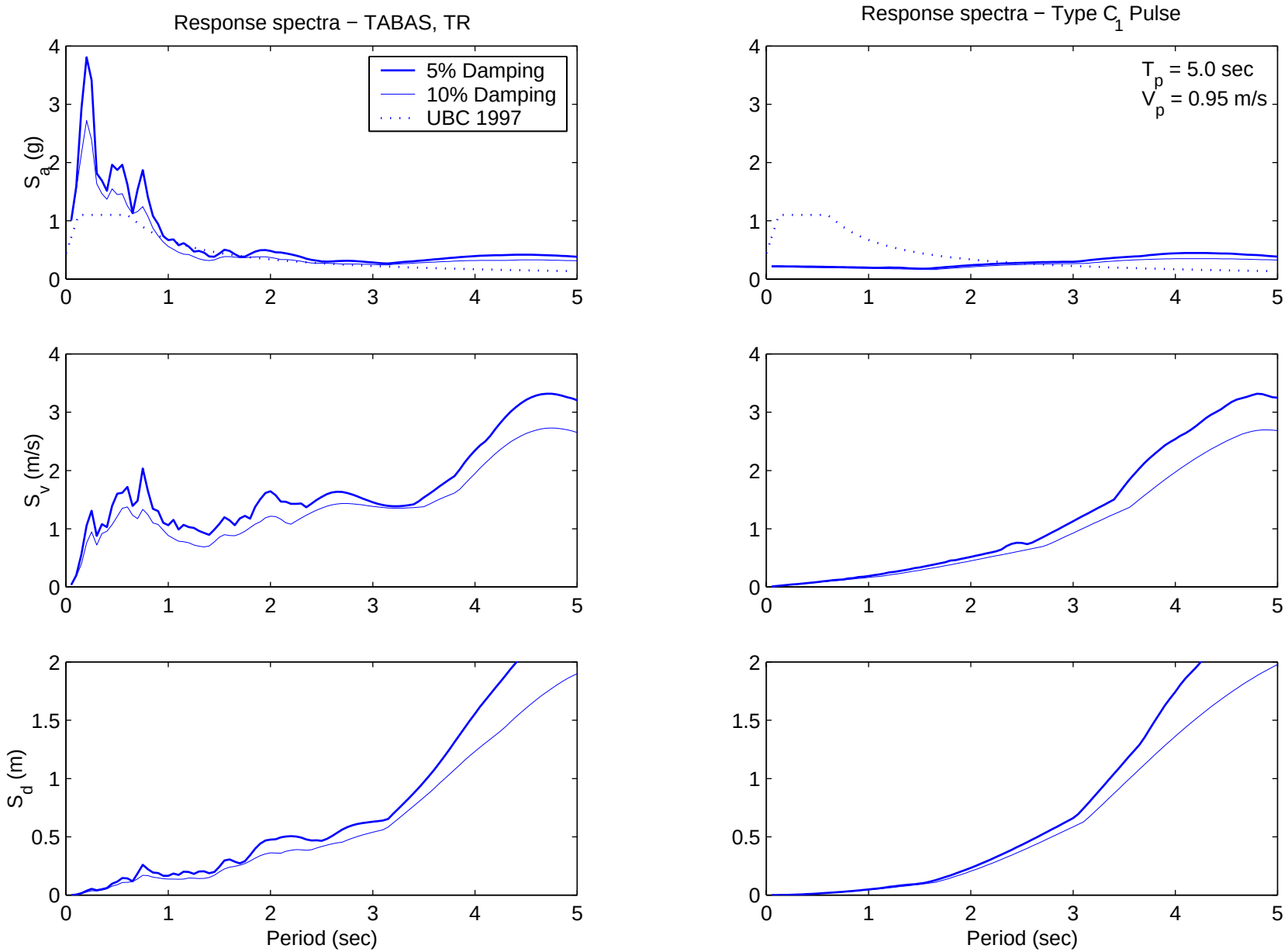

Figure 4.4. Acceleration, velocity, and displacement response spectra due to the Tabas record (left), and the associated type C_1 pulse (right).

$T_p \approx 1.3\,\text{sec}$ while Figure 4.4 (center-left) shows that the peak spectral velocity occurs at a period near 4.5 sec. These period values are very close to the pulse periods of the trigonometric approximations shown in Figures 4.1 and 4.3.

Figure 4.5 (left) shows the acceleration, velocity, and displacement histories of the fault-normal motions recorded at the El Centro Station, Array No. 5 during the October 15, 1979, Imperial Valley, California, earthquake. This motion resulted in a forward-and-back pulse with a 3.2 sec duration. In this case, the coherent long-period pulse is distinguishable not only in the displacement and velocity records, but also in the acceleration record. Figure 4.5 (right) shows the acceleration, velocity, and displacement histories of a type B cycloidal pulse (Makris 1997):

$$\ddot{u}_g(\tau) = \omega_p V_p \cos(\omega_p \tau), \qquad 0 \le \tau \le T_p \tag{49}$$

$$\dot{u}_g(\tau) = V_p \sin(\omega_p \tau), \qquad 0 \le \tau \le T_p \tag{50}$$

$$u_g(\tau) = \frac{V_p}{\omega_p} - \frac{V_p}{\omega_p}\cos(\omega_p \tau), \qquad 0 \le \tau \le T_p. \tag{51}$$

In constructing Figure 4.5 (right) the values of $T_p = 3.2\,\text{sec}$ and $V_p = 0.7\,m/\text{sec}$ were used. Figure 4.6 plots the true acceleration, velocity, and displacement response spectra due to the Array #5 record and the associated trigonometric pulse. It is noted again that the peak spectral velocity appears at $T_p \approx 3.2\,\text{sec}$ — that is the period of the trigonometric approximation.

Figure 4.7 (left) shows the acceleration, velocity, and displacement histories recorded at the Los Gatos Station during the October 15, 1989, Loma Prieta, California, earthquake. The right plots in Figure 4.7 show a type C_1 ($T_p = 3.0\,\text{sec}$ and $V_p = 0.75\,\text{m/sec}$) pulse that captures the peak ground displacement and part of the strong velocity pulse; however, many of the kinematic characteristics of this record are not represented with the trigonometric approximation. This becomes evident in the response spectra shown in Figure 4.8 in which appreciable differences are apparent, especially in the acceleration and velocity spectrum.

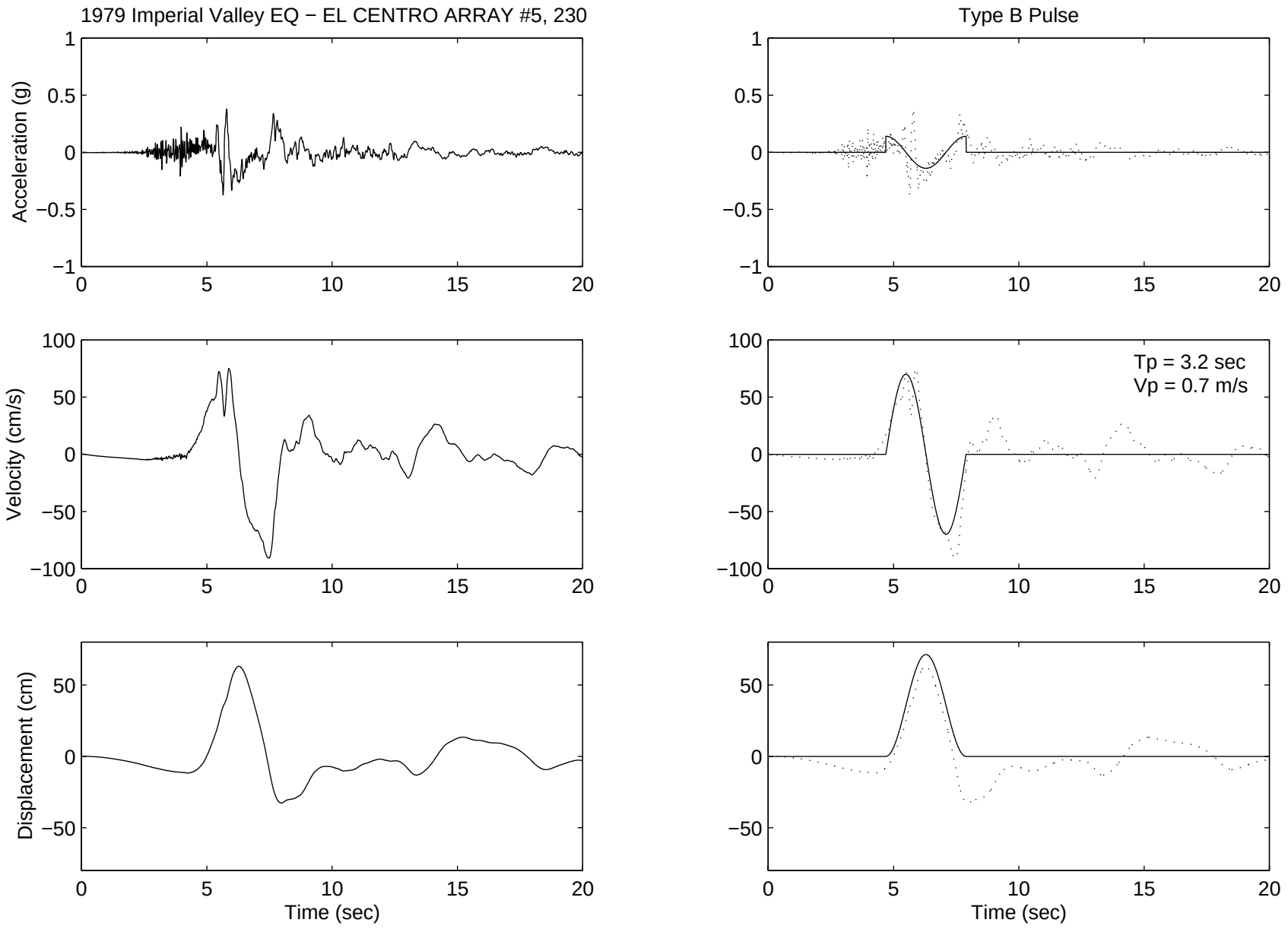

Figure 4.5. Fault-normal components of the acceleration, velocity, and displacement time histories recorded at the El Centro Array No. 5 Station during the October 15, 1979, Imperial Valley, California, earthquake (left), and a cycloidal type *B* pulse (right).

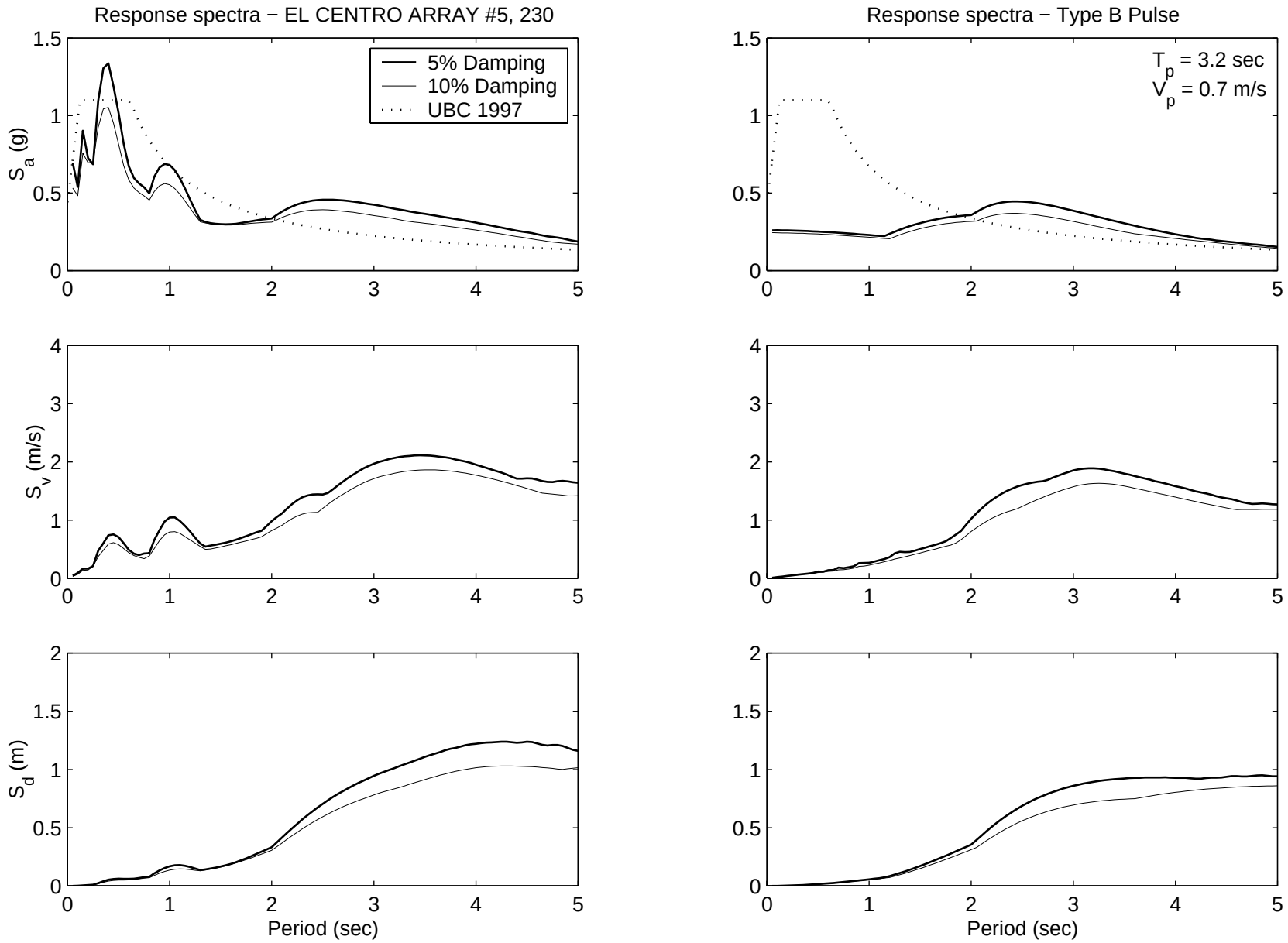

Figure 4.6. Acceleration, velocity, and displacement response spectra due to the El Centro Array No. 5 record (left), and the associated cycloidal type *B* pulse (right).

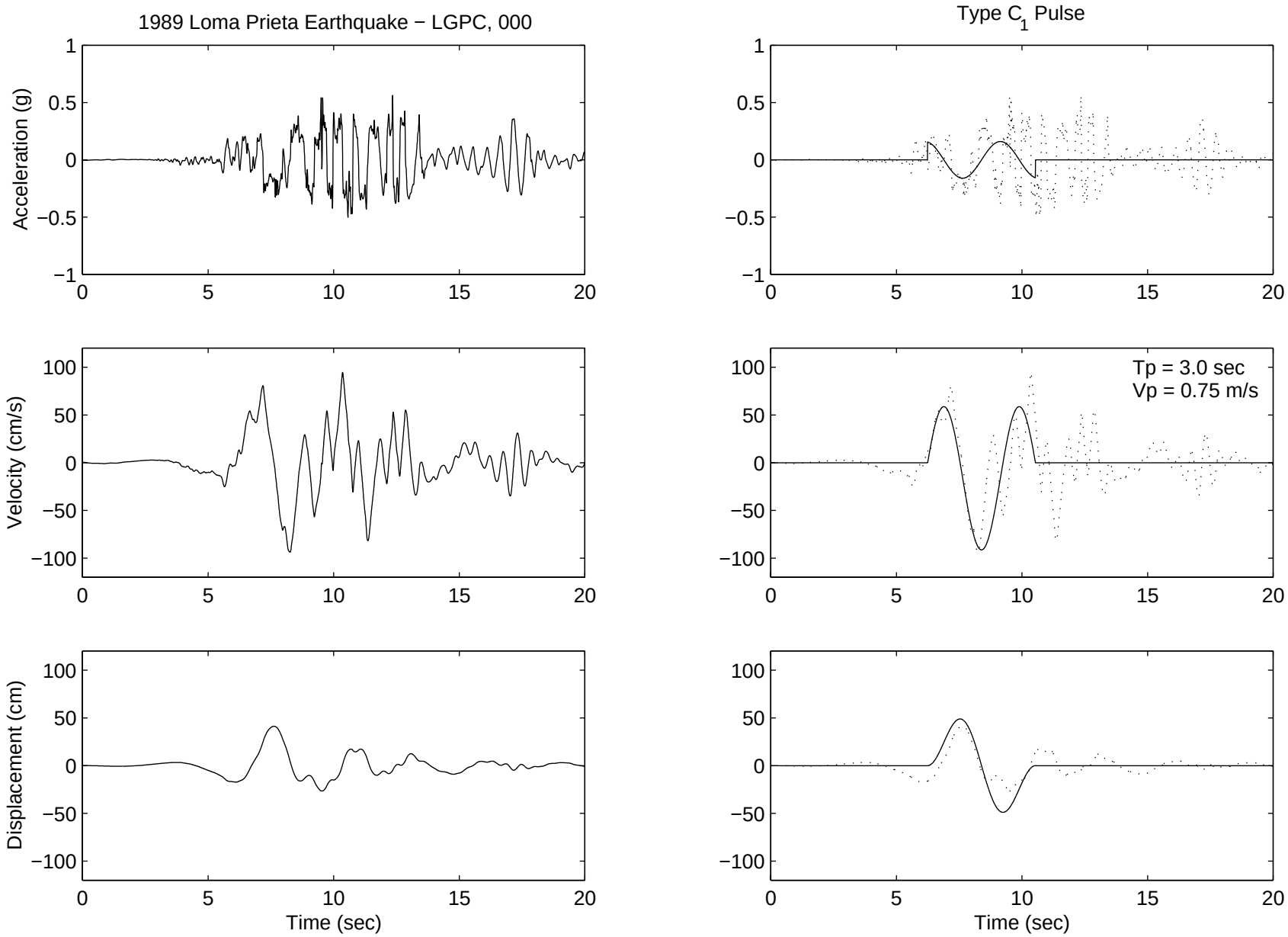

Figure 4.7. East-west components of the acceleration, velocity, and displacement time histories recorded at the Los Gatos Station during the October 18, 1989, Loma Prieta, California, earthquake (left), and a cycloidal type C_1 pulse (right).

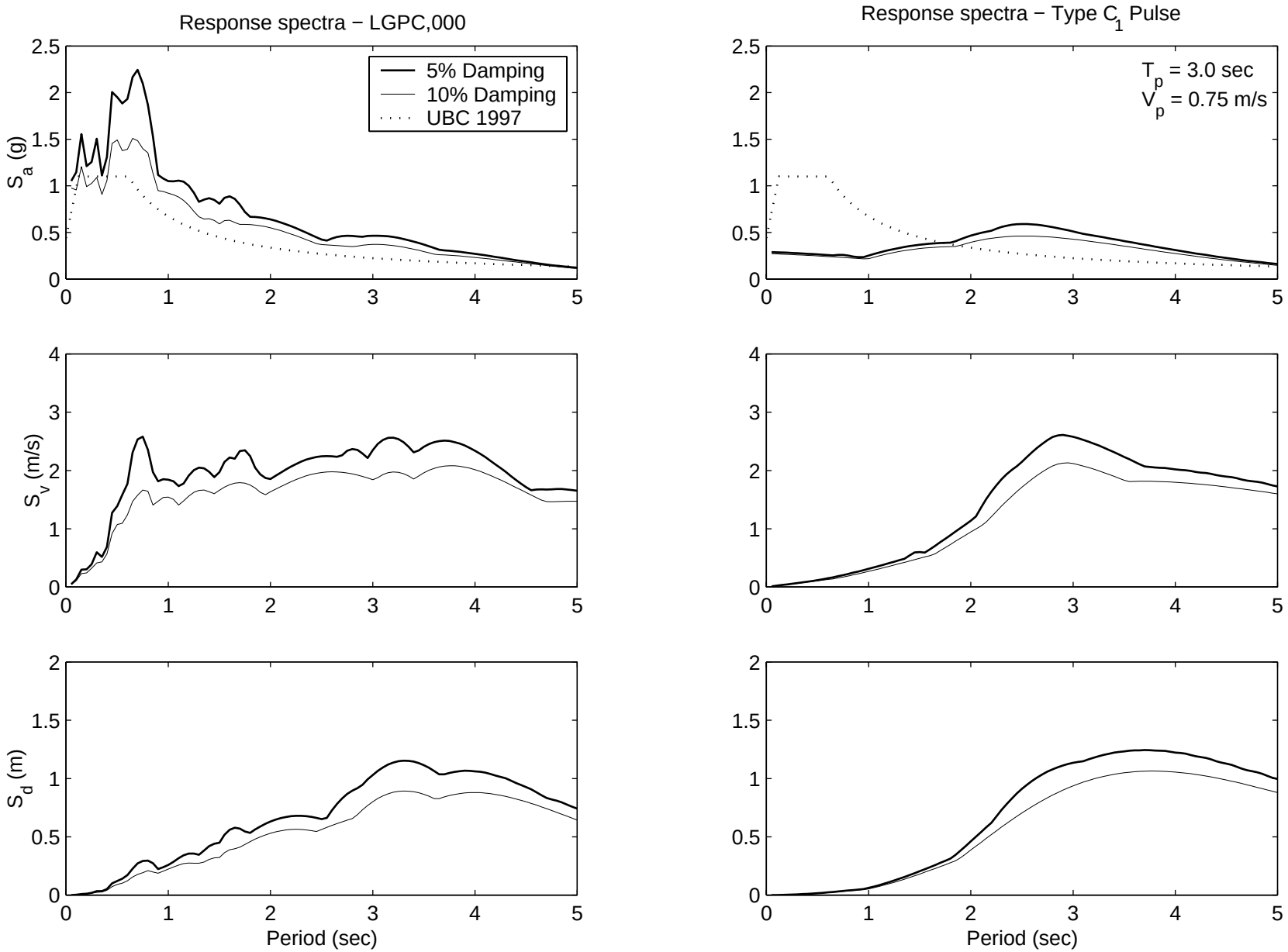

Figure 4.8. Acceleration, velocity, and displacement response spectra due to the Los Gatos Station record (left), and the associated cycloidal type C_1 pulse (right).

Figure 4.9 shows the acceleration, velocity, and displacement histories recorded during the March 13, 1992, Erzikan, Turkey, earthquake (left) and their approximation with a type C_1 pulse. In this case the type C_1 pulse captures with fidelity not only the displacement and velocity histories but also many features of the acceleration history. In constructing Figure 4.9 (right) the values of $T_p = 1.8\,\text{sec}$ and $V_p = 0.7\,m/\text{sec}$ were used. The close resemblance of the Erzikan record to a type C_1 pulse is reflected in the corresponding spectra shown in Figure 4.10 which exhibits striking similarities.

Figure 4.11 (left) shows the north-south components of the displacement histories recorded during the April 25, 1992, Cape Mendocino earthquake. The interesting aspect of this record is that it exhibits a sharp acceleration pulse with a peak ground acceleration that reaches 1.5g and a much longer displacement pulse with duration that reaches 4.5 sec. Figure 4.11 (center) indicates how the local acceleration pulse can be approximated with a type A pulse, whereas, Figure 4.11 (right) shows the kinematic characteristics of a 4.4-sec-long type C_1 pulse. A type A cycloidal pulse is given by (Jacobsen and Ayre, 1958; Makris 1997):

$$\ddot{u}_g(\tau) = \omega_p \frac{V_p}{2} \sin(\omega_p \tau), \qquad 0 \le \tau \le T_p \tag{52}$$

$$\dot{u}_g(\tau) = \frac{V_p}{2} - \frac{V_p}{2} \cos(\omega_p \tau), \qquad 0 \le \tau \le T_p \tag{53}$$

$$u_g(\tau) = \frac{V_p}{2} \tau - \frac{V_p}{2\omega_p} \sin(\omega_p \tau), \qquad 0 \le \tau \le T_p \tag{54}$$

The effects of the distinct pulses on elastic structures are shown in Figure 4.12. The center column of Figure 4.12 shows that the type A pulse with a period of 0.55 sec produces acceleration and velocity spectra which closely resemble the earthquake spectra for periods larger than 0.5 sec. On the other hand, the displacement spectrum of the pulse grossly underestimates the earthquake spectrum for periods longer than 2.8 sec. The right column of Figure 4.12 shows that the type C_1 pulse with a period of 4.4 sec produces the wrong acceleration and velocity spectra as compared to the earthquake spectra; while the displacement spectrum captures some of the trends of the earthquake spectrum at longer periods.

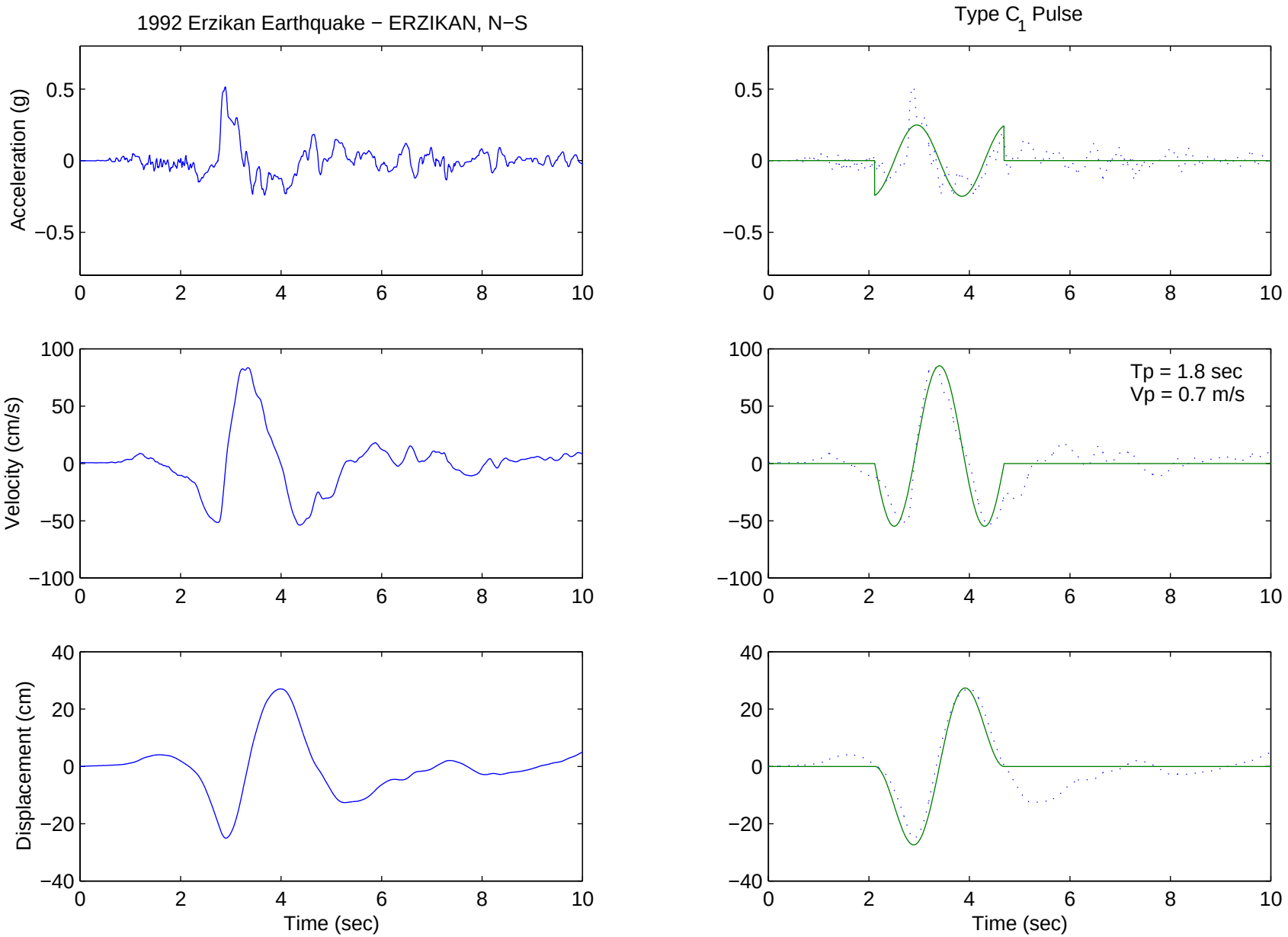

Figure 4.9. North-south components of the acceleration, velocity, and displacement time histories recorded during the March 13, 1992, Erzikan, Turkey, earthquake (left), and a cycloidal type C_1 pulse (right).

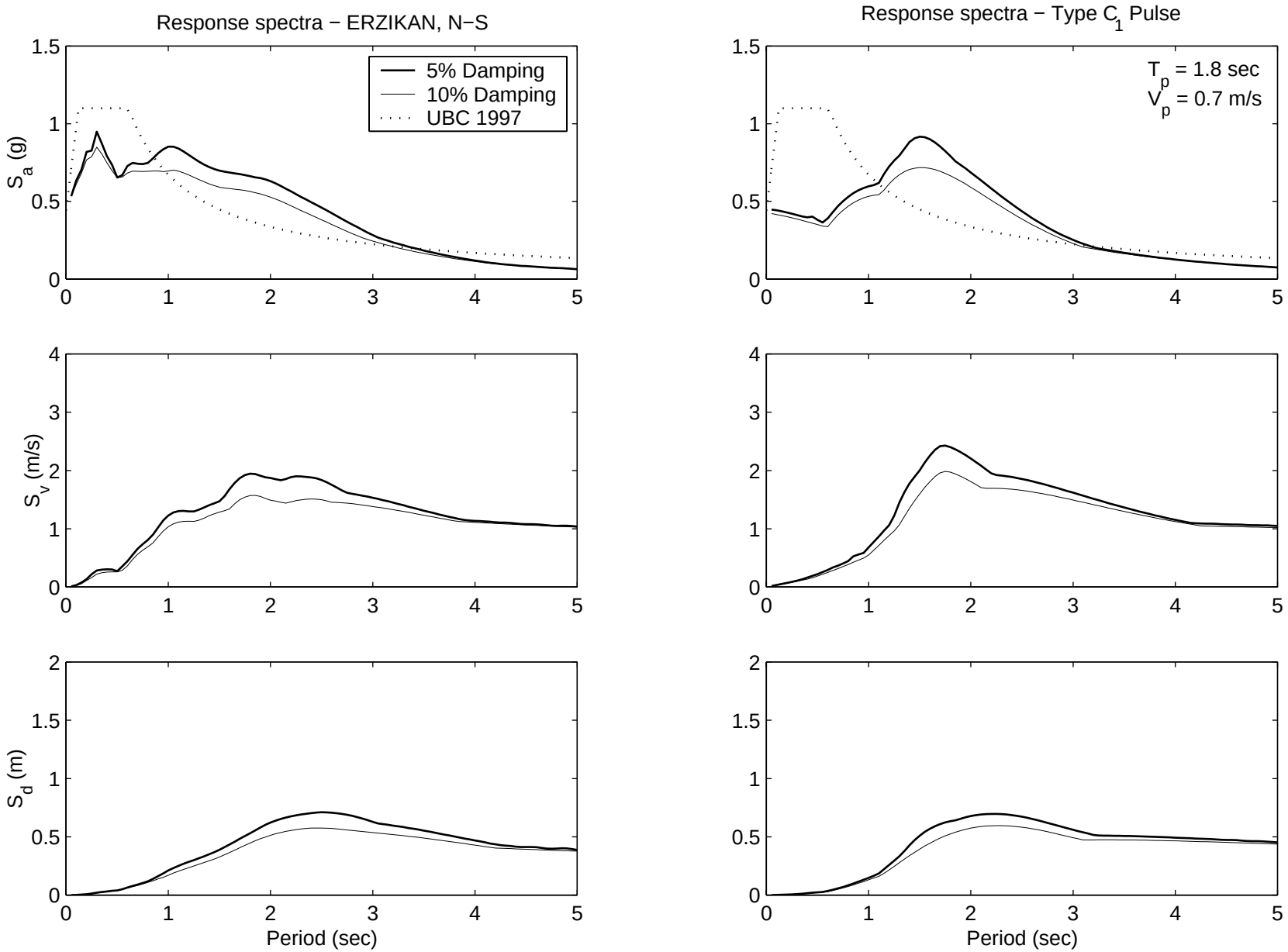

Figure 4.10. Acceleration, velocity, and displacement response spectra due to the Erzikan record (left), and the associated cycloidal type C_1 pulse (right).

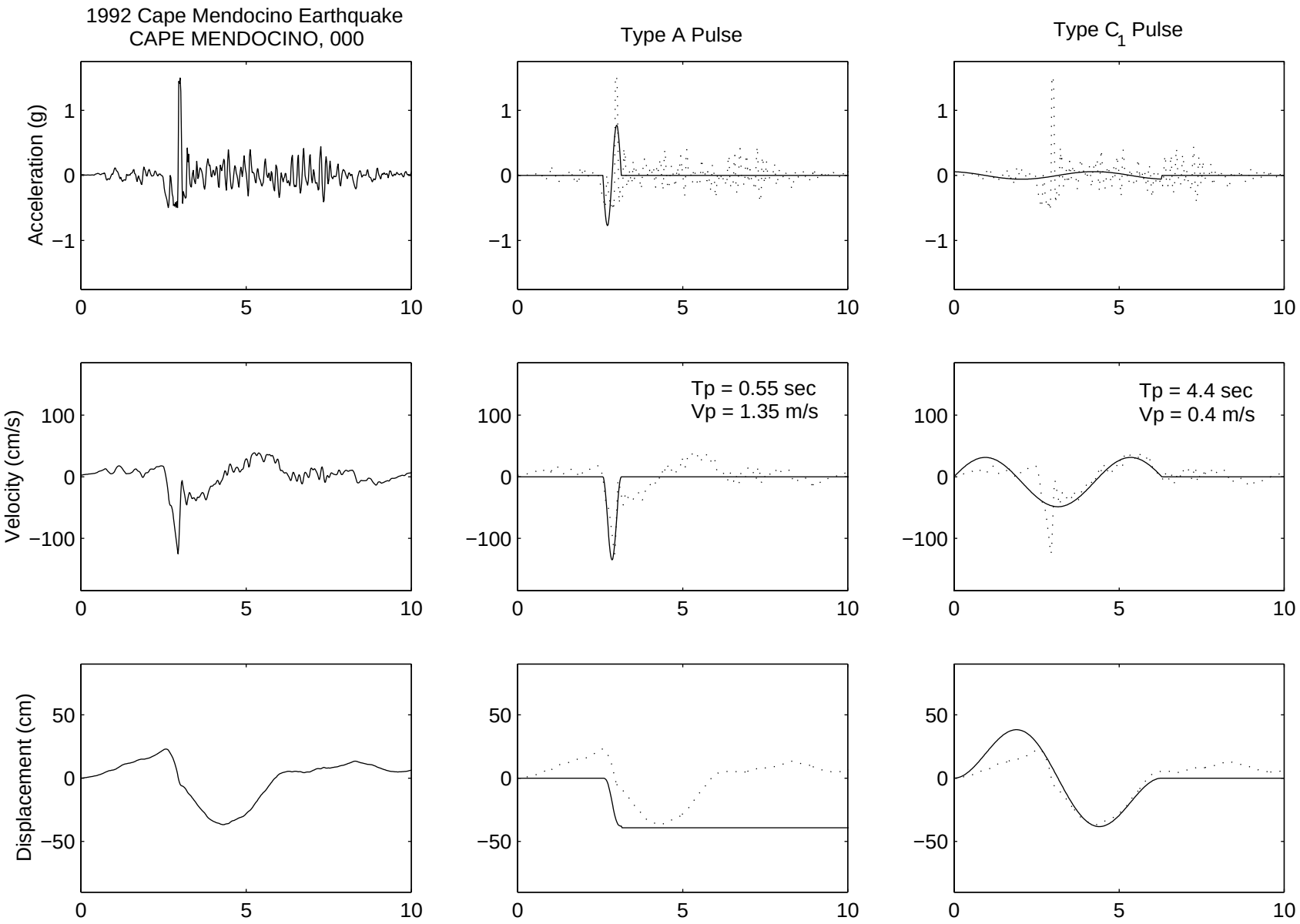

Figure 4.11. North-south components of the acceleration, velocity, and displacement time histories recorded during the April 25, 1992, Cape Mendocino earthquake (left), a cycloidal type *A* pulse (center), and a cycloidal type C_1 pulse (right).

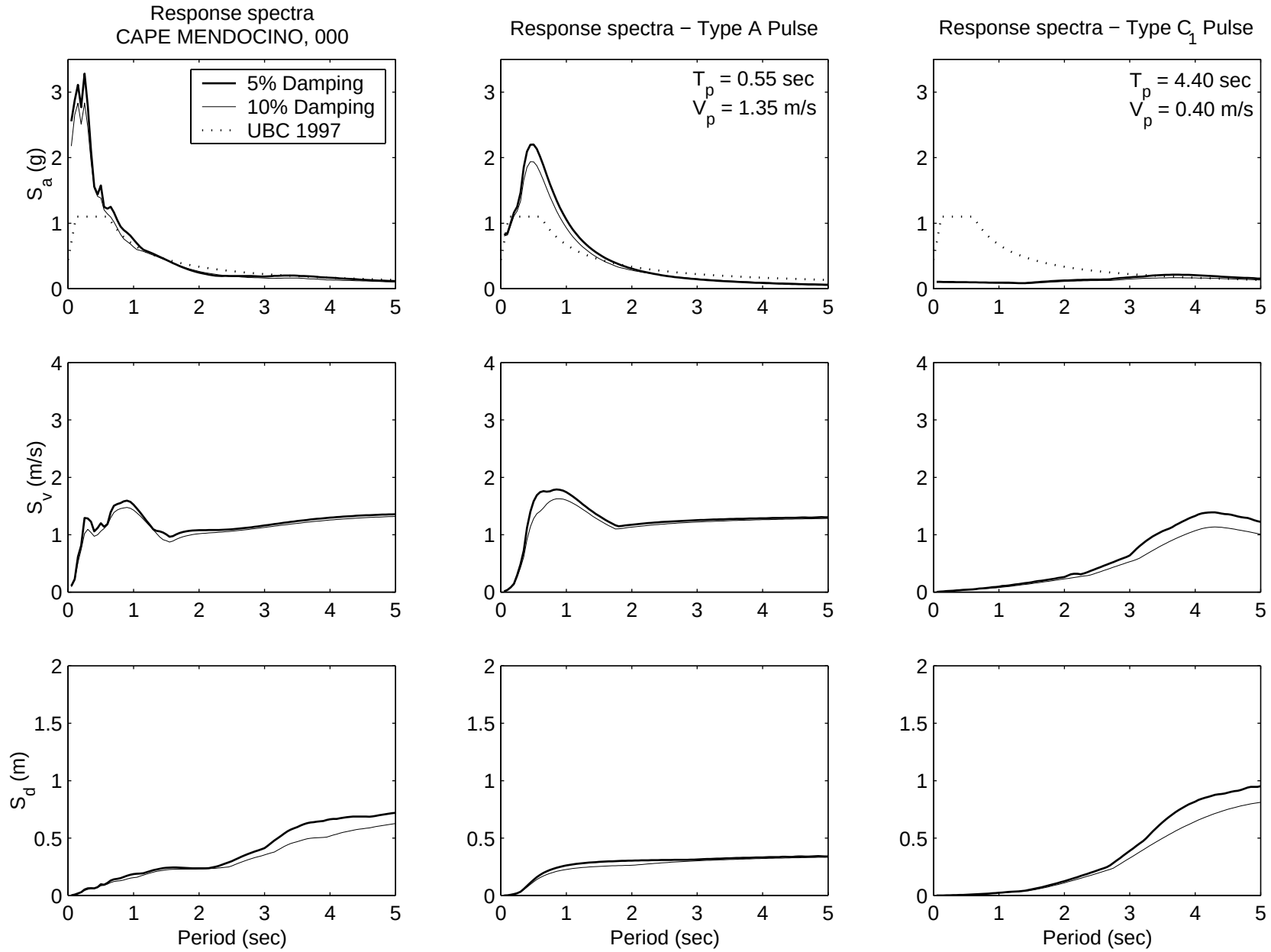

Figure 4.12. Acceleration, velocity, and displacement response spectra due to the Cape Mendocino N-S record (left), a cycloidal type *A* pulse (center), and a cycloidal type C_1 pulse (right).

Figure 4.13 (left) portrays the fault-normal components of the acceleration, velocity, and displacement histories recorded at the Rinaldi Station during the January 17, 1994, Northridge, California, earthquake. This motion resulted in a forward ground motion that recovered partially. Figure 4.13 (center) shows the acceleration, velocity, and displacement histories of a type *A* cycloidal pulse where $T_p = 0.8\,\text{sec}$ and $V_p = 1.75\,m/\text{sec}$. Figure 4.13 (right) shows the acceleration, velocity, and displacement of a type B cycloidal pulse where $T_p = 1.3\,\text{sec}$ and $V_p = 1.3\,m/\text{sec}$. When observing Figure 4.14, which offers the corresponding response spectra, one concludes that both trigonometric pulses provide good approximations.

Figure 4.15 shows the fault-normal component of the acceleration, velocity, and displacement time histories recorded at the Sylmar Station during the January 17, 1994, Northridge earthquake. The ground displacement consists of two main long-period cycles, the first cycle being the largest and the subsequent ones decaying. These long-period pulses are also distinguishable in the ground velocity history where the amplitude of the positive pulses is larger than the amplitude of the negative pulses. Figure 4.15 (right) shows the acceleration, velocity, and displacement of a type C_2 cycloidal pulse where $T_p = 2.3\,\text{sec}$ and $V_p = 0.6\,m/\text{sec}$. Although many of the kinematic characteristics of the Sylmar record are not captured with the type C_2 trigonometric approximation, the velocity spectrum shown in Figure 4.16 exhibits an amplification near 2.5 sec that is very close to the 2.3 sec period of the proposed type C_2 pulse.

Figure 4.17 shows the fault-normal and fault-parallel components of the ground motion recorded at the Takatori Station during the January 16, 1995, Kobe earthquake. This strong motion exhibited several appreciable cycles that do not resemble any of the simple trigonometric pulses used in this study. Their elastic response spectra shown in Figure 4.18 show high spectral accelerations and unusually high spectral velocities.

Figures 4.19 and 4.21 show the fault-normal and fault-parallel components of the ground motions recorded at the TCU068 station during the September 20, 1999, Chi-Chi, Taiwan, earthquake. Among other unique characteristics, the motion exhibits a very large and long displacement pulse.

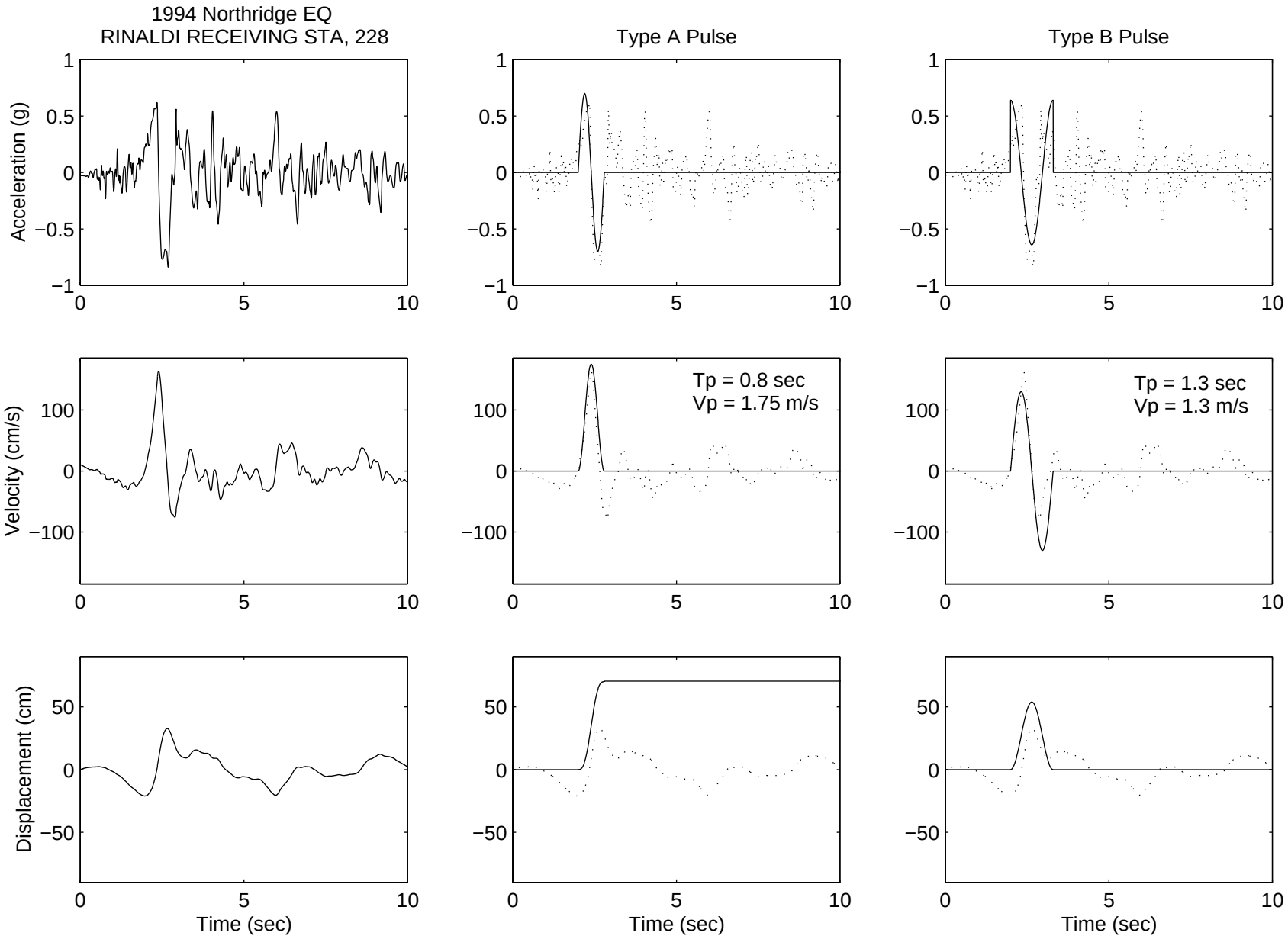

Figure 4.13. Fault-normal components of the acceleration, velocity, and displacement time histories recorded at the Rinaldi Station during the January 17, 1994, Northridge earthquake (left), a cycloidal type *A* pulse (center) and type *B* pulse (right).

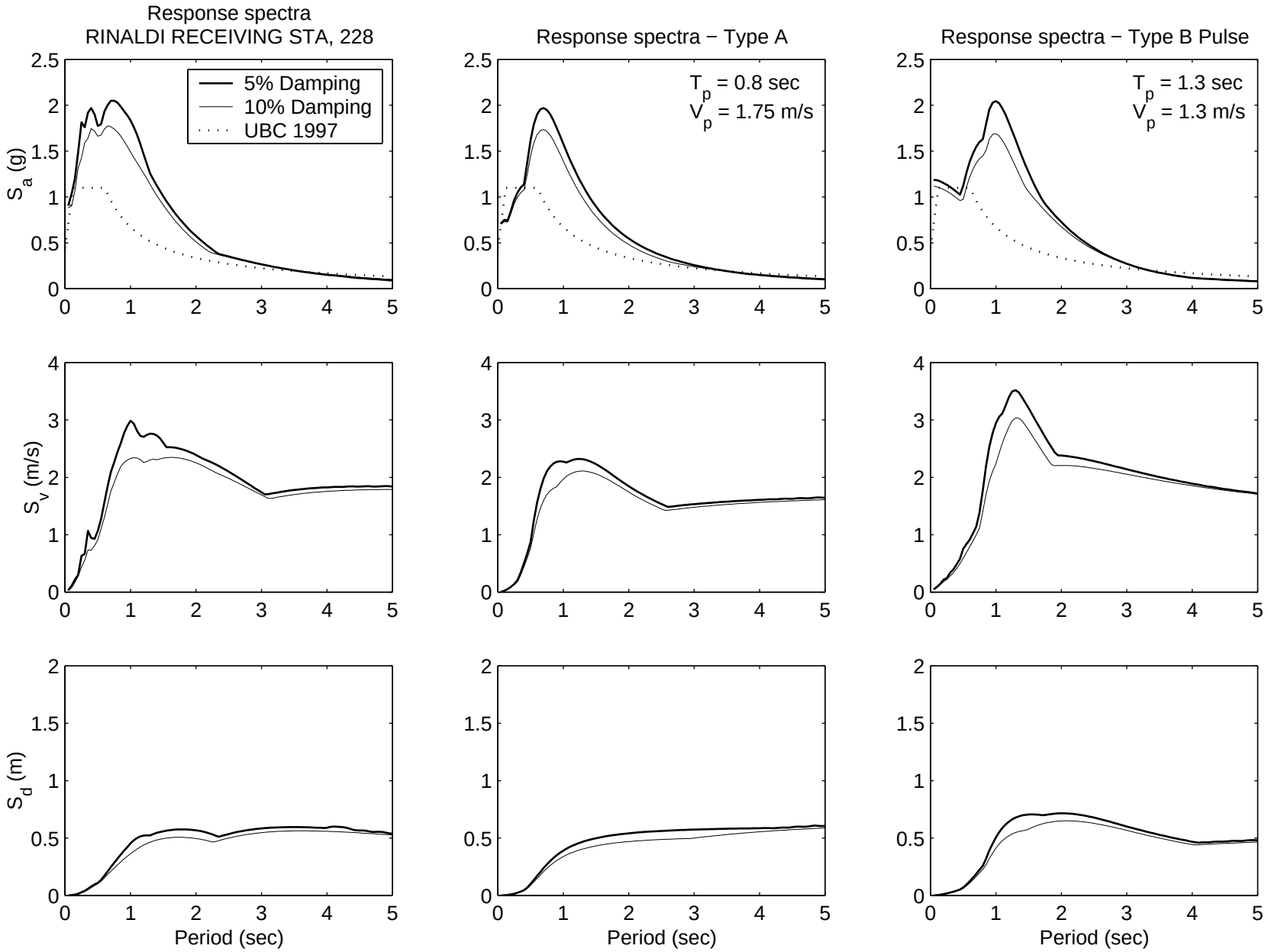

Figure 4.14. Acceleration, velocity, and displacement response spectra due to the Rinaldi Station record (left), and the associated cycloidal type *A* pulse (center), and the cycloidal type *B* pulse (right).

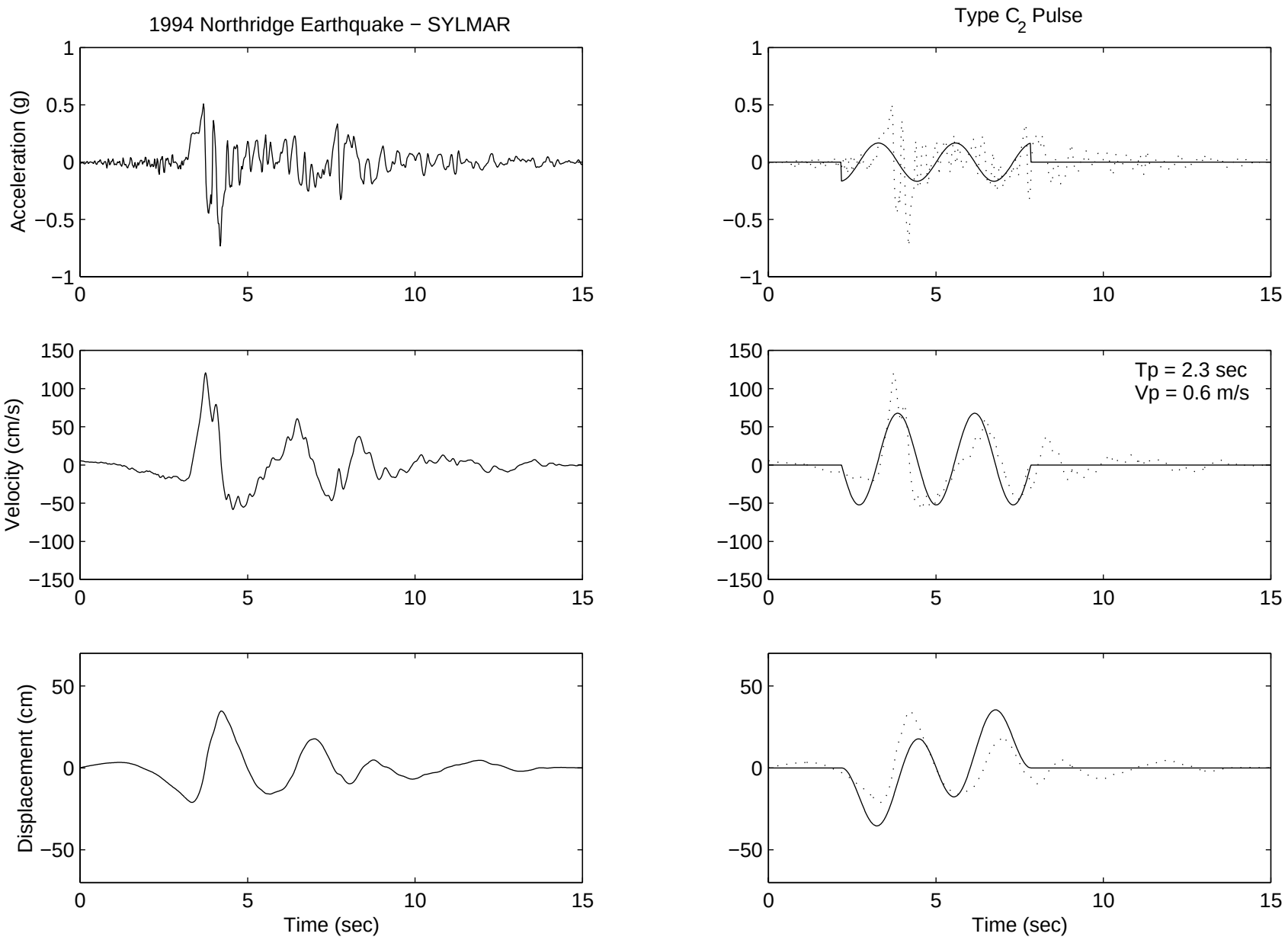

Figure 4.15. Fault-normal components of the acceleration, velocity, and displacement time histories recorded at the Sylmar Station during the January 17, 1994, Northridge, California, earthquake (left), and a cycloidal type C_2 pulse (right).

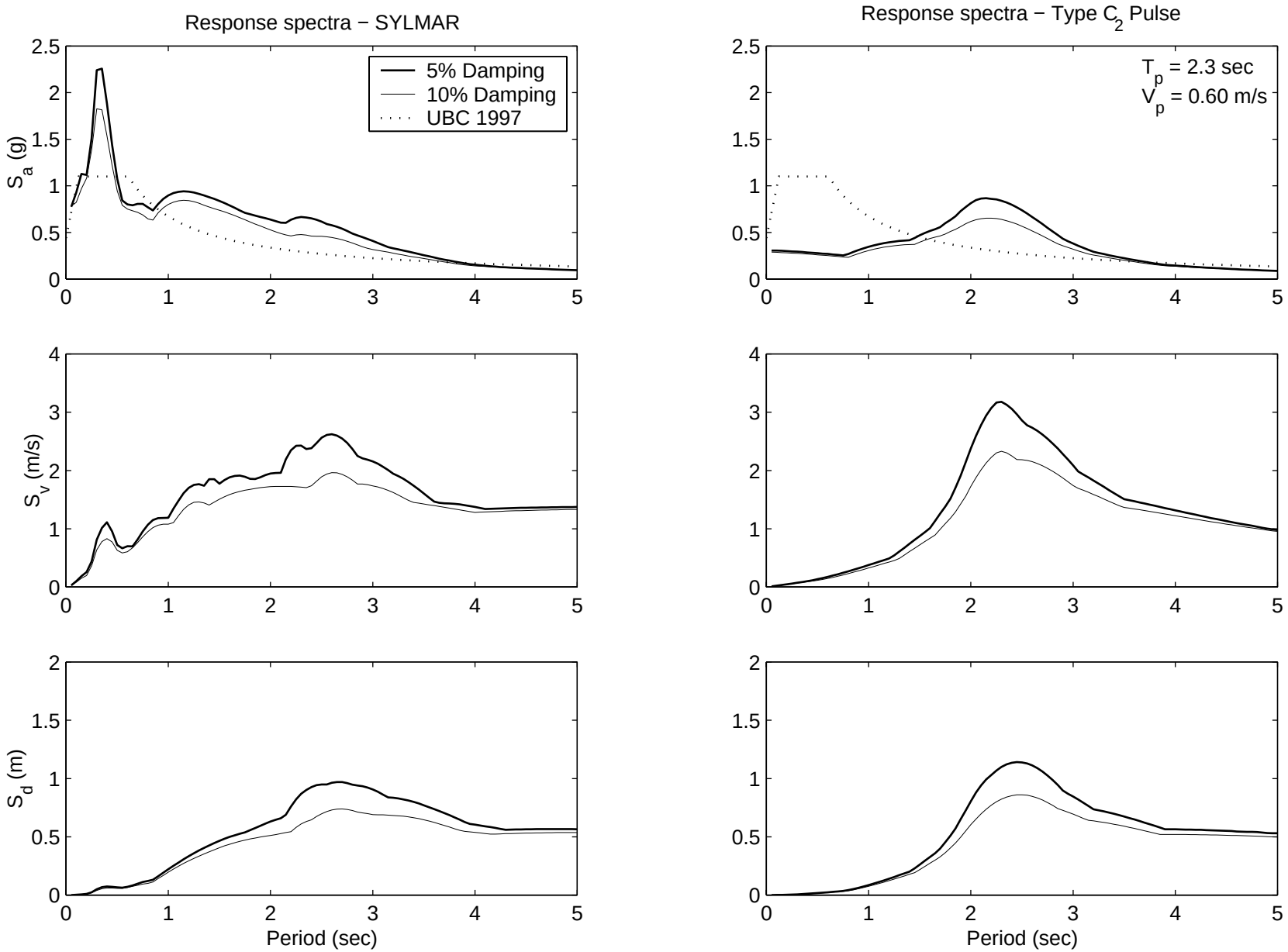

Figure 4.16. Acceleration, velocity, and displacement response spectra due to the Sylmar Station record (left), and the associated cycloidal type C_2 pulse (right).

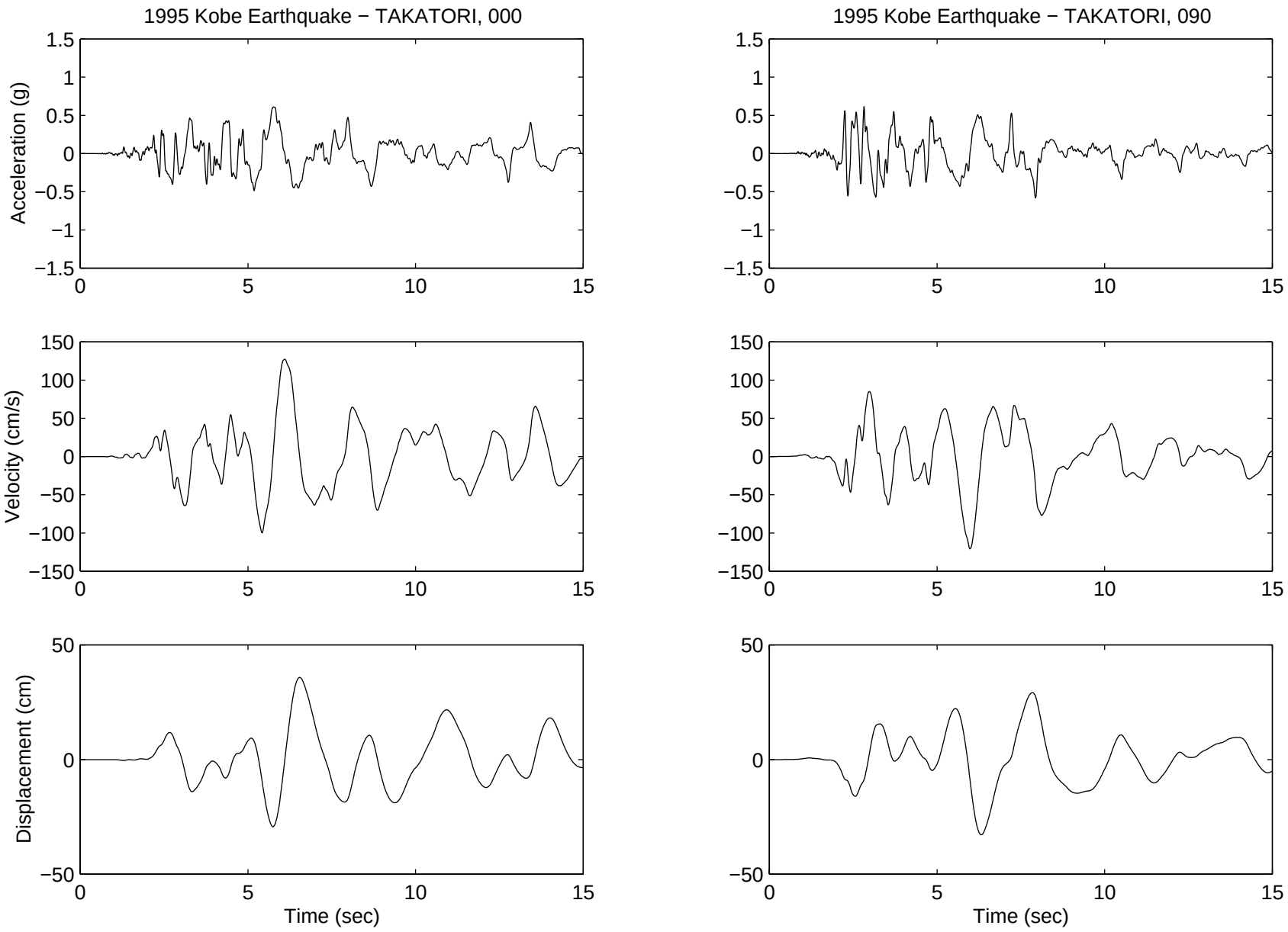

Figure 4.17. Fault-normal (left) and fault-parallel (right) components of the acceleration, velocity, and displacement time histories recorded during the January 16, 1995, Kobe earthquake.

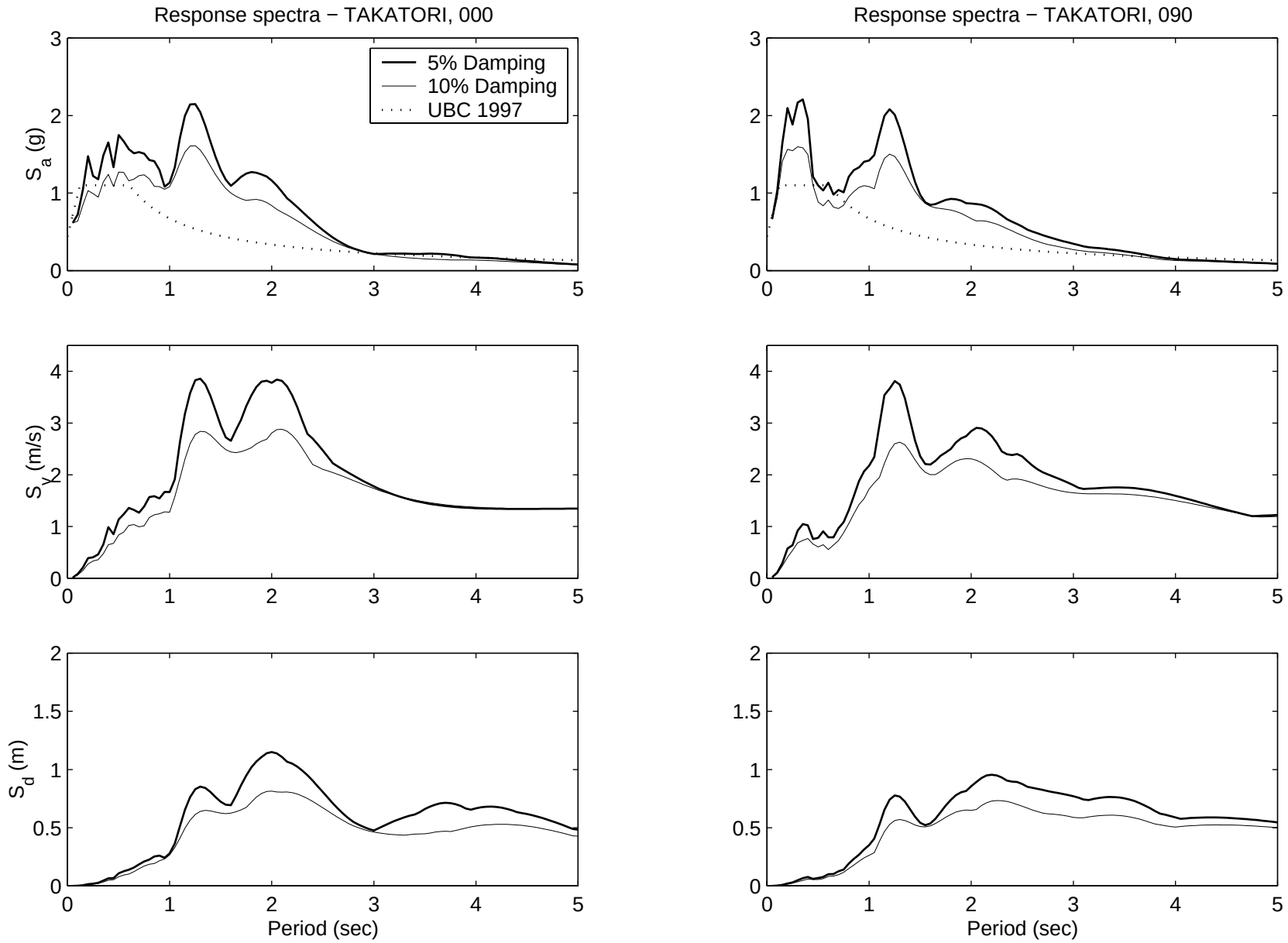

Figure 4.18. Acceleration, velocity, and displacement response spectra due to the fault-normal (left) and fault-parallel (right) components of the Kobe earthquake.

The E-W component of the TCU068 record can be approximated with a type A pulse with $T_p = 6.5\,\text{sec}$ and $V_p = 2.4 m/\text{sec}$. This extremely large ground velocity in association with the 6.5-sec long pulse resulted in a permanent ground displacement on the order of 8 m. The large ground displacements and velocities that resulted from the TCU068 motion are also present in the fault-parallel component shown in Figure 4.21. Figures 4.20 and 4.22 show that the trigonometric approximations are useful only for estimating spectral displacements as the acceleration and velocity spectra are sensitive to higher-frequency pulses other than the pulse which is responsible for the main ground displacement.

The exceptionally large displacements and velocities generated during the 1999 Chi-Chi, Taiwan, earthquake are also observable in the TCU052 record. Figure 4.23 (left) shows the fault-normal component of the acceleration, velocity, and displacement time histories; whereas, Figure 4.23 (right) shows the acceleration, velocity, and displacement of a type C_1 pulse with $T_p = 5.5\,\text{sec}$ and $V_p = 1.0 m/\text{sec}$. Figure 4.25 (left) shows the fault-parallel component of the acceleration, velocity, and displacement time histories; whereas, Figure 4.25 (right) shows the acceleration, velocity, and displacement of a type A pulse with $T_p = 6.5\,\text{sec}$ and $V_p = 2.0 m/\text{sec}$. The acceleration, velocity and ground displacement spectra for the fault-normal and fault-parallel components of the TCU052 motions are shown in Figures 4.24 and 4.26, respectively. Similar to the TCU068 motions, the trigonometric approximations are useful only for estimating spectral displacements.

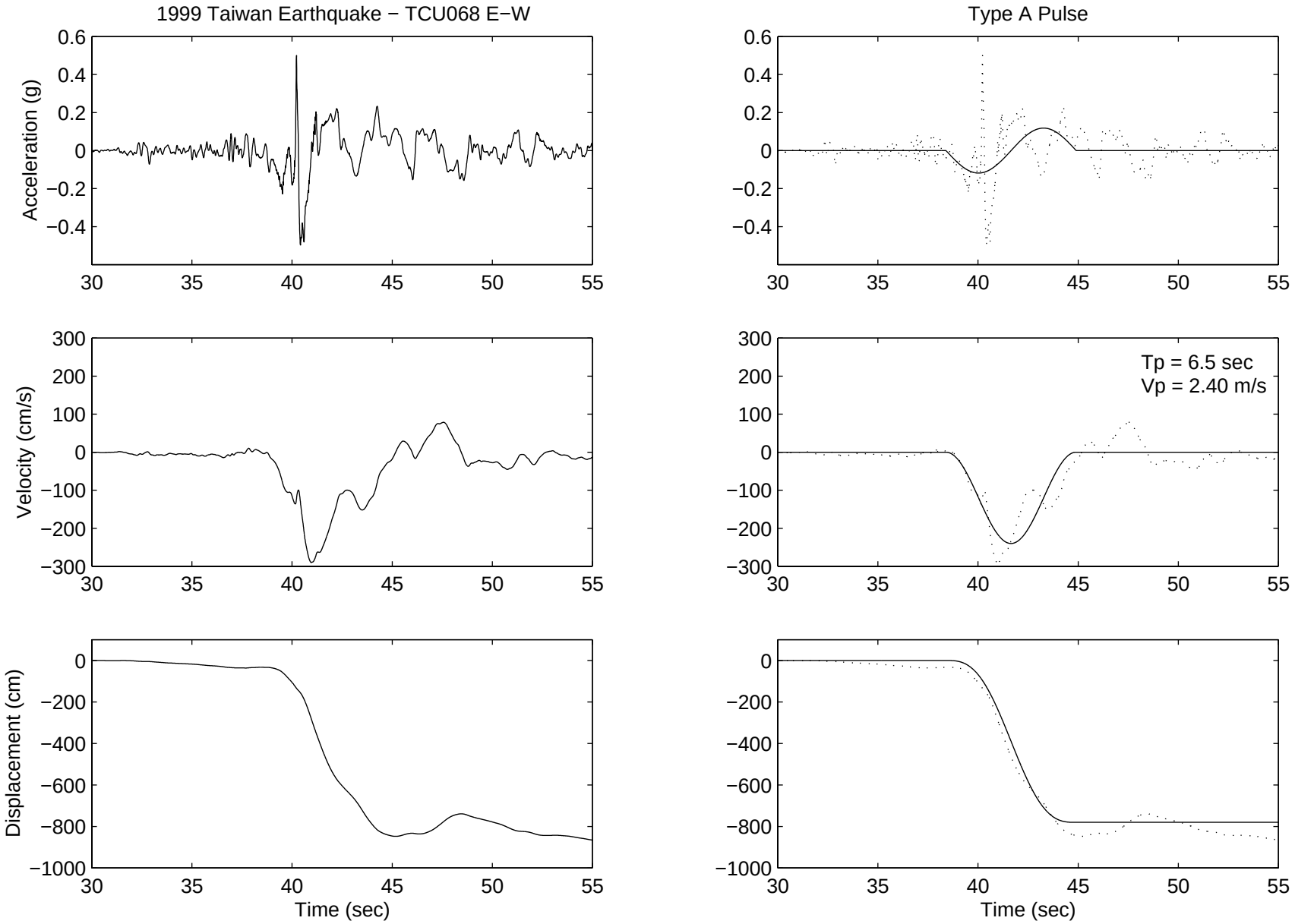

Figure 4.19. East-west components of the acceleration, velocity, and displacement time histories of the TCU068 E-W record from the September 20, 1999, Chi-Chi, Taiwan, earthquake (left), and a cycloidal type *A* pulse (right).

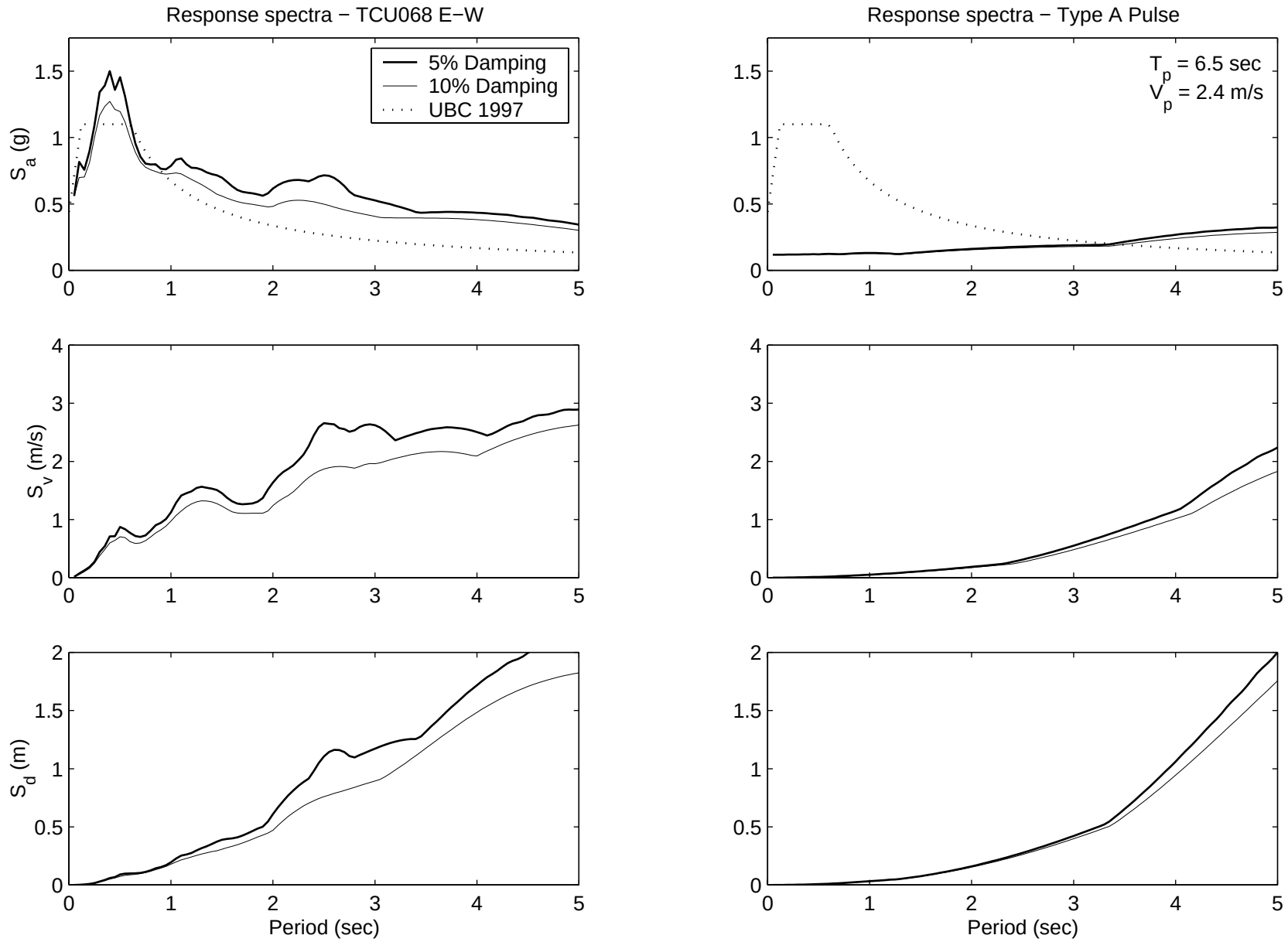

Figure 4.20. Acceleration, velocity, and displacement response spectra due to the TCU068 E-W record (left), and the associated cycloidal type *A* pulse (right).

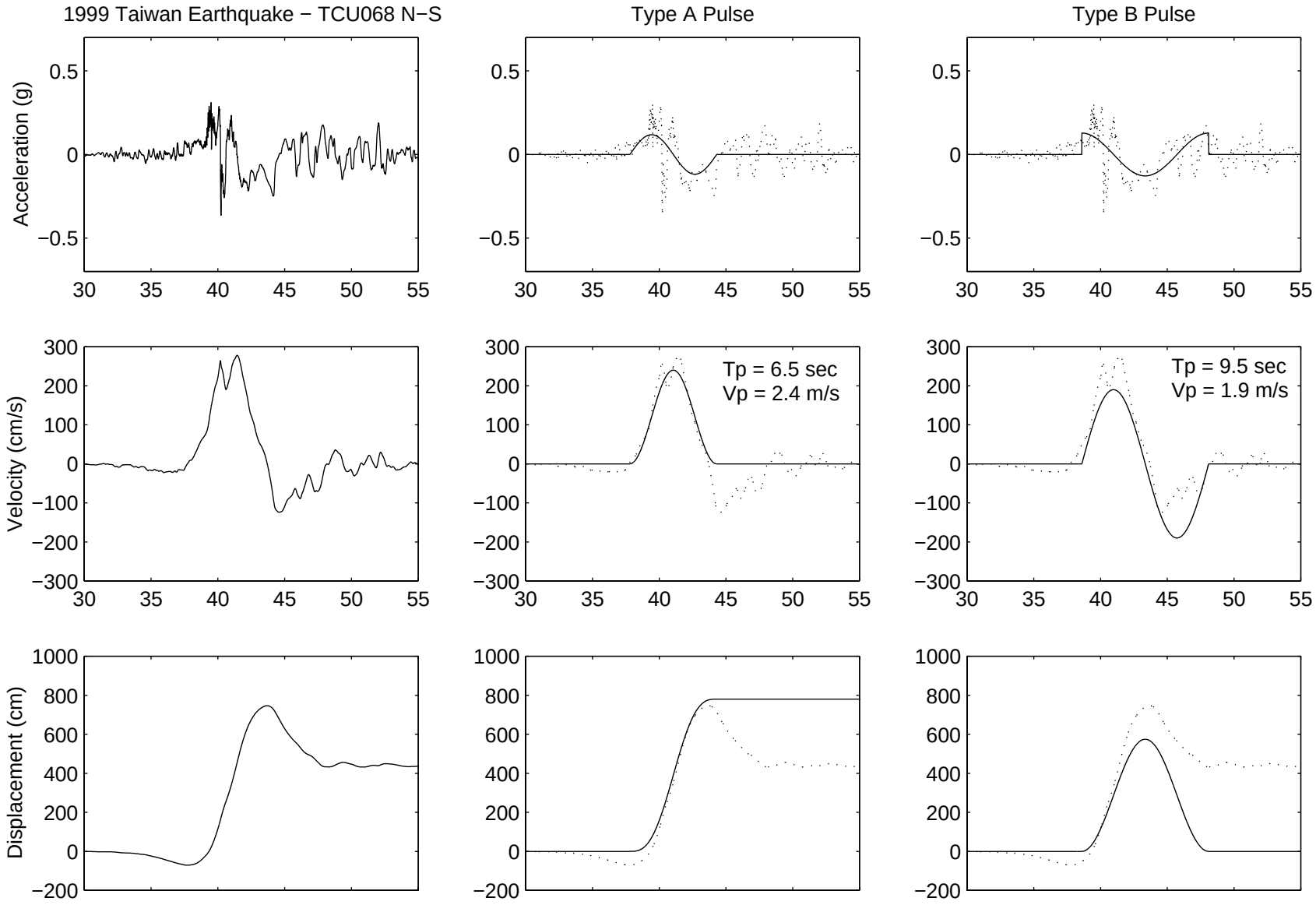

Figure 4.21. North-south components of the acceleration, velocity, and displacement time histories of the TCU068 N-S record from the September 20, 1999, Chi-Chi, Taiwan, earthquake (left), a cycloidal type *A* pulse (center) and a type *B* pulse (right).

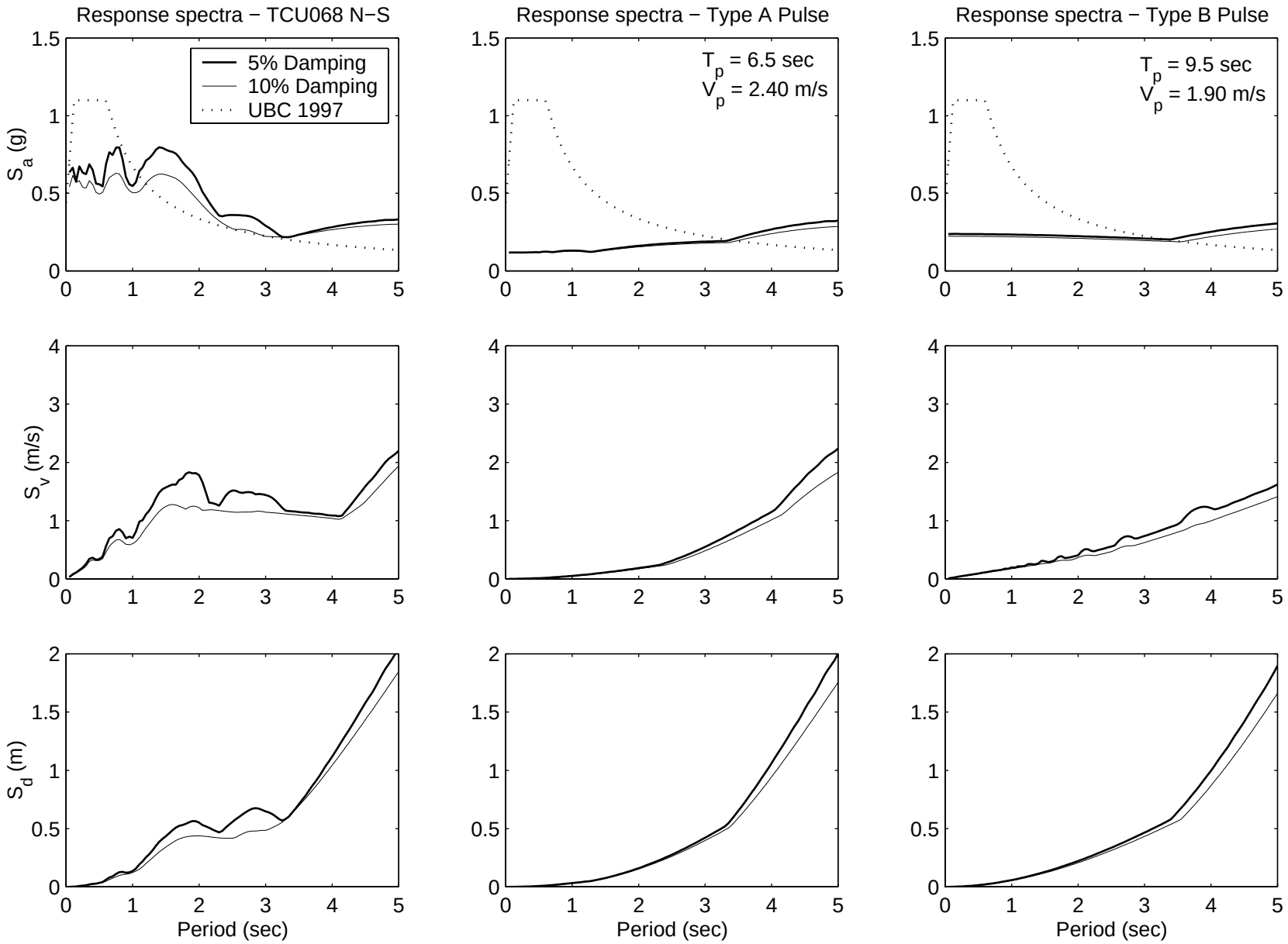

Figure 4.22. Acceleration, velocity, and displacement response spectra due to the TCU068 N-S record (left), and the associated cycloidal type *A* pulse (center) and a type *B* pulse (right).

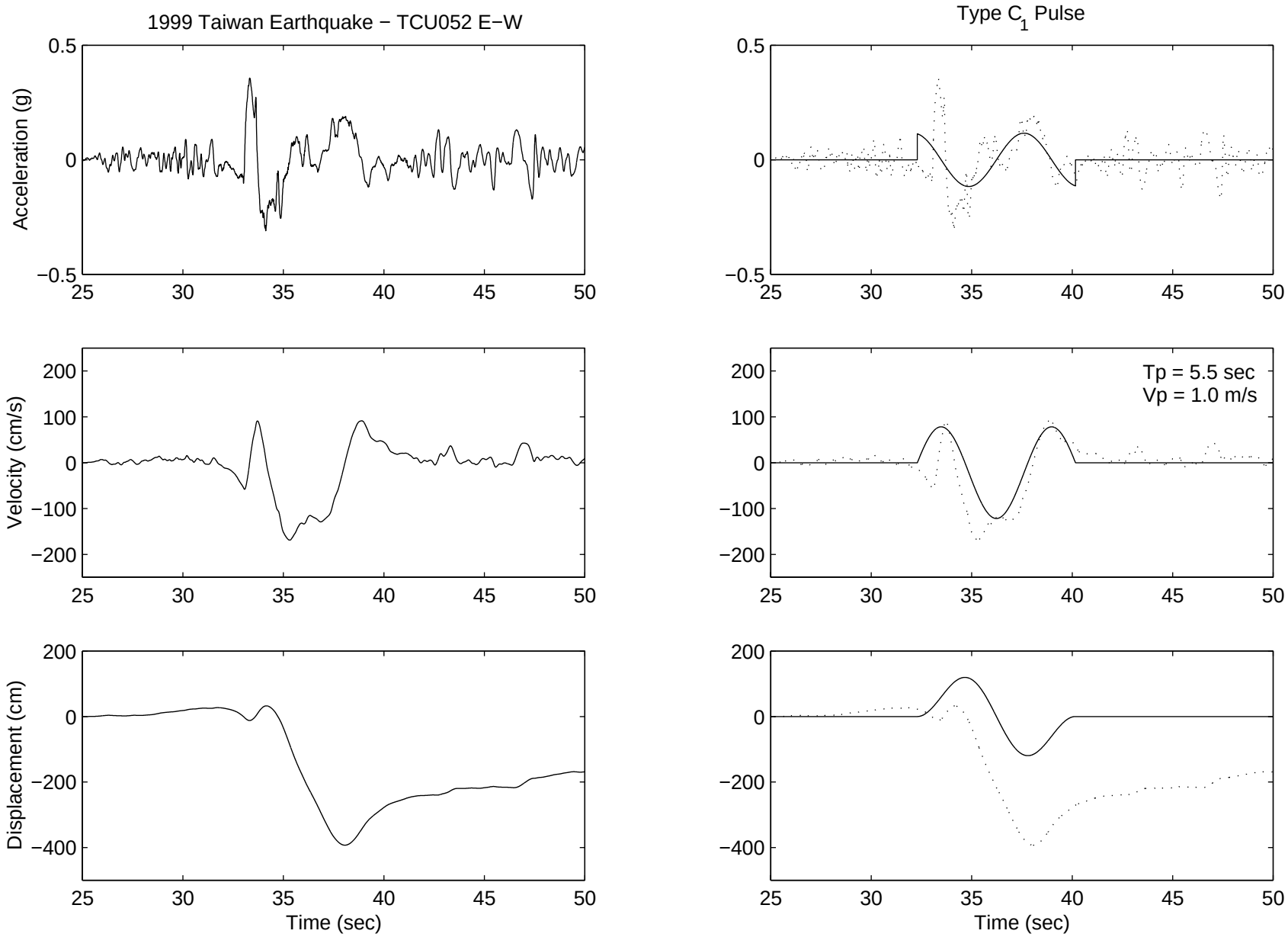

Figure 4.23. East-west components of the acceleration, velocity, and displacement time histories of the TCU052 E-W record from the September 20, 1999, Chi-Chi, Taiwan, earthquake (left), and a cycloidal type C_1 pulse (right).

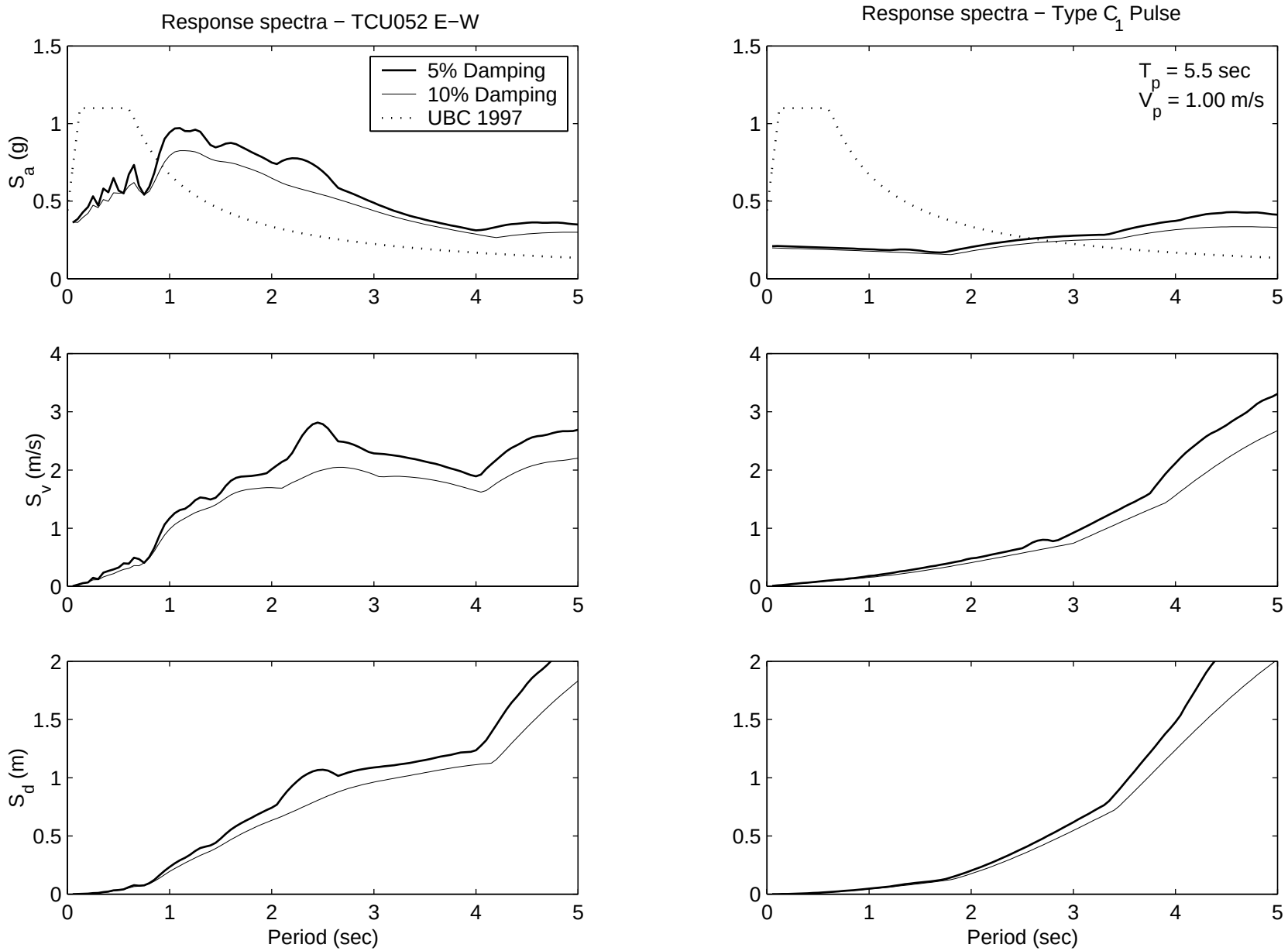

Figure 4.24. Acceleration, velocity, and displacement response spectra due to the TCU052 E-W record (left), and the associated cycloidal type C_1 pulse (right).

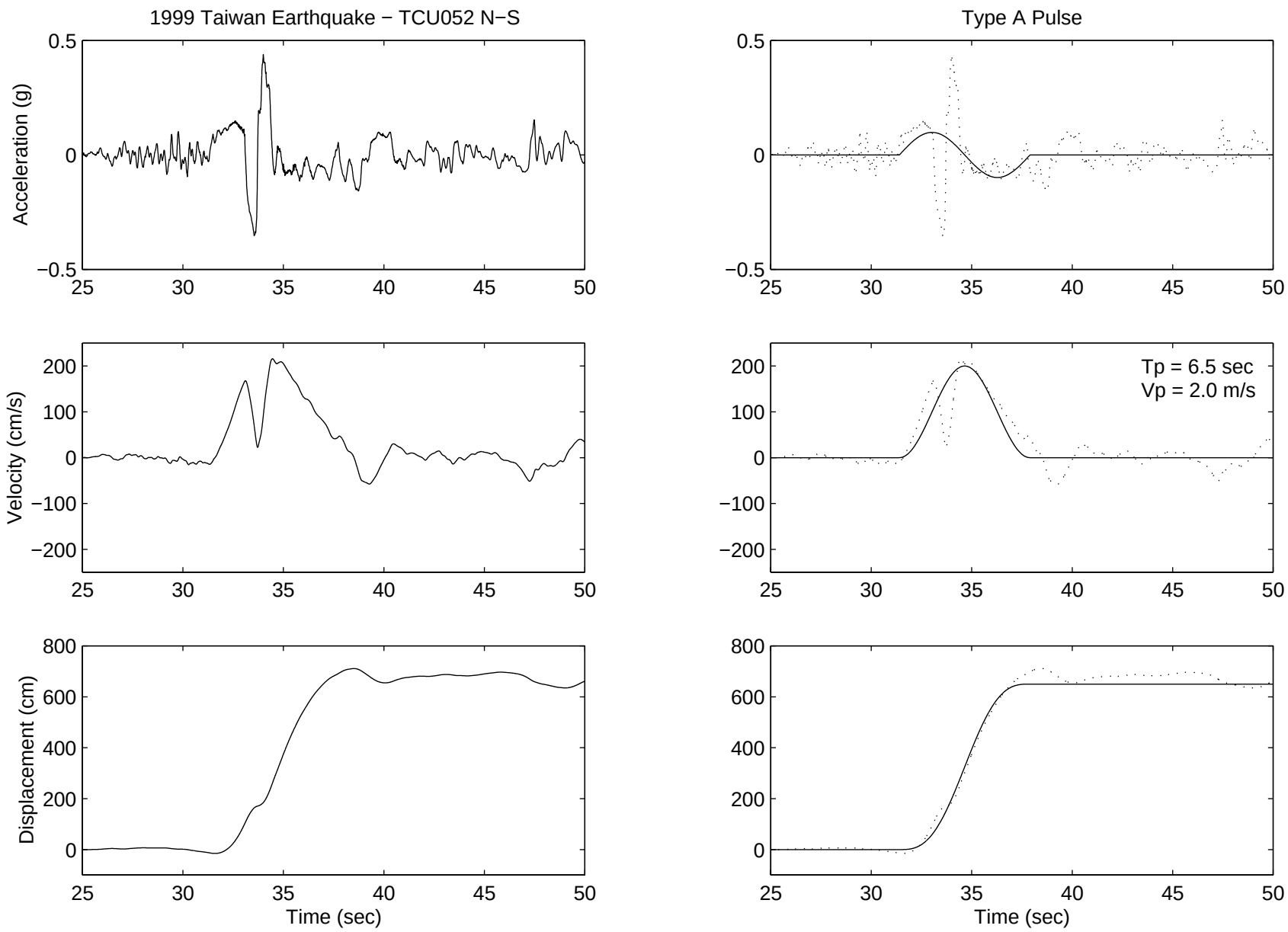

Figure 4.25. North-south components of the acceleration, velocity, and displacement time histories of the TCU052 N-S record from the September 20, 1999, Chi-Chi, Taiwan, earthquake (left), and a cycloidal type *A* pulse (right).

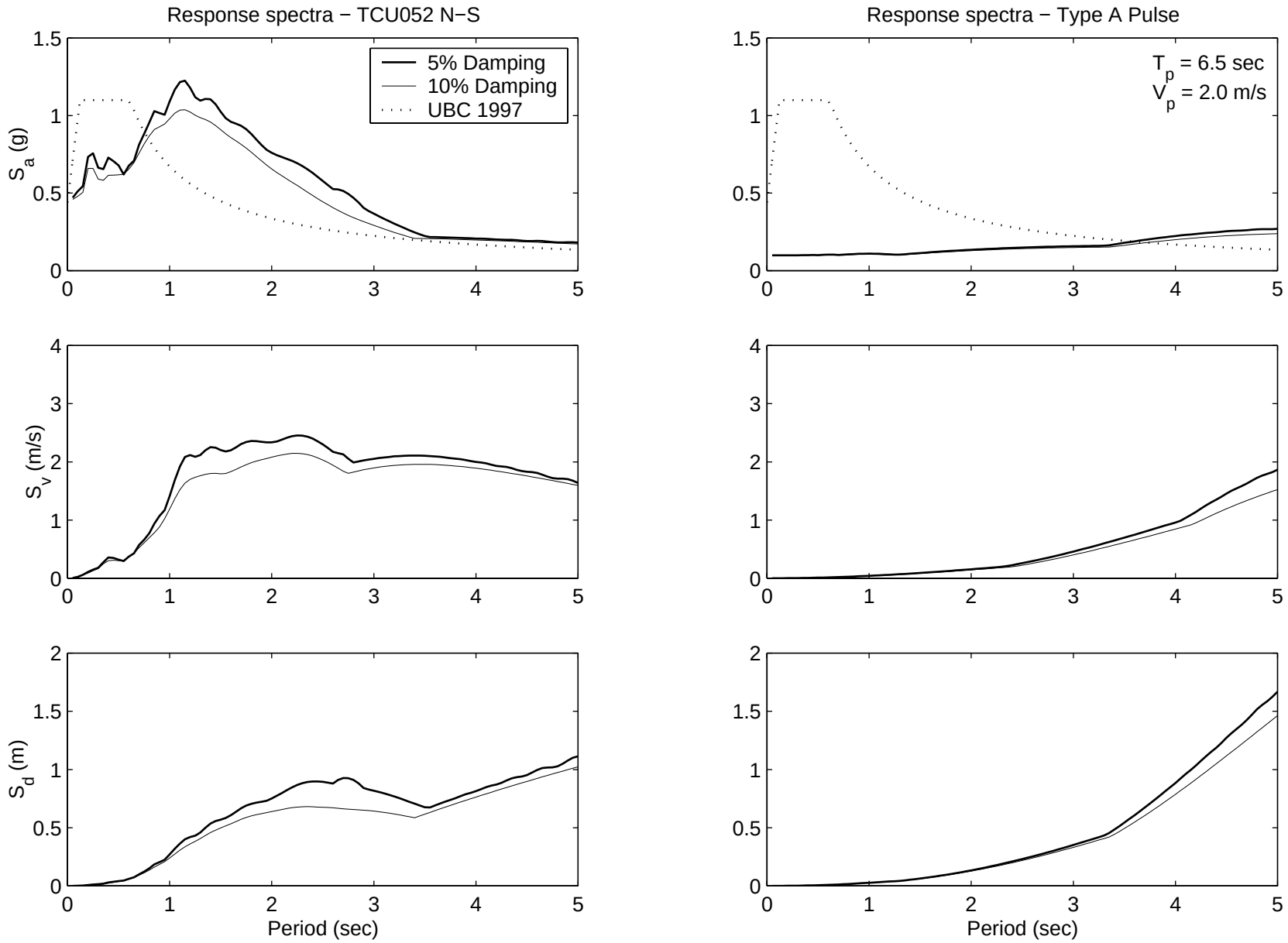

Figure 4.26. Acceleration, velocity, and displacement response spectra due to the TCU052 N-S record (left), and the associated cycloidal type *A* pulse (right).

5 Evaluation of Minimum Restrainer Strength

The presence of the foundation slab that extends on each side of the elevation view of the equipment increases the rocking stability of the structure, provided that the anchorages (restrainers) are strong enough to engage the foundation in rocking motion. Rocking of the equipment with the slab is desirable because (a) it is a less slender configuration than the equipment alone and (b) the maximum coefficient of restitution that will allow rocking motion after the first impact is significantly smaller than the maximum coefficient of restitution of the equipment alone. As an example, for the most slender configuration considered in this investigation (60 kip transformer, see Table 2) the maximum coefficient of restitution for which rocking of the equipment alone can happen is $\sqrt{r_{max}} = 0.803$; whereas the maximum coefficient of restitution for which rocking of the equipment with its base can happen is $\sqrt{r_{max}} = 0.577$. In view of these beneficial effects that result from the participation of the foundation base in the rocking motion, our study examines the minimum strength of the anchorages needed to engage the foundation base of the equipment in rocking motion. For the case where additional energy is lost due to local plastic deformations when the foundation base impacts the underlying soil, the coefficient of restitution is even smaller offering further stability.

Because of the many parameters involved, our study concentrates on the rocking response of two typical transformers used by PG&E. The geometrical and physical characteristics of the three equipment of interest are summarized in Table 2. Schematics of the two transformers are shown in Figure 5.1 to scale.

5.1 Rocking Response of Equipment Subjected to Pulse Motions

The foregoing discussion on the coherence of selected near-source ground motions indicated that some of their kinematic characteristics can be approximated with trigonometric pulses that are

Table 2: Geometrical and physical characteristics of two typical electrical transformers.

Equipment Weight (kips)	b (in)	h (in)	Fu (kips)	k (kips/in)	Slab dimension: length, width, thickness (in)	Slab Weight (kips)
60	35	90	26	500	114,114,10	16
60	35	90	27	920	114,114,10	16
60	35	90	47	1570	114,114,10	16
230	38	90	79	1500	234,150,12	50
230	38	90	80	2760	234,150,12	50
230	38	90	143	3200	234,150,12	50

uniquely defined by their type, pulse period, T_p, and velocity amplitude, V_p. Tables 3 through 5 present the acceleration and velocity levels of selected pulses (type *A*, type *B*, and type C_1 respectively) that are needed to overturn each of the two transformers of interest. The values listed under the column heading “Equipment on Foundation” are for the case when the restrainers are strong enough to engage the base in rocking motion, while those listed under “Equipment (anchored) on a Rigid Base” correspond to the values needed to overturn the transformers by failing their restrainers. The restrainer strengths, F_u/W, indicated in Tables 3 through 5 are high-end values used by PG&E; whereas, the columns with $F_u/W = 0$ correspond to freestandingfreestanding equipment.

Tables 3 through 5 indicate that, in general, the intensity of the trigonometric pulses needed to overturn the equipment exceeds by far the intensity of the pulses that approximate strong near-source ground motions. This is true not only for the case where the transformers are anchored to their base, but also for the case where they are free standing. As an example, consider the Rinaldi Station record shown in Figure 4.13. It can be approximated either with a type *A* or type *B* pulse with approximate duration $T_p \approx 1\,\text{sec}$. Table 3 indicates that the velocity amplitude of a 1 sec type A pulse that is needed to overturn the freestanding 60 kip transformer is $V_p = 2.19\,\text{m/sec}$, a value that exceeds the $1.5\,\text{m/sec}$ peak velocity of the Rinaldi Station record. As seen in Table 4, the velocity amplitude for a type *B* pulse, with duration $T_p = 1\,\text{sec}$, which is needed to overturn the

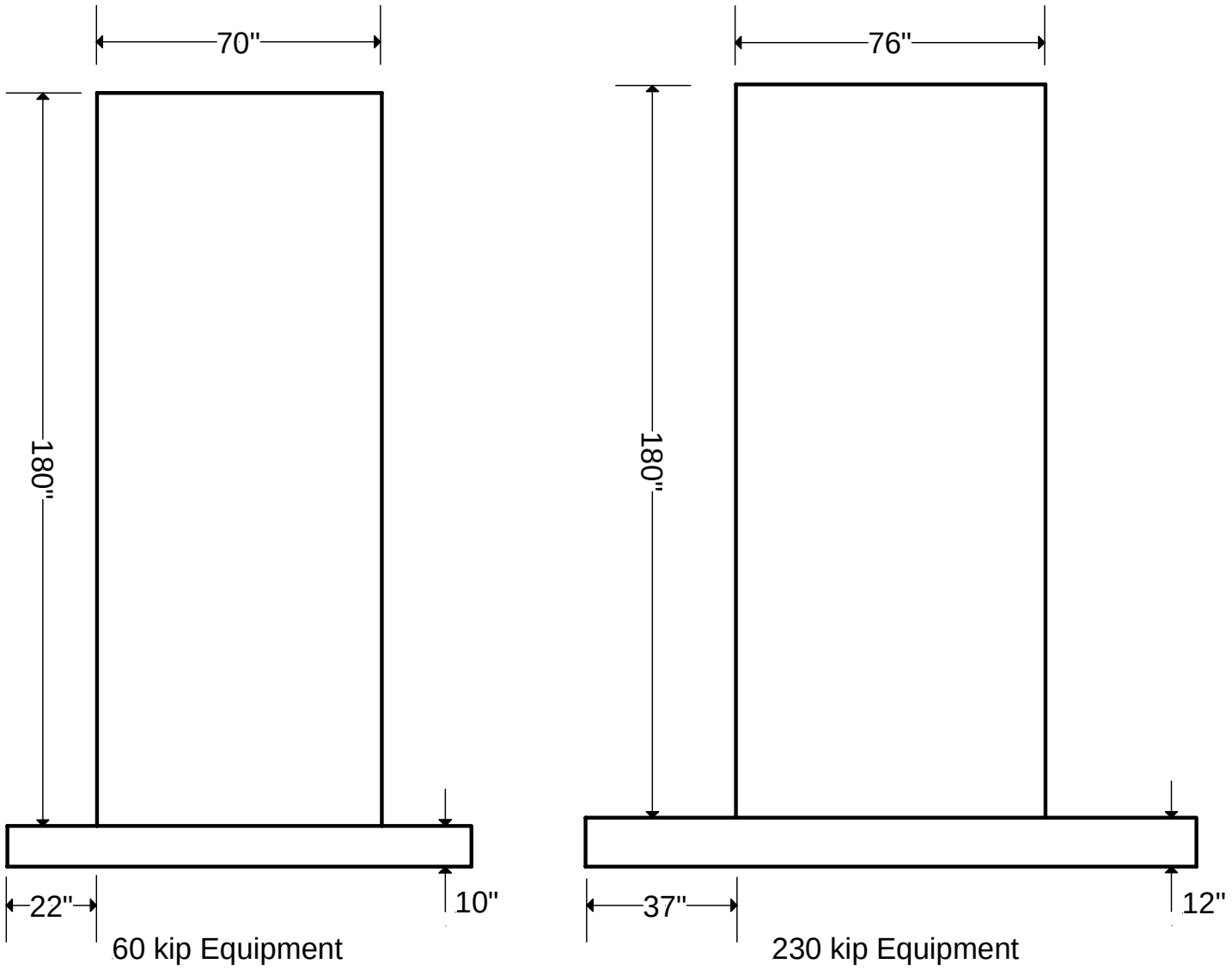

Figure 5.1. Schematic showing the 60 kip and 230 kip electrical equipment configurations to scale.

equipment is drastically larger (V_p = 9.34 m/sec). This high-velocity value is due to the inherent nonlinearity of the rocking problem.

Table 3: Overturning acceleration and velocity amplitudes of selected type *A* trigonometric pulses for the 60 kip and 230 kip equipment.

Equipment Weight		60 kip			230 kip		
		Equipment on Foundation	Equipment (anchored) on a Rigid Base		Equipment on Foundation	Equipment (anchored) on a Rigid Base	
Equipment Configuration		b = 35", h = 90" d = 22", s = 5" R = 108.35", R_o = 123.94" $\sqrt{r}$ = 0.577, p = 1.650 α = 0.554 rad = 31.75°	b = 35", h = 90" R = 96.57", R_o = 111.50" $\sqrt{r}$ = 0.803, p = 1.732 α = 0.371 rad = 21.25°		b = 38", h = 90" d = 37", s = 6" R = 117.80", R_o = 133.62" $\sqrt{r}$ = 0.370, p = 1.596 α = 0.690 rad = 39.55°	b = 38", h = 90" R = 97.68", R_o = 112.80" $\sqrt{r}$ = 0.773, p = 1.722 α = 0.400 rad = 22.89°	
Fu/W		Large Enough	0.00	0.78	Large Enough	0.00	0.62
Type A Tp = 1 sec	w_p/p	3.81	3.63	3.63	3.94	3.65	3.65
	$A_p/\alpha g$	5.85	1.89	2.83	6.77	2.06	2.53
	A_p (g)	3.24	0.70	1.05	4.67	0.82	1.01
	V_p (m/s)	10.12	2.19	3.28	14.58	2.56	3.15
Type A Tp = 2 sec	w_p/p	1.90	1.81	1.81	1.97	1.82	1.82
	$A_p/\alpha g$	1.41	1.29	2.75	1.65	1.30	2.46
	A_p (g)	0.78	0.48	1.02	1.14	0.52	0.98
	V_p (m/s)	4.87	3.00	6.37	7.12	3.25	6.12
Type A Tp = 3 sec	w_p/p	1.27	1.21	1.21	1.31	1.22	1.22
	$A_p/\alpha g$	1.32	1.21	2.75	1.45	1.23	2.43
	A_p (g)	0.73	0.45	1.02	1.00	0.49	0.97
	V_p (m/s)	6.84	4.22	9.56	9.37	4.59	9.09
Type A Tp = 4 sec	w_p/p	0.76	0.73	0.73	0.79	0.73	0.73
	$A_p/\alpha g$	1.28	1.19	2.72	1.39	1.20	2.41
	A_p (g)	0.71	0.44	1.01	0.96	0.48	0.96
	V_p (m/s)	8.87	5.50	12.62	11.99	6.00	11.99
Type A Tp = 5 sec	w_p/p	0.76	0.73	0.73	0.79	0.73	0.73
	$A_p/\alpha g$	1.26	1.19	2.72	1.36	1.18	2.41
	A_p (g)	0.70	0.44	1.01	0.94	0.47	0.96
	V_p (m/s)	10.93	6.87	15.77	14.68	7.34	14.99
Type A Tp = 6 sec	w_p/p	0.63	0.60	0.60	0.66	0.61	0.61
	$A_p/\alpha g$	1.23	1.16	2.72	1.33	1.15	2.41
	A_p (g)	0.68	0.43	1.01	0.92	0.46	0.96
	V_p (m/s)	12.74	8.06	18.92	17.24	8.62	17.99

Aspects of the nonlinear nature of the overturning problem are shown in Figure 5.2 which plots the overturning spectra for the 60 kip equipment due to a type *B* pulse. It is seen in Figure 5.2 that when the ratio ω_p/p is small the problem of overturning is multi-valued. The lower values of accelerations capable of toppling the transformer induce rocking motion with impact, whereas, the higher acceleration values induce rocking and eventually toppling without impact. This dual pattern of overturning vanishes when ω_p/p is beyond a threshold value where overturning happens without impact; this requires significantly larger accelerations.

Table 4: Overturning acceleration and velocity amplitudes of selected type *B* trigonometric pulses for the 60 kip and 230 kip equipment.

Equipment Weight		60 kip			230 kip		
		Equipment on Foundation	Equipment (anchored) on a Rigid Base		Equipment on Foundation	Equipment (anchored) on a Rigid Base	
Equipment Configuration		b = 35", h = 90" d = 22", s = 5" R = 108.35", R_o = 123.94" √r = 0.577, p = 1.650 α = 0.554 rad = 31.75°	b = 35", h = 90" R = 96.57", R_o = 111.50" √r = 0.803, p = 1.732 α = 0.371 rad = 21.25°		b = 38", h = 90" d = 37", s = 6" R = 117.80", R_o = 133.62" √r = 0.370, p = 1.596 α = 0.690 rad = 39.55°	b = 38", h = 90" R = 97.68", R_o = 112.80" √r = 0.773, p = 1.722 α = 0.400 rad = 22.89°	
Fu/W		Large Enough	0.00	0.78	Large Enough	0.00	0.62
Type B Tp = 1 sec	w_p/p	3.81	3.63	3.63	3.94	3.65	3.65
	$A_p/\alpha g$	18.19	16.15	2.99	20.48	16.37	16.62
	A_p (g)	10.08	5.99	1.11	14.13	6.53	6.63
	V_p (m/s)	15.74	9.35	1.73	22.06	10.20	10.35
Type B Tp = 2 sec	w_p/p	1.90	1.81	1.81	1.97	1.82	1.82
	$A_p/\alpha g$	1.66	1.46	2.56	2.20	1.48	2.31
	A_p (g)	0.92	0.54	0.95	1.52	0.59	0.92
	V_p (m/s)	2.87	1.69	2.97	4.75	1.84	2.87
Type B Tp = 3 sec	w_p/p	1.27	1.21	1.21	1.31	1.22	1.22
	$A_p/\alpha g$	1.46	1.21	2.53	1.61	1.25	2.28
	A_p (g)	0.81	0.45	0.94	1.11	0.50	0.91
	V_p (m/s)	3.79	2.11	4.40	5.20	2.34	4.26
Type B Tp = 4 sec	w_p/p	0.96	0.91	0.91	0.98	0.91	0.91
	$A_p/\alpha g$	1.32	1.21	2.53	1.52	1.23	2.26
	A_p (g)	0.73	0.45	0.94	1.05	0.49	0.90
	V_p (m/s)	4.56	2.81	5.87	6.56	3.06	5.62
Type B Tp = 5 sec	w_p/p	0.76	0.73	0.73	0.79	0.73	0.73
	$A_p/\alpha g$	1.28	1.19	2.53	1.48	1.20	2.26
	A_p (g)	0.71	0.44	0.94	1.02	0.48	0.90
	V_p (m/s)	5.54	3.43	7.34	7.96	3.75	7.03
Type B Tp = 6 sec	w_p/p	0.63	0.60	0.60	0.66	0.61	0.61
	$A_p/\alpha g$	1.25	1.16	2.53	1.35	1.18	2.26
	A_p (g)	0.69	0.43	0.94	0.93	0.47	0.90
	V_p (m/s)	6.46	4.03	8.81	8.71	4.40	8.43

The 60 kip transformer has a frequency parameter, $p = 1.73$ rad/sec and with a pulse duration $T_p = 1$ sec, ($\omega_p = 6.28$ rad/sec) the resulting dimensionless frequency parameter $\omega_p/p = 3.628$. It so happens that for a type *B* pulse with $\omega_p/p = 3.628$, the freestanding 60 kip transformer marginally escapes the multi-valued region of the graph and can only overturn without impact. To achieve this with a one-second duration type *B* pulse one needs $5.98g$ of acceleration amplitude. Interestingly, when the block is anchored the multi-valued region extends into higher values of ω_p/p and in this case the transformer overturns with impact. This explains the substantially lower acceleration amplitude, $A_p = 1.08g$, that is needed to overturn the anchored ($F_u/W = 0.78$) 60 kip trans-

Table 5: Overturning acceleration and velocity amplitudes of selected type C_1 trigonometric pulses for the 60 kip and 230 kip equipment.

Equipment Weight		60 kip			230 kip		
		Equipment on Foundation	Equipment (anchored) on a Rigid Base		Equipment on Foundation	Equipment (anchored) on a Rigid Base	
Equipment Configuration		b = 35", h = 90" d = 22", s = 5" R = 108.35", Ro = 123.94" √r = 0.577, p = 1.650 α = 0.554 rad = 31.75°	b = 35", h = 90" R = 96.57", Ro = 111.50" √r = 0.803, p = 1.732 α = 0.371 rad = 21.25°		b = 38", h = 90" d = 37", s = 6" R = 117.80", Ro = 133.62" √r = 0.370, p = 1.596 α = 0.690 rad = 39.55°	b = 38", h = 90" R = 97.68", Ro = 112.80" √r = 0.773, p = 1.722 α = 0.400 rad = 22.89°	
Fu/W		Large Enough	0.00	0.78	Large Enough	0.00	0.62
Type C1 Tp = 1 sec	wp/p	3.81	3.63	3.63	3.94	3.65	3.65
	Ap/αg	8.48	2.67	2.96	28.13	2.83	2.88
	Ap (g)	4.70	0.99	1.10	19.41	1.13	1.15
	Vp (m/s)	14.68	3.09	3.43	60.61	3.53	3.59
Type C1 Tp = 2 sec	wp/p	1.90	1.81	1.81	1.97	1.82	1.82
	Ap/αg	1.77	1.56	2.72	2.06	1.58	2.46
	Ap (g)	0.98	0.58	1.01	1.42	0.63	0.98
	Vp (m/s)	6.12	3.62	6.31	8.87	3.93	6.12
Type C1 Tp = 3 sec	wp/p	1.27	1.21	1.21	1.31	1.22	1.22
	Ap/αg	1.57	1.32	2.64	1.74	1.30	2.41
	Ap (g)	0.87	0.49	0.98	1.20	0.52	0.96
	Vp (m/s)	8.15	4.59	9.18	11.24	4.87	8.99
Type C1 Tp = 4 sec	wp/p	0.95	0.91	0.91	0.98	0.91	0.91
	Ap/αg	1.48	1.21	2.64	1.64	1.23	2.38
	Ap (g)	0.82	0.45	0.98	1.13	0.49	0.95
	Vp (m/s)	10.24	5.62	12.24	14.11	6.12	11.87
Type C1 Tp = 5 sec	wp/p	0.76	0.73	0.73	0.79	0.73	0.73
	Ap/αg	1.39	1.19	2.64	1.51	1.20	2.36
	Ap (g)	0.77	0.44	0.98	1.04	0.48	0.94
	Vp (m/s)	12.02	6.87	15.30	16.24	7.49	14.68
Type C1 Tp = 6 sec	wp/p	0.63	0.60	0.60	0.66	0.61	0.61
	Ap/αg	1.25	1.16	2.61	1.36	1.18	2.33
	Ap (g)	0.69	0.43	0.97	0.94	0.47	0.93
	Vp (m/s)	12.93	8.06	18.17	17.61	8.81	17.42

former. The multi-valued nature of overturning problem is further apparent in Figure 5.3 that plots overturning spectra due to the type C_1 pulse.

Our results for the rocking stability of the 60 kip and 230 kip equipment under pulse motions are summarized in Figures 5.4 and 5.5. Figure 5.4 shows that the protrusion of the foundation base increases the rocking stability of the equipment assuming that the restrainers are strong enough to engage the foundation plate in rocking motion. Figure 5.4 also shows that anchorages with $F_u/W = 0.78$ are capable in most cases of sustaining accelerations higher than those needed to overturn the equipment with its foundation base as designed by PG&E. The restrainers exhibit less capacity under shorter duration pulses (say $T_p \le 2\,\text{sec}$) for all three pulse types. Similar pat-

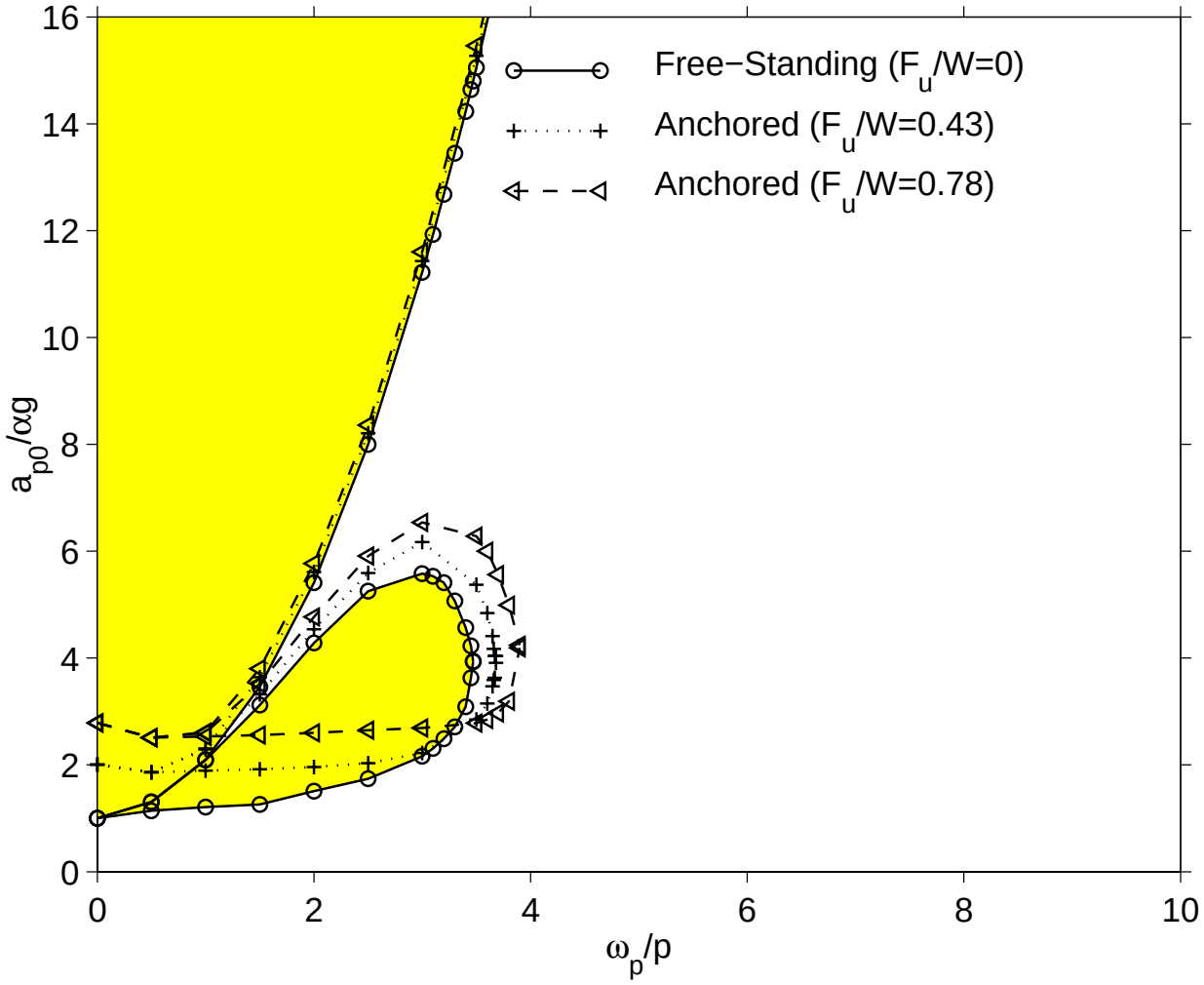

Figure 5.2. Overturning acceleration spectra of the anchored 60 kip equipment due to a one-cosine pulse ($\alpha = 0.371 rad = 21.25°$, $p = 1.732$, $\eta = \sqrt{r} = 0.803$ and $\mu = 5$) with restrainer strength $F_u/W = 0$, 0.43 and 0.78.

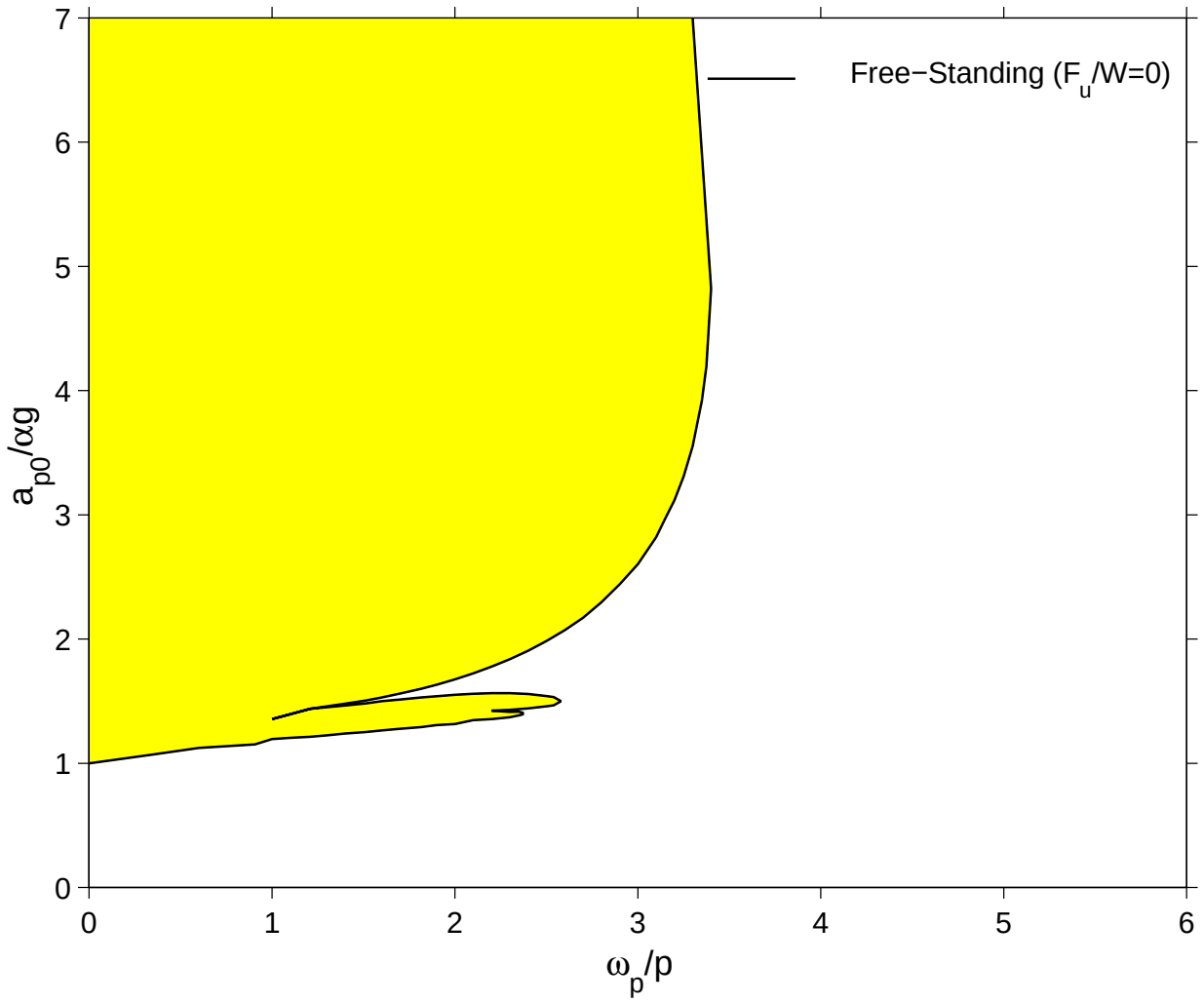

Figure 5.3. Overturning acceleration spectra of the freestanding 60 kip equipment due to a type C_1 cycloidal pulse ($\alpha = 0.371 rad = 21.25°$, $p = 1.732$, $\eta = \sqrt{r} = 0.803$).

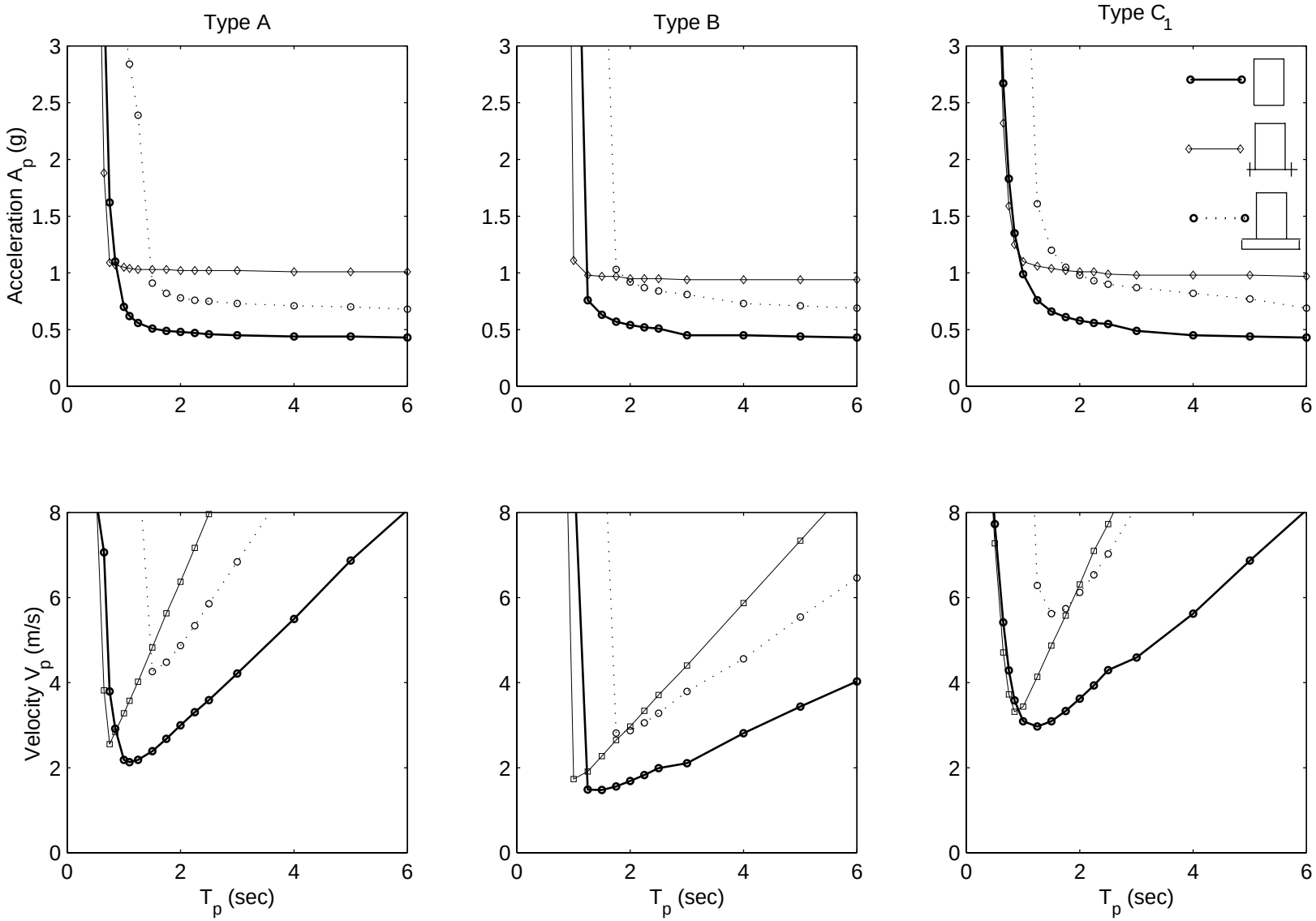

Figure 5.4. Acceleration and velocity amplitudes of types *A*, *B*, and C_1 pulses needed to overturn the 60 kip transformer. Thick line: Free standing ($\alpha = 0.371 rad = 21.25°$, $p = 1.732$, $\eta = \sqrt{r} = 0.803$). Thin line: Anchored ($F_u/W = 0.78$, $\mu = 5$). Dotted line: With foundation base ($\alpha = 0.55 rad = 31.18°$, $\eta = \sqrt{r} = 0.58$, $d/b = 0.66$).

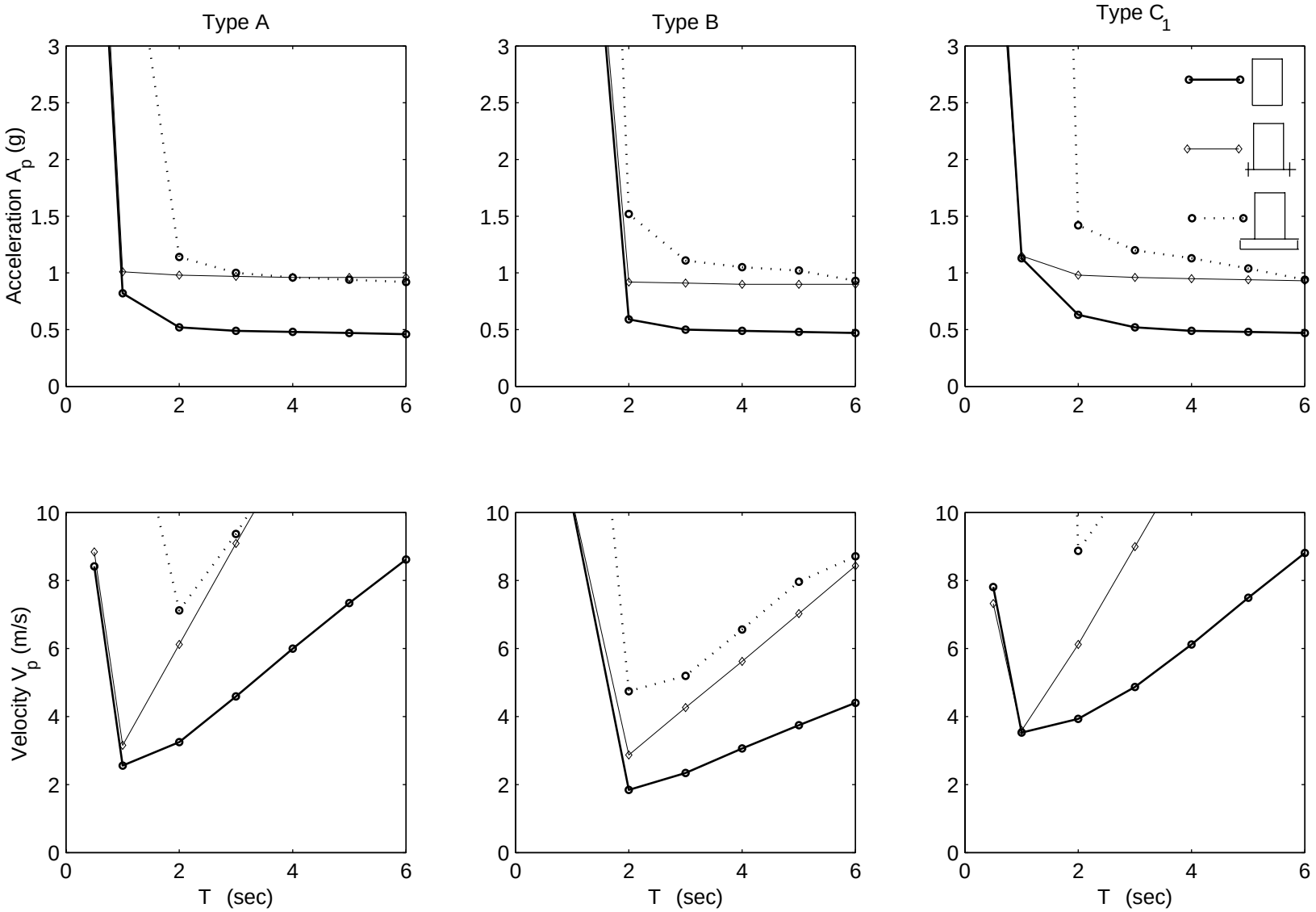

Figure 5.5. Acceleration and velocity amplitudes of types *A*, *B*, and C_1 pulses needed to overturn the 230 kip transformer. Thick line: Free standing ($\alpha = 0.4rad = 22.89°$, $p = 1.722$, $\eta = \sqrt{r} = 0.773$). Thin line: Anchored ($F_u/W = 0.62$, $\mu = 5$). Dotted line: With foundation base ($\alpha = 0.69rad = 39.53°$, $\eta = \sqrt{r} = 0.37$, $d/b = 0.97$).

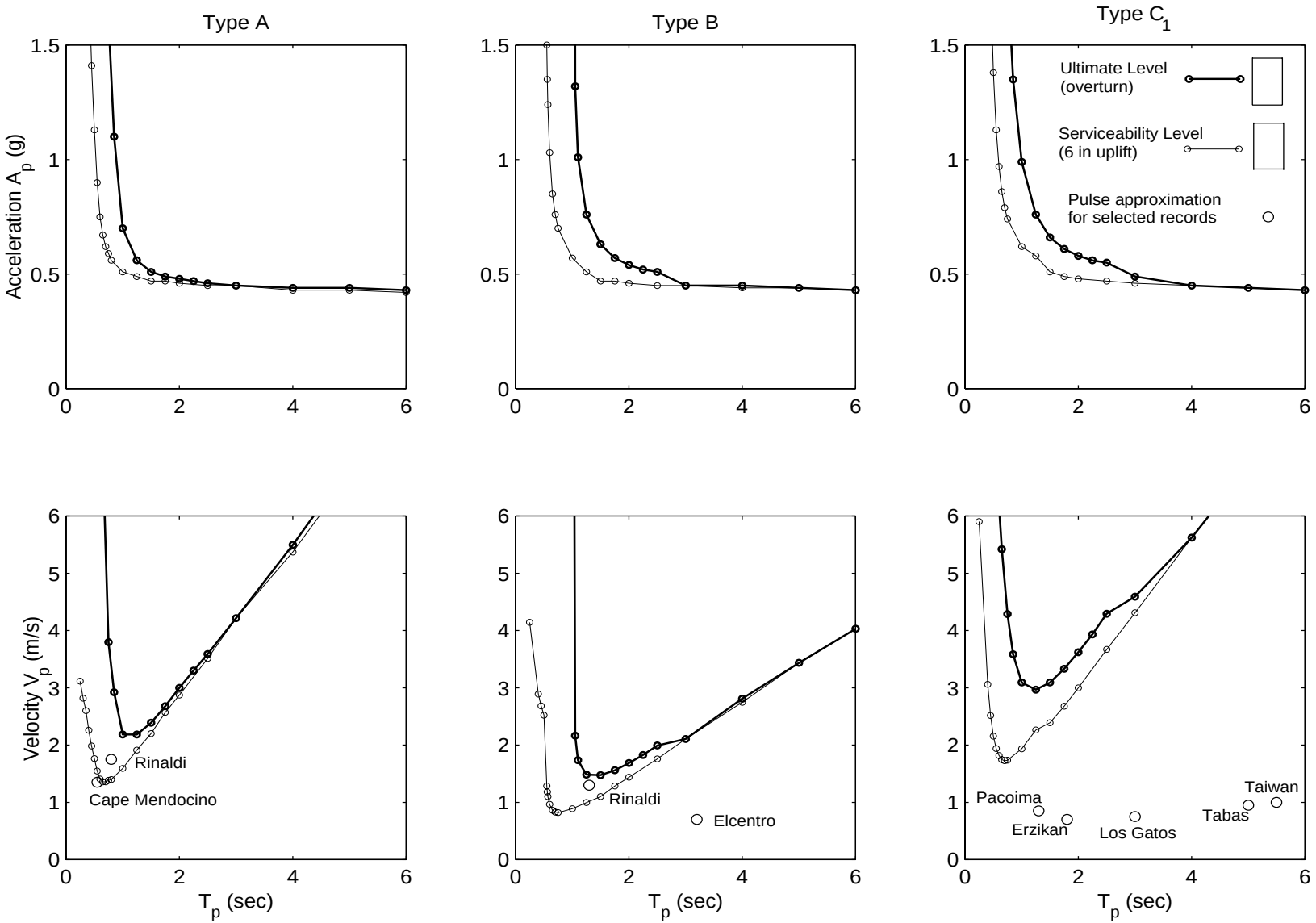

Figure 5.6. Acceleration and velocity amplitudes of types *A*, *B*, and C_1 pulses needed to uplift the 60 kip transformer by 6 in. (thin line), and overturn the 60 kip transformer (thick line). The circles show the velocity amplitude of the trigonometric approximations of selected records.

terns are observed in Figure 5.5 that shows spectra of overturning accelerations and velocities of types *A*, *B*, and C_1 pulses for the 230 kip transformer. In this case the anchorages with $F_u/W = 0.62$ exhibit less capacity than the base-supported equipment for pulses as long as $T_p \approx 3\,\text{sec}$. What is important to note in Figures 5.4 to 5.6 is that the longer the pulse duration, the smaller is the acceleration amplitude needed to create overturning. Accordingly, a static calculation will result in the lowest acceleration amplitude needed to create overturning — an over-conservative calculation.

Our investigation proceeds with the rocking response analysis of freestanding and anchored equipment. In addition to overturning (failure) the investigation is concerned with levels of uplift that exceed the serviceability level. Although different electrical equipment configurations might be able to tolerate various levels of uplift and remain operational, in this study, a global upper bound of the serviceability level has been established from experience as an uplift of 6 in. (Fujisaki 2001). The thin line in Figure 5.6 plots the acceleration and velocity amplitudes of types *A*, *B*, and C_1 pulses that are needed to uplift the 60 kip transformer by 6 in. As the duration of the excitation pulse increases, these values converge rapidly to the acceleration and velocity amplitudes needed to overturn the transformer. Figure 5.6 indicates that as the duration of the pulse increases, the margin between serviceability levels and overturning (failure) is minimal and eventually vanishes. In addition, Figure 5.6 indicates the velocity amplitude of the trigonometric approximations of the ground motions considered in this study. We see that the pulse approximation of the Rinaldi record is the only one which has a velocity in excess of that needed to uplift the 60 kip transformer by 6 in. With reference to Table 1, we see that the Rinaldi record is indeed the only record that exhibits a distinguishable pulse which is capable of producing an uplift of 6 in. The Takatori records are also capable of uplifting the equipment by 6 in. but do not have identifiable pulses and thus are not represented in Figure 5.6. The velocity amplitudes of type C_1 pulses needed to exceed the serviceability limit are several multiples higher than the amplitudes of the C_1 pulse approximations of the indicated records. These levels are substantially larger than the percentage that one has to amplify the actual record to create an uplift of 6 in. This difference is likely due to the presence of acceleration spikes which when added to the underlying pulses result in motions which are capable of causing the 6 in. uplift.

5.2 Rocking Response of Equipment Subjected to Recorded Motions

Next, the rocking response analysis of freestanding and anchored equipment subjected to the selected earthquake records listed in Table 1 is examined. The records listed in Table 1 are primarily near fault records which have been chosen in part due to the proximity of electrical substations to active faults. These records were also chosen as near fault records often contain large duration pulses for which a relatively low acceleration is needed to induce uplifting and eventual overturning. Figures 5.7 to 5.22 plot time histories of the rotation, θ, the angular velocity, $\dot{\theta}$ and the reaction force, $N(t)$, at the pivot point. Our analysis distinguishes between intensity levels of the ground shaking that will affect serviceability; and intensity levels of the ground shaking that will result in overturning. The serviceability level has been established from experience as an uplift of 6 inches.

The left column of Figure 5.7 plots the response of the 60 kip transformer subjected to 100% of the Pacoima Dam record. The thick line shows the response of the freestanding equipment; whereas, the thin line plots the rocking response of the equipment supported on its foundation base. The freestanding equipment (no base) exhibits some uplifting with its peak value reaching approximately 3 in., whereas, the equipment with its base does not visually uplift, although, there is some fluctuation of the vertical reaction. The dotted horizontal lines in the rotation plots show the rotations that correspond to a 6 in. uplift of the freestanding block ($\theta = (6in)/(2b)$), and to a 6 in. uplift of the block-foundation system ($\theta = (6in)/(2b + 2d)$). The second column of Figure 5.7 plots the response of the 60 kip transformer subjected to 123% of the Pacoima Dam record — that is the level needed for the freestanding equipment to reach an uplift of approximately 6 in. Under the 123% level the block-foundation system exhibits more noticeable rotations, than under the 100% level; yet they are below the $(6in)/(2b + 2d)$ serviceability limit. The third column of Figure 5.7 compares the response of the freestanding block with the response of the same block when it is anchored with restrainers that have the low level strength ($F_u/W = 0.43$) used by PG&E. Interestingly, the 123% level of the Pacoima Dam record is capable of fracturing the restrainers which have been modeled as elasto-plastic element with a ductility $\mu = 5$. Nevertheless, the presence of the restrainers suppress the response which exhibits rotations well below the serviceability limit. When comparing the response of the block-foundation system shown in the second column and

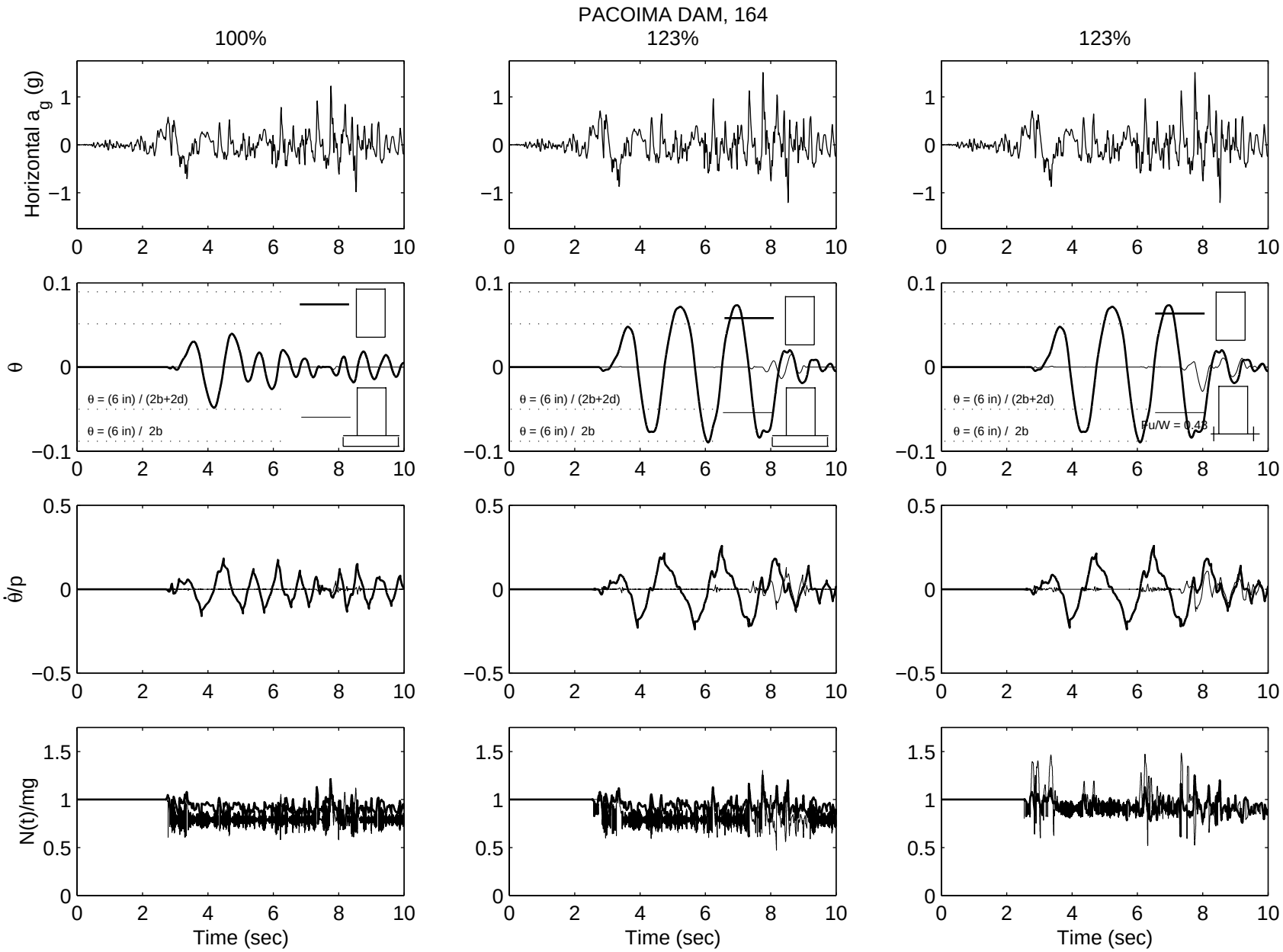

Figure 5.7. Rocking response of the 60 kip equipment to the 1971 San Fernando earthquake — Pacoima Dam at the serviceability level.

the response of the anchored block ($F_u/W = 0.43$) shown in the right column one concludes that under the 123% level of the Pacoima Dam record, the two systems have about the same capacity. The bottom plots of Figure 5.7. show vertical reactions at the pivot points. When the ductile restrainers fracture, the angular accelerations of the equipment is nearly zero and the vertical reaction is $N = mg + F_u$. The bottom right plot shows that when the restrainers with $F_u/W = 0.43$ fractures, the vertical reaction is $N = 1.48W$ which is the expected result.

Figure 5.8 examines the response of the 60 kip transformer on the verge of overturning. When the level of excitation is 285% of the recorded motion, both the freestanding block and the block-foundation system escape overturning, however the anchored block with $F_u/W = 0.43$ topples (see second column). This is an interesting example where the anchored 60 kip transformer can sustain less acceleration than the freestanding equipment. This behavior can be predicted with the results shown in Figure 5.4 that have been derived from trigonometric pulses. With reference to Figure 4.1, the Pacoima Dam record can be approximated with a type C_1 pulse with $T_p = 1.3$ sec and $V_p = 0.85$ m/sec. The last column of Figure 5.4 indicates that whereas the anchored 60 kip transformer can sustain a higher acceleration than the transformer with its base for most of the pulse-period range; at the low pulse period range the situation is reversed. As a result when $T_p = 1.3$ sec Figure 5.4 indicates that the 60 kip transformer can sustain less acceleration than the base-supported equipment. The right column of Figure 5.8 indicates that a slight increase in the acceleration level (286%) topples the freestanding block but also the anchored block with $F_u/W = 0.78$. Although 285% of the Pacoima Dam record is an unrealistically high excitation this analysis shows that for the specific frequency content, the overturning capacity of the 60 kip transformer is governed by its restrainers.

Figure 5.9 plots the rocking response of the 60 kip transformer subjected to the Los Gatos record. The 100% level of the record induces an uplift of the free standing equipment to the order of 3 inches; whereas, when it is fixed to the base, the motion the equipment/foundation system is negligible when the base is engaged in the motion. The second column of Figure 5.9 plots the response of the 60 kip transformer subjected to 105% of the Los Gatos record — that is the level

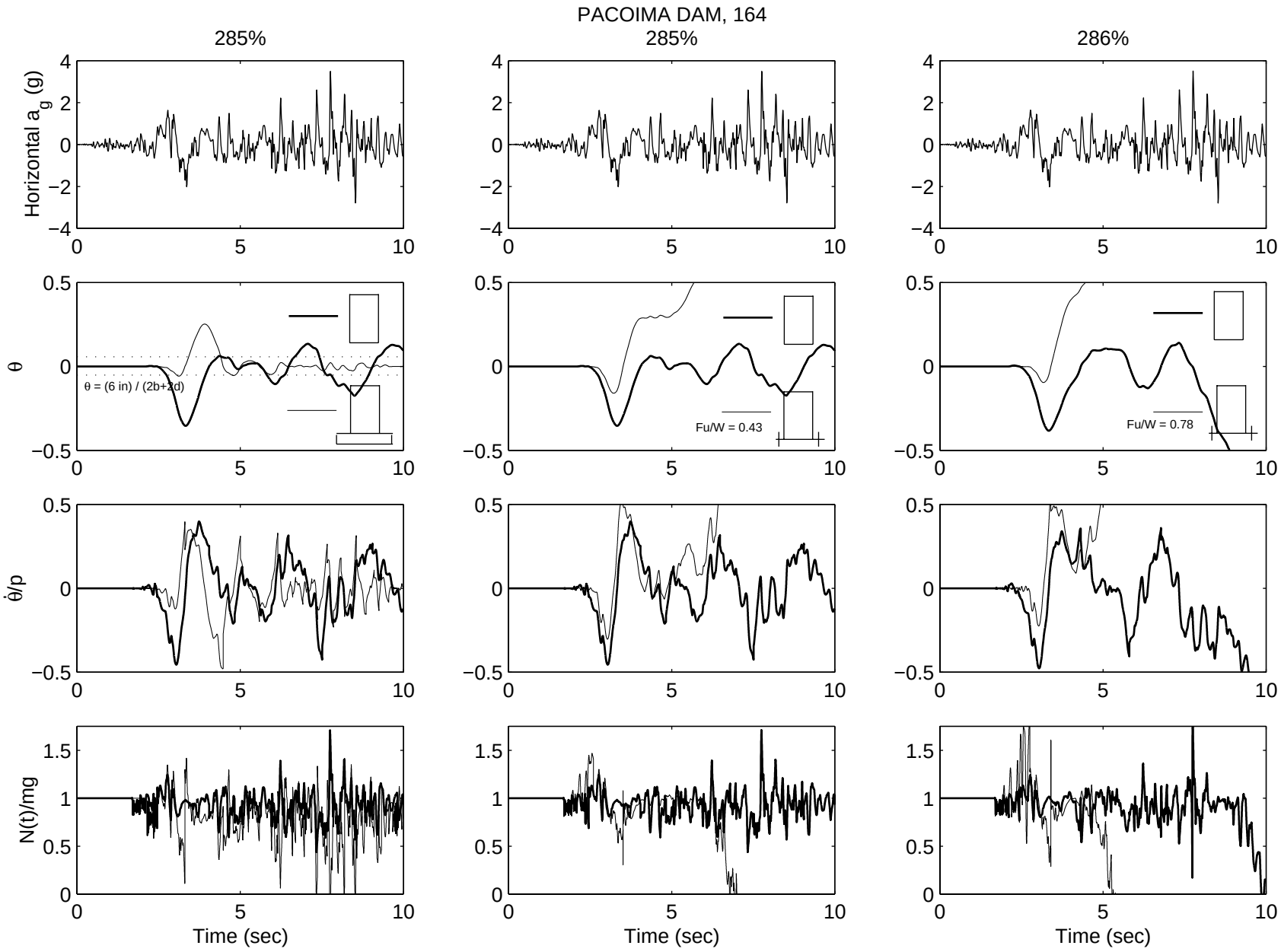

Figure 5.8. Rocking response of the 60 kip equipment to the 1971 San Fernando earthquake — Pacoima Dam record at ultimate state.

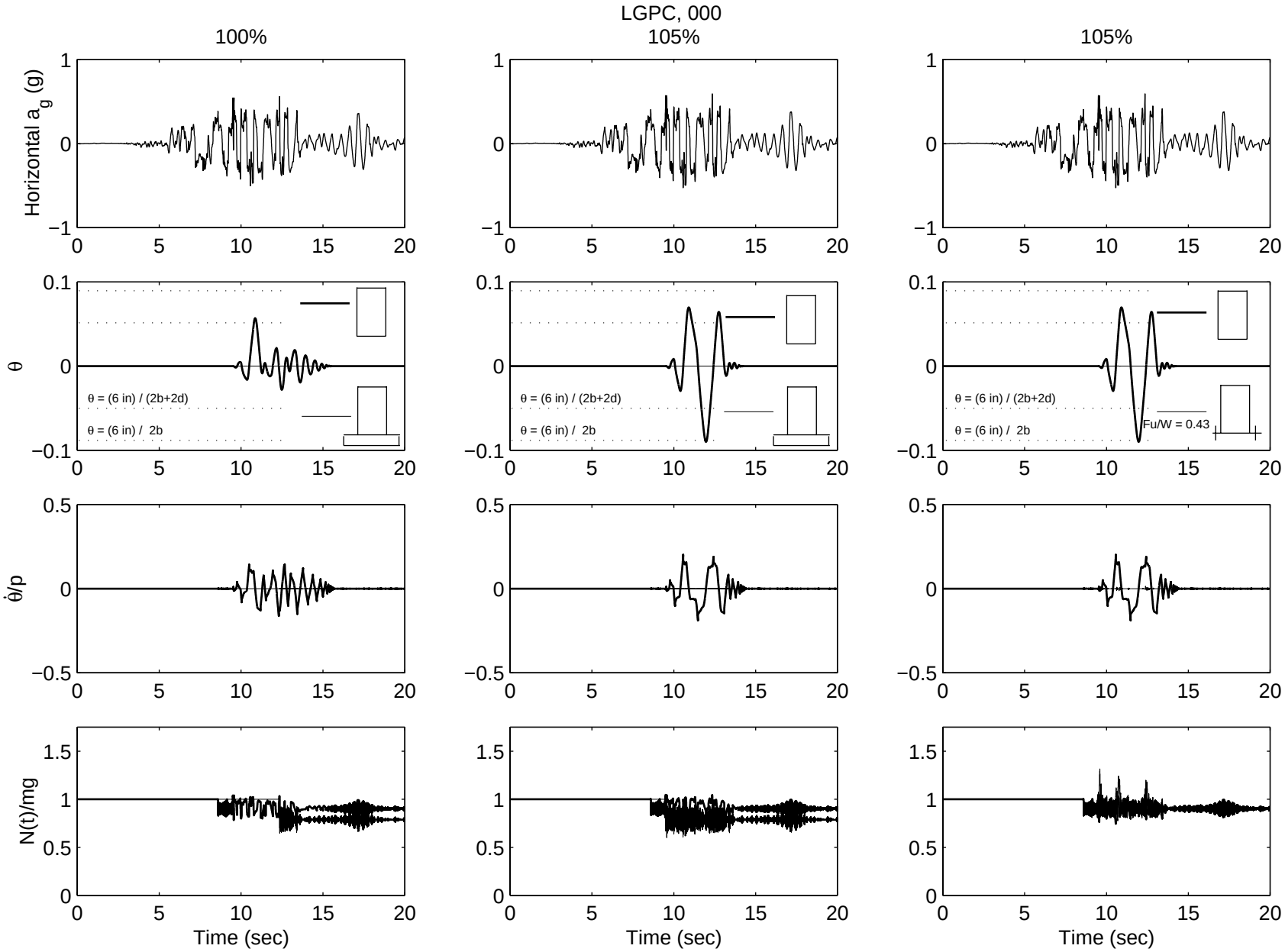

Figure 5.9. Rocking response of the 60 kip equipment to the 1989 Loma Prieta earthquake — Los Gatos record at the serviceability level.

needed for the freestanding equipment to reach the 6 in. uplift serviceability limit. Under the 105% level, neither the block-foundation system nor the anchored block with $F_u/W = 0.43$ exhibit any appreciable uplift.

Figure 5.10 indicates that more than 200% of the Los Gatos record is needed to overturn the free-standing 60 kip transformer. Under this level of shaking both the base-supported and the anchored equipment survive the rotation as is expected from the indications of Figure 5.4.

Figure 5.11 plots the rocking response of the 60 kip transformer subjected to the 1992 Erzikan, Turkey, record. The 100% level of the record does not create any noticeable uplift even to the freestanding block. The 139% level however results in an uplift of 6 in. of the freestanding block yet does not move either the equipment-foundation system nor the anchored equipment with $F_u/W = 0.43$.

Figure 5.12 examines the response of the 60 kip transformer on the verge of overturning. At a level of 170%, the freestanding equipment, the equipment-foundation system and the anchored ($F_u/W = 0.78$) equipment survive the motion with the equipment-foundation system being the most stable. At the 171% level however, the freestanding block topples, the anchored equipment with $F_u/W = 0.43$ rocks violently after fracturing the restrainers yet survives toppling; whereas, the anchored equipment with $F_u/W = 0.78$ essentially does not rock although it stretches the restrainers appreciably. For this record the equipment with its base foundation and the anchored equipment with $F_u/W = 0.78$ exhibit approximately the same capacity.

A ground motion with a rocking potential comparable to the 1992 Erzikan, Turkey, earthquake is the Sylmar motion recorded during the 1994 Northridge earthquake. The 100% level of the record shown at the top left of Figure 5.13 is capable of producing uplift in the freestanding system and 138% of the motion results in an uplift equal to the 6 in. serviceability level. Under this excitation level the equipment-foundation system experiences minimum uplift, whereas the anchored equip-

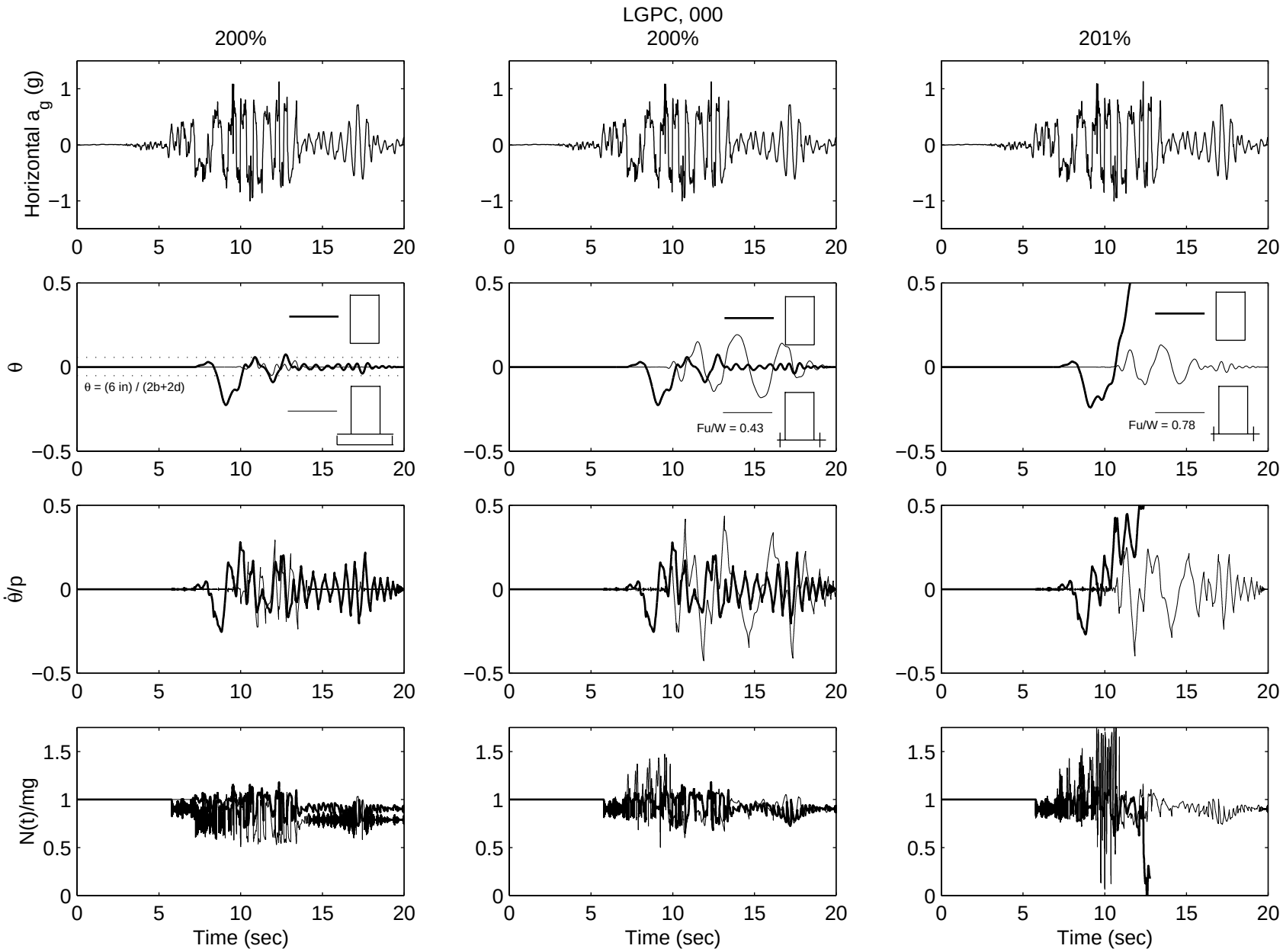

Figure 5.10. Rocking response of the 60 kip equipment to the 1989 Loma Prieta earthquake — Los Gatos record at the ultimate state.

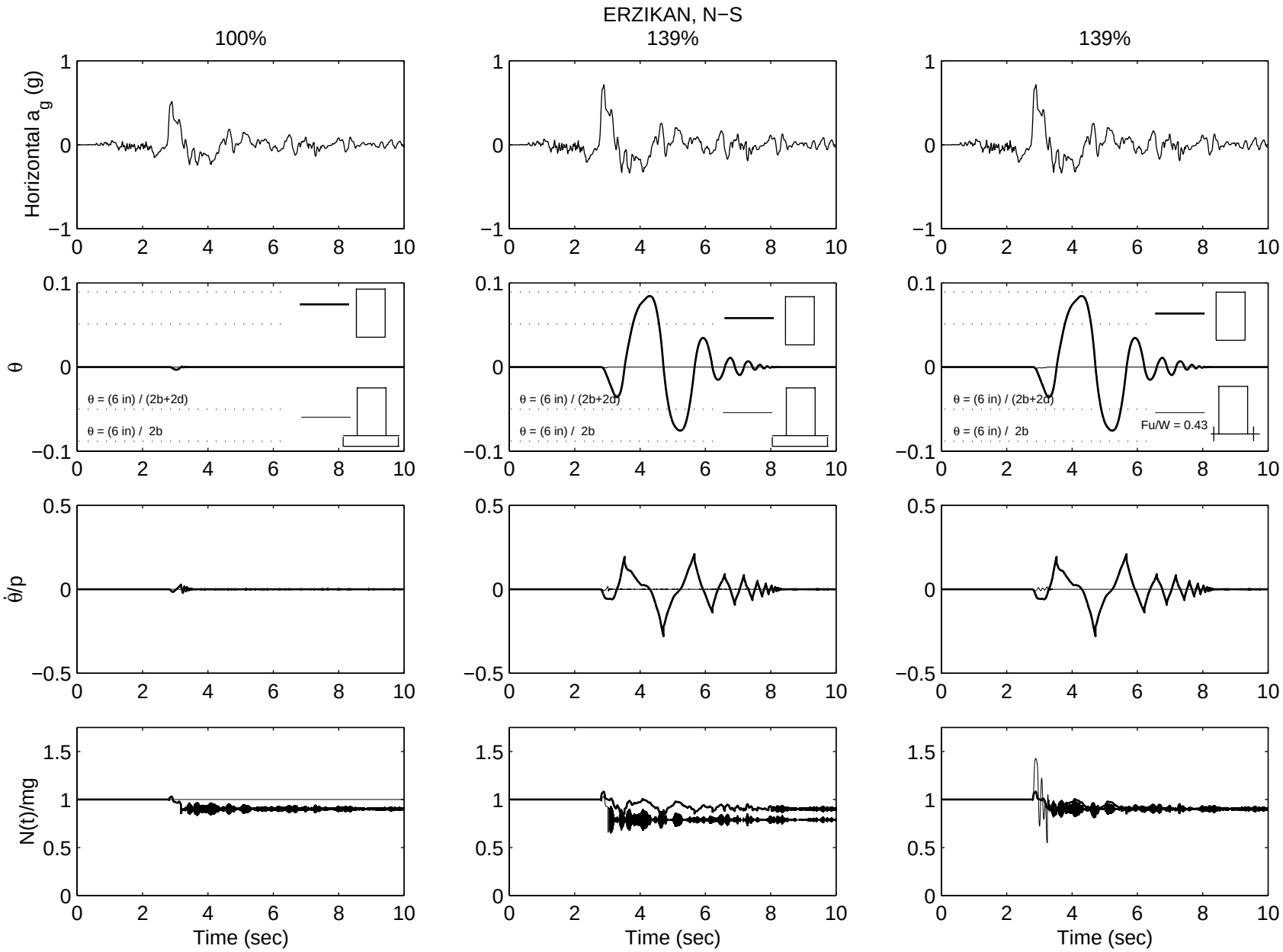

Figure 5.11. Rocking response of the 60 kip equipment to the 1992 Erzikan, Turkey, earthquake at the serviceability level.

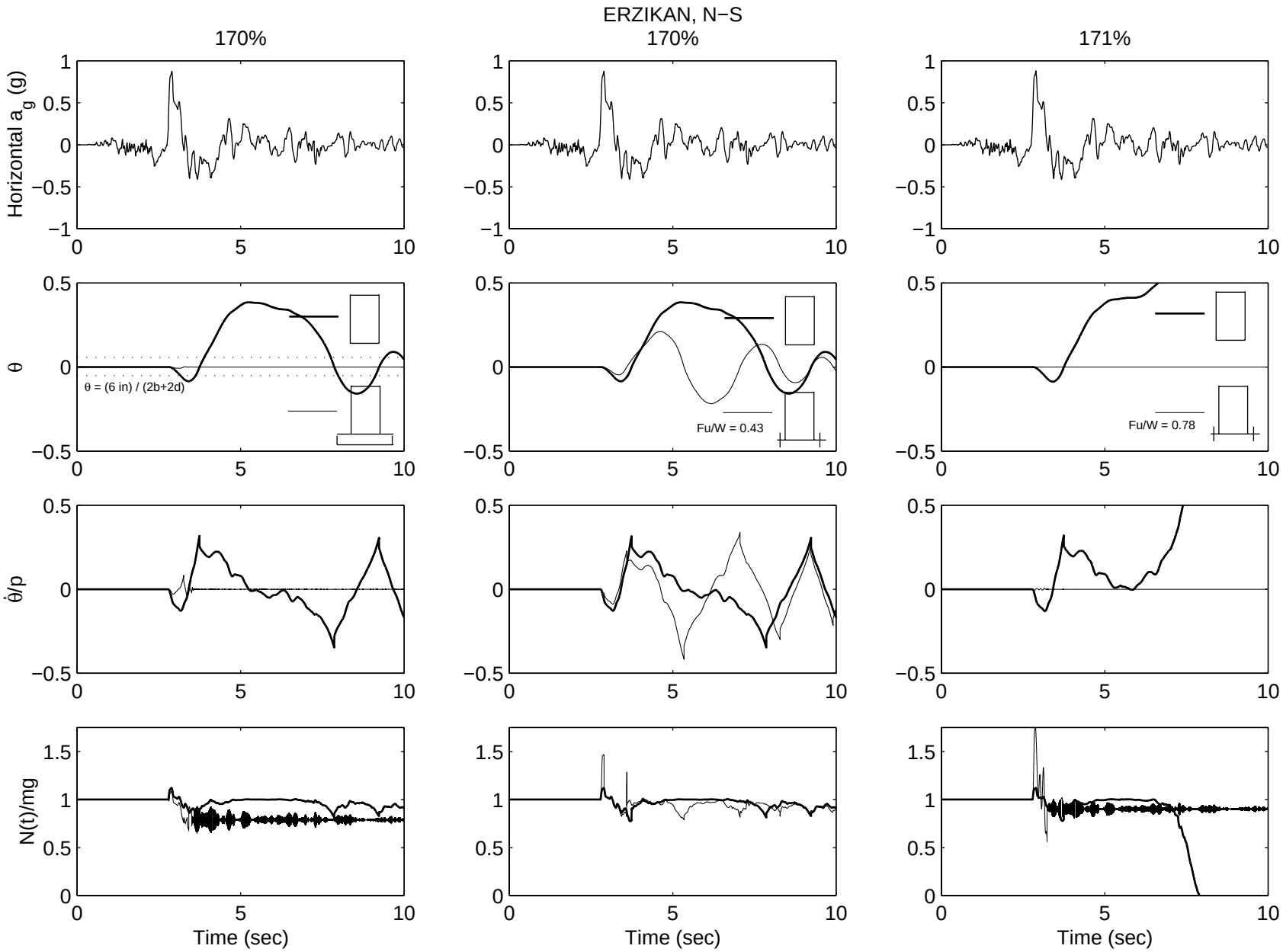

Figure 5.12. Rocking response of the 60 kip equipment to the 1992 Erzikan, Turkey, earthquake at the ultimate level.

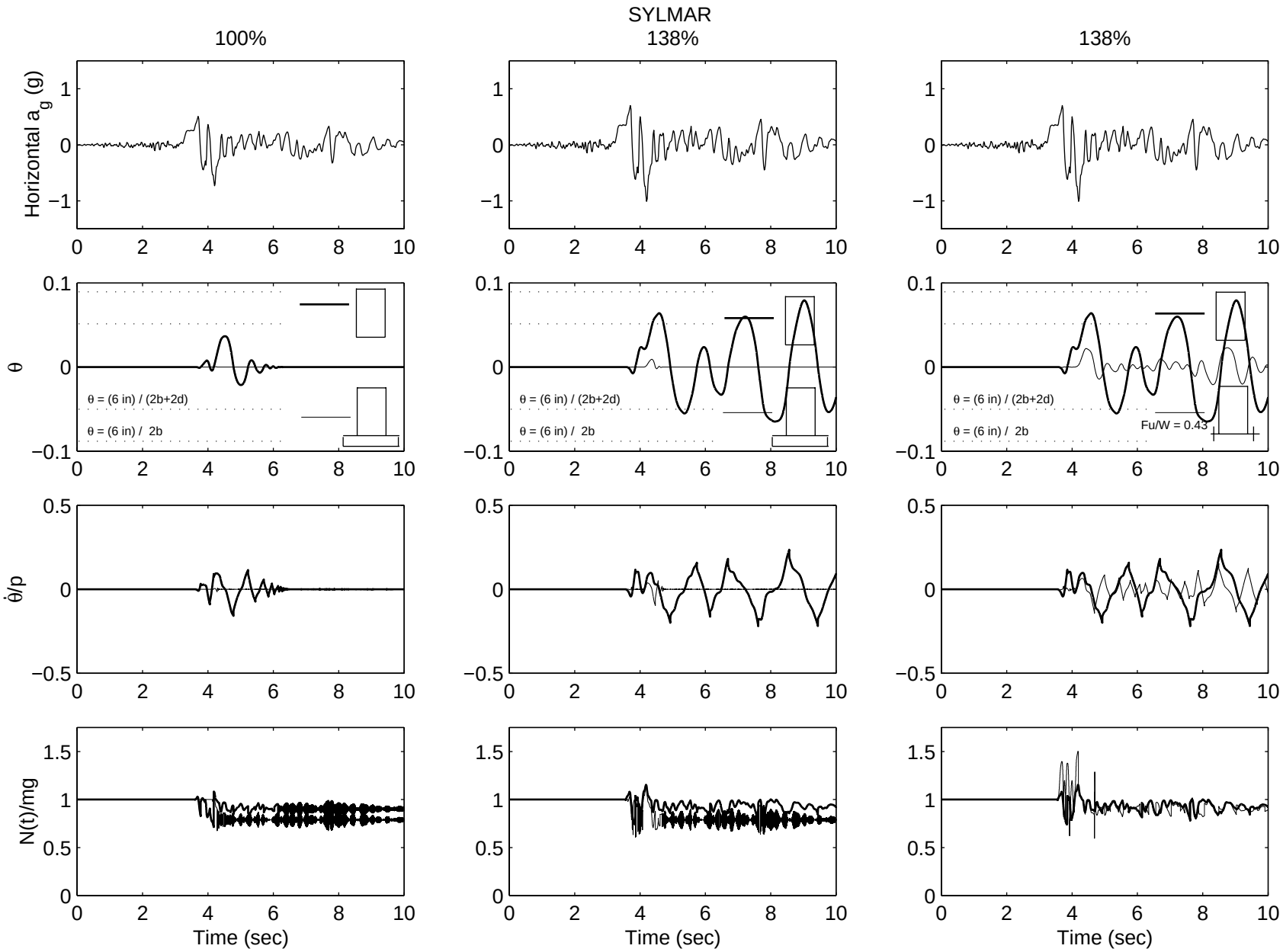

Figure 5.13. Rocking response of the 60 kip equipment to the 1994 Northridge earthquake — Sylmar Station at the serviceability level.

ment experiences some moderate rotations which are large enough to fracture the restrainer with $F_u/W = 0.43$.

The ultimate level response of the equipment to the Sylmar record shown in Figure 5.14 indicates a response very similar to that seen for the Erzikan record (Figure 5.12).

Figure 5.15 shows that the 100% level of the Rinaldi record induces rotations in the freestanding equipment which exceed the 6 in. serviceability uplift. When the record is increased to 136%, the freestanding 60 kip transformer topples and the equipment-base system exceeds its serviceability limit (see Figure 5.16). A similar situation happens with the Takatori record. The 100% level of the Takatori record induces rotations in the freestanding equipment that exceeds the 6 in. serviceability uplift (Figure 5.17). When the record is increased to 163% both the freestanding 60 kip transformer and the anchored transformer with $F_u/W = 0.43$ topple and the equipment base system exceeds its serviceability limit (Figure 5.18).

Next we investigate the uplifting and overturning potential of the TCU068 and the TCU052 motions recorded during the 1999 Chi-Chi, Taiwan, earthquake. The interesting characteristics of these motions is that whereas they exhibit moderate ground accelerations the ground velocities are unusually high, exceeding 2 m/sec and the durations of the main pulse periods reach 6 sec or more. The left column of Figure 5.19 plots the response of the 60 kip transformer subjected to 100% of the TCU068 E-W record. The freestanding equipment experiences a small uplift whereas the equipment anchored to its foundation does not move. The center column of Figure 5.19 indicates that 118% of the record induces rotations that reach serviceability levels; however it is incapable of moving the anchored equipment. Figure 5.20 indicates that a further minor increase of the excitation level (120%) is capable to overturn the freestanding equipment but leaving intact the anchored equipment. This behavior is consistent with the behavior observed from the rocking response of blocks under long-duration trigonometric pulses. A behavior similar to the one discussed in Figures 5.19 and 5.20 is observed in Figures 5.21 and 5.22.

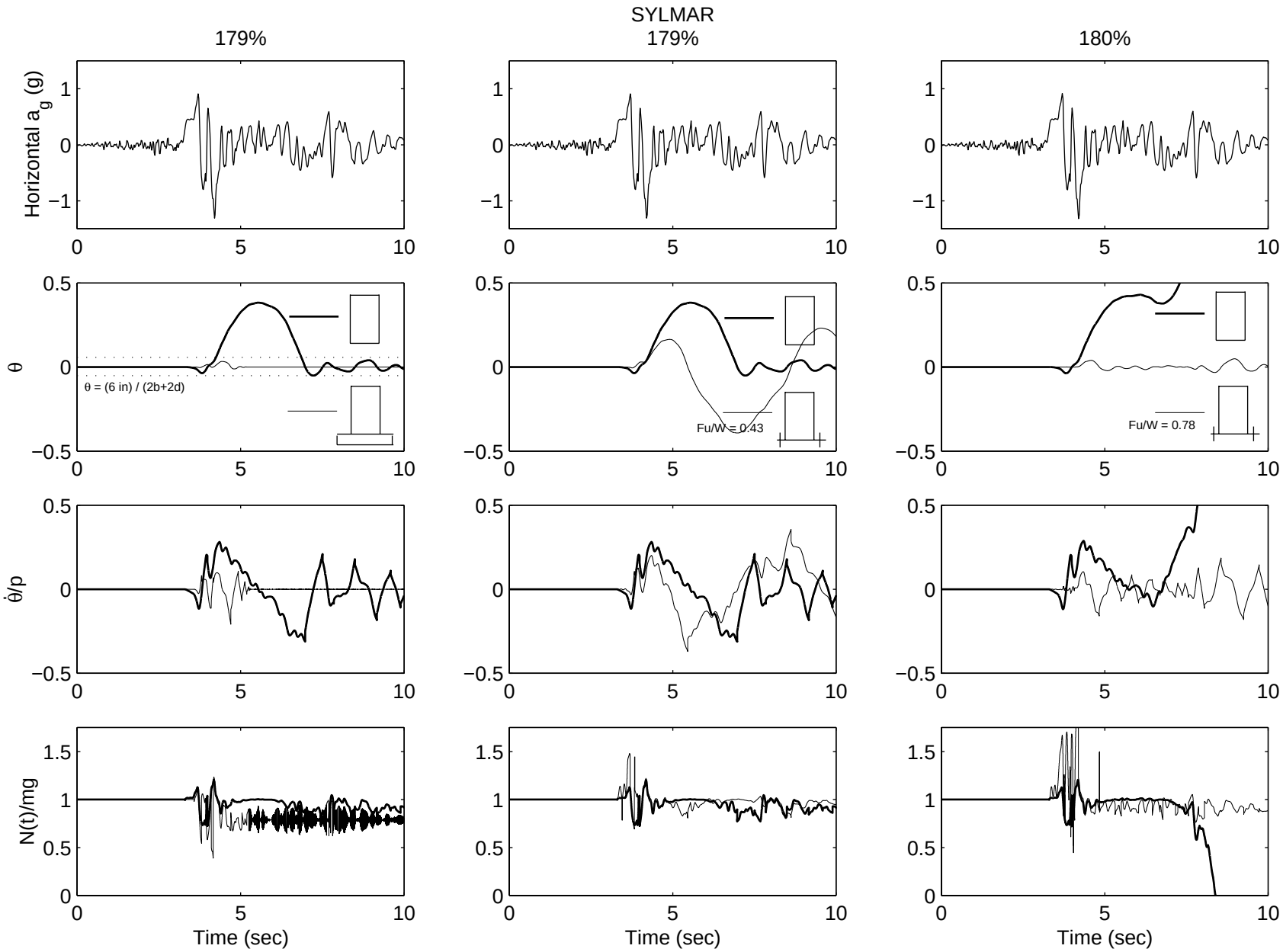

Figure 5.14. Rocking response of the 60 kip equipment to the 1994 Northridge earthquake — Sylmar Station record at the ultimate state.

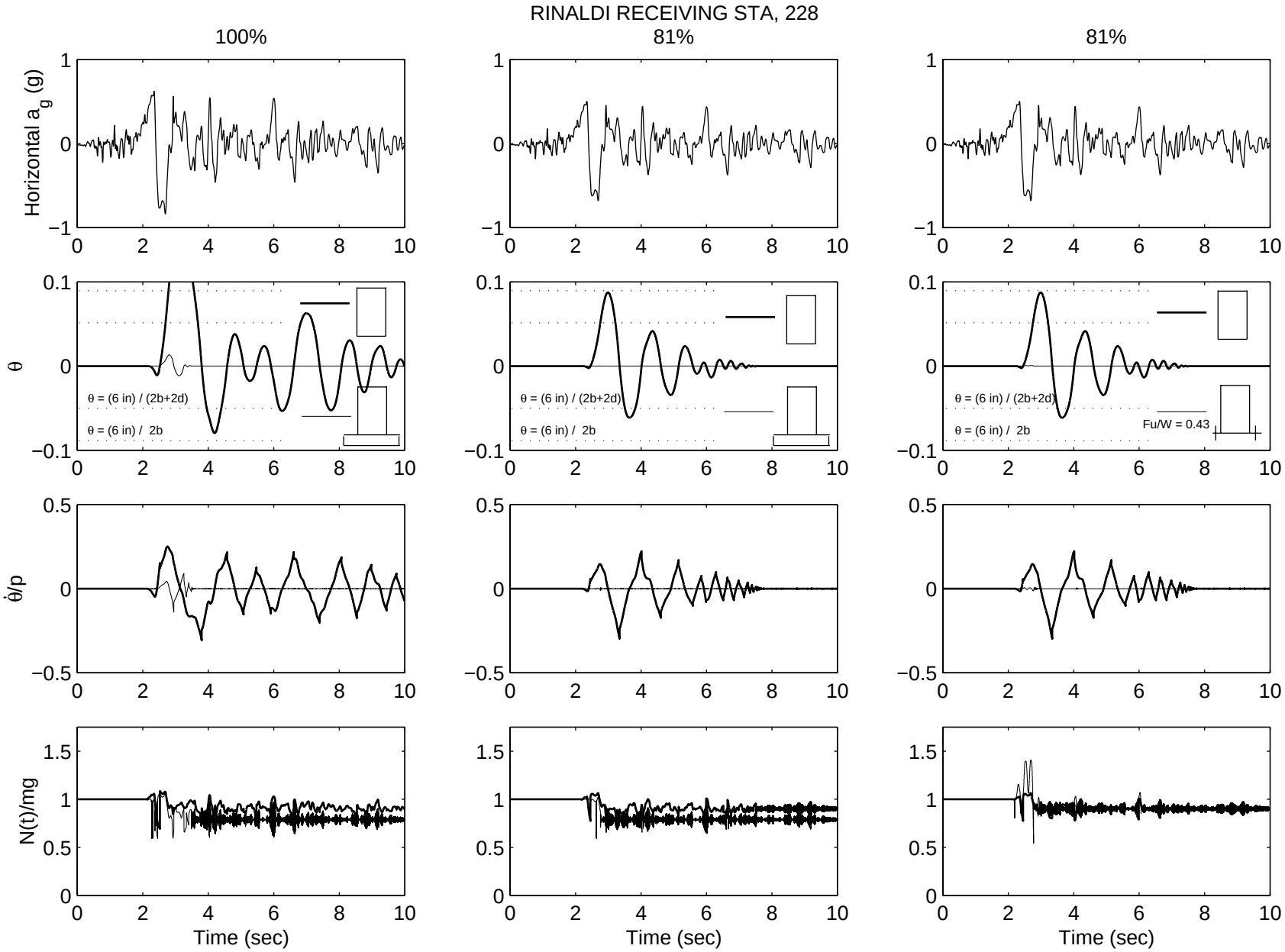

Figure 5.15. Rocking response of the 60 kip equipment to the 1994 Northridge earthquake — Rinaldi record at the serviceability level.

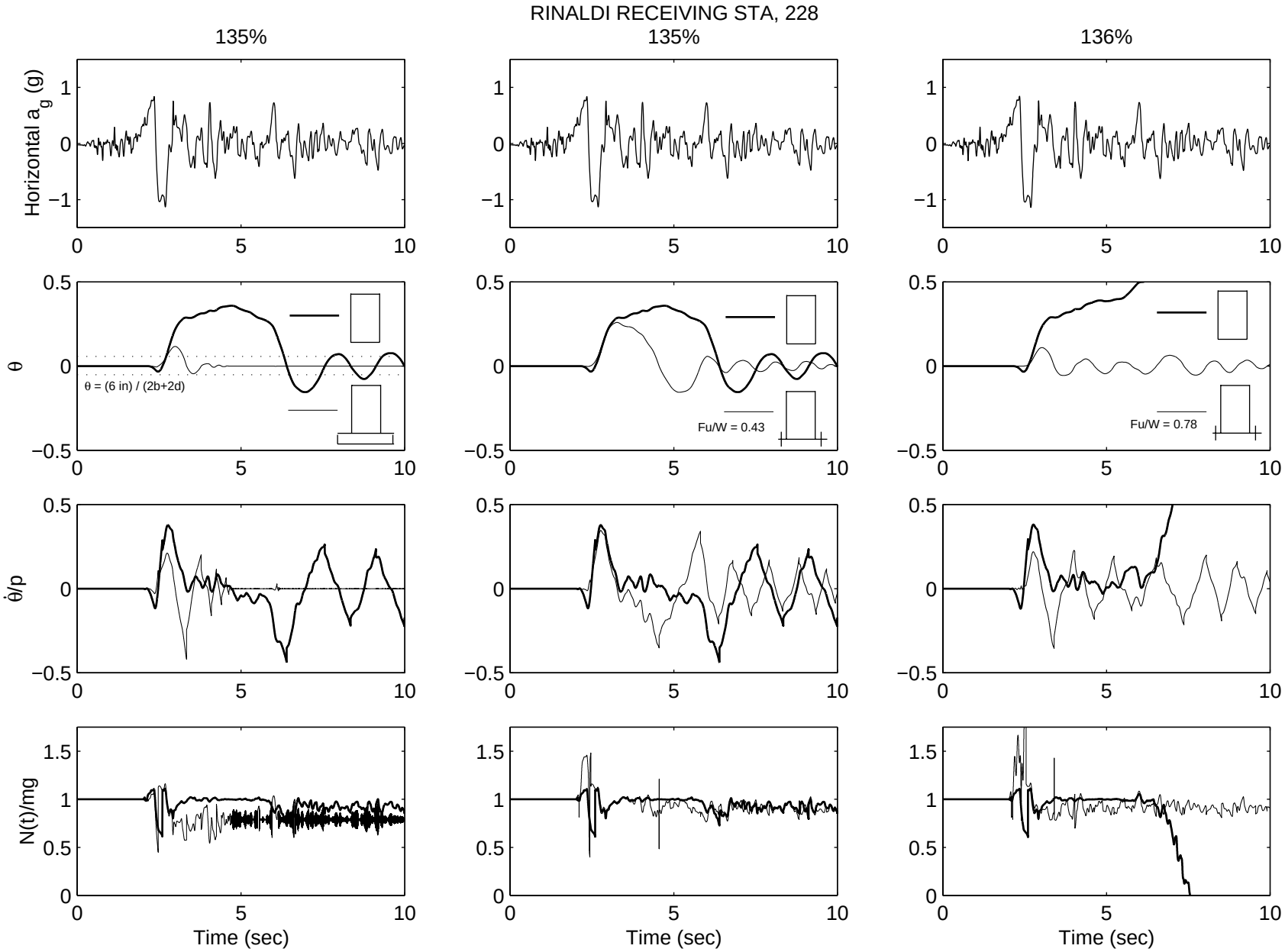

Figure 5.16. Rocking response of the 60 kip equipment to the 1994 Northridge earthquake — Rinaldi record at the ultimate state.

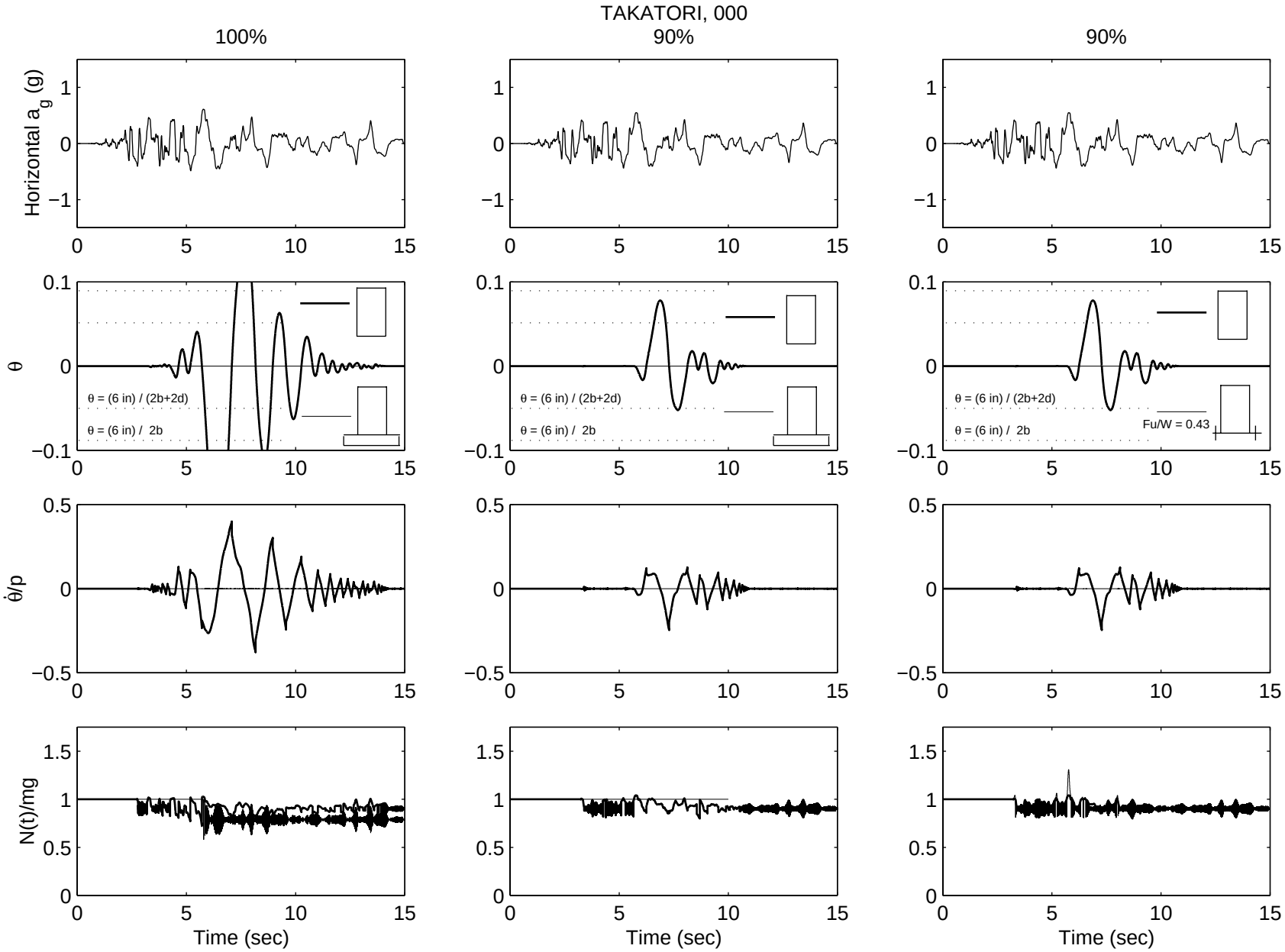

Figure 5.17. Rocking response of the 60 kip equipment to the 1995 Kobe earthquake — Takatori 000 record at the serviceability level.

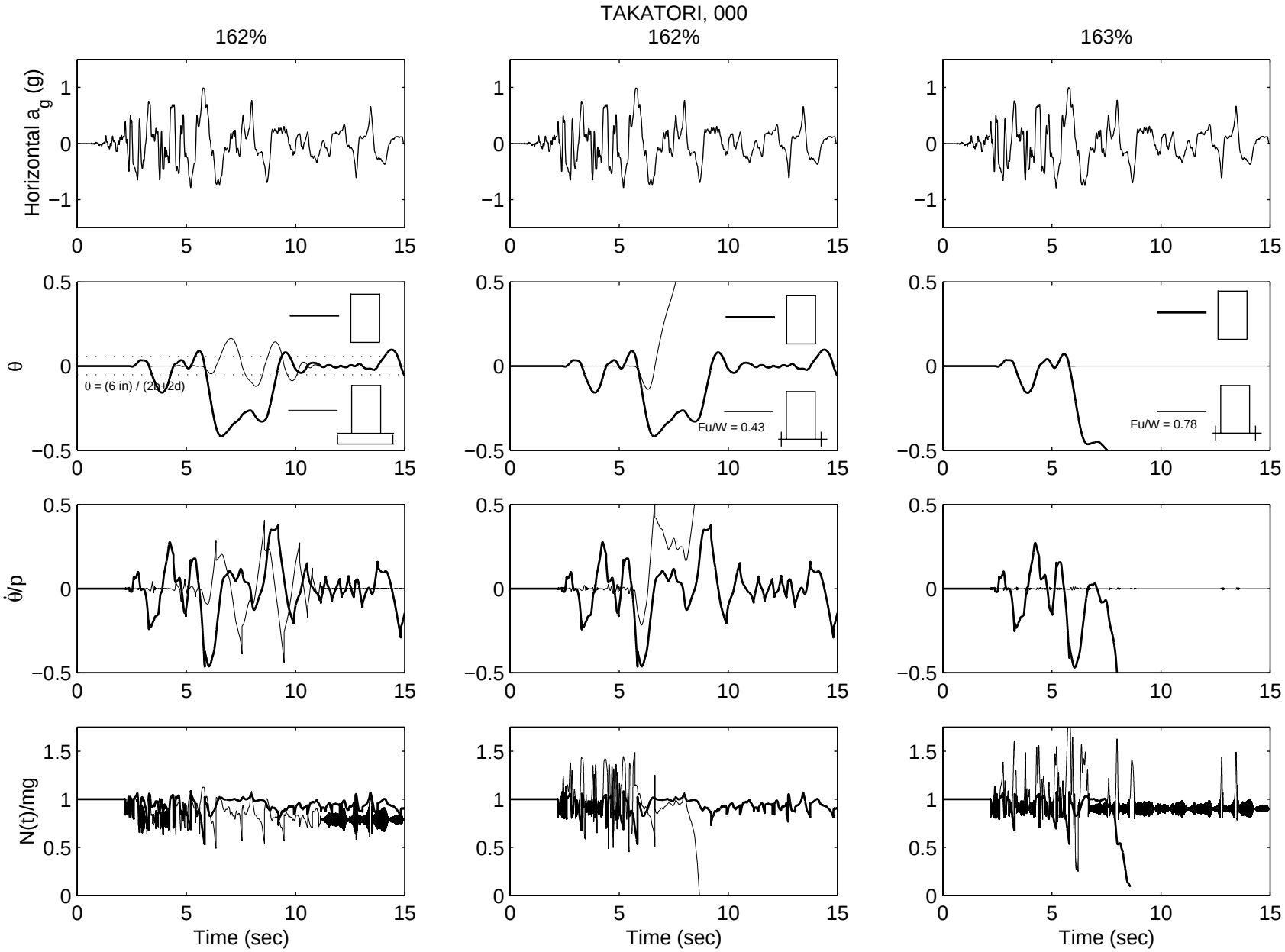

Figure 5.18. Rocking response of the 60 kip equipment to the 1995 Kobe earthquake — Takatori 000 record at the ultimate state.

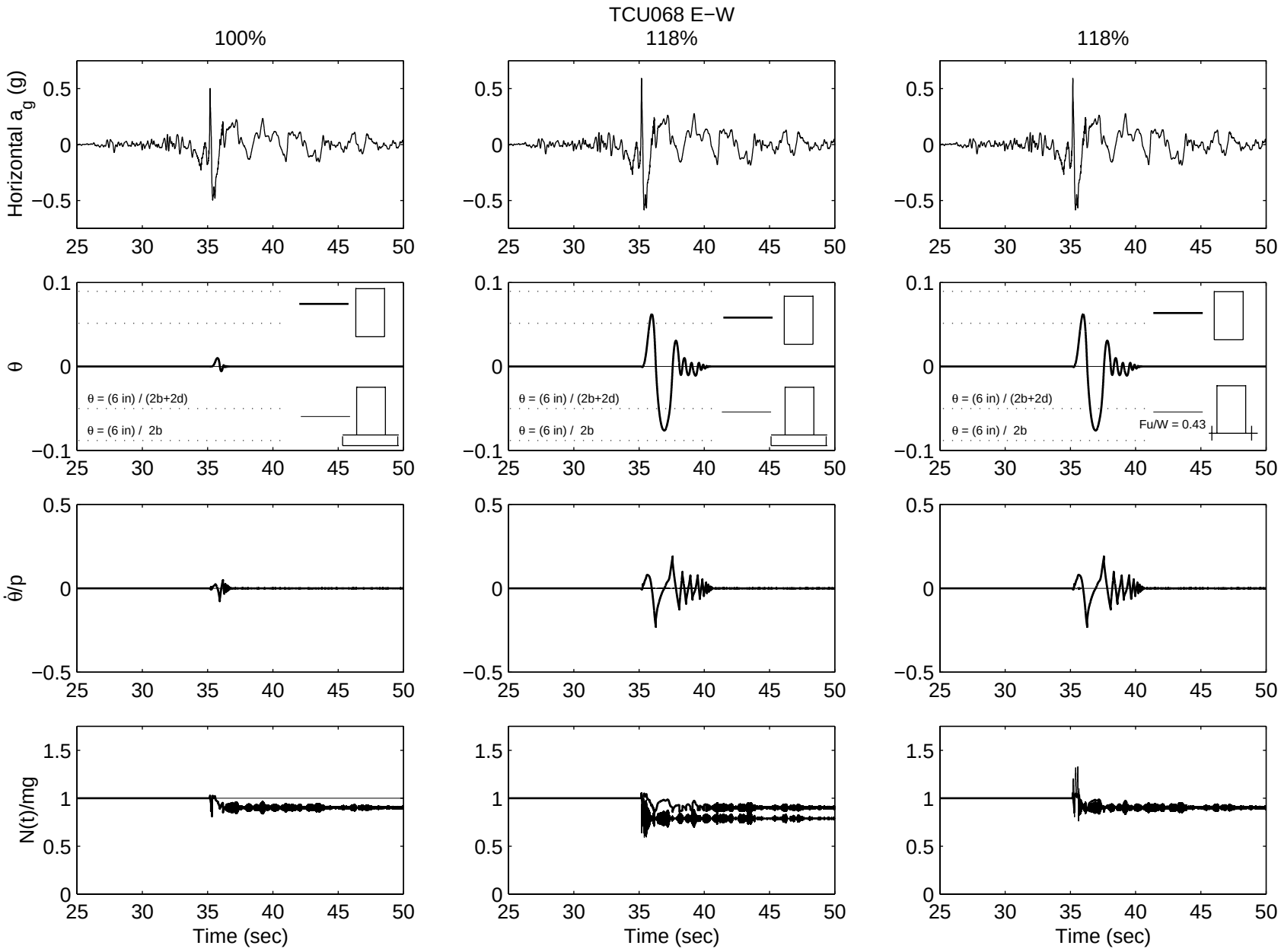

Figure 5.19. Rocking response of the 60 kip equipment to the 1999 Chi-Chi, Taiwan, earthquake — TCU068 EW at serviceability level.

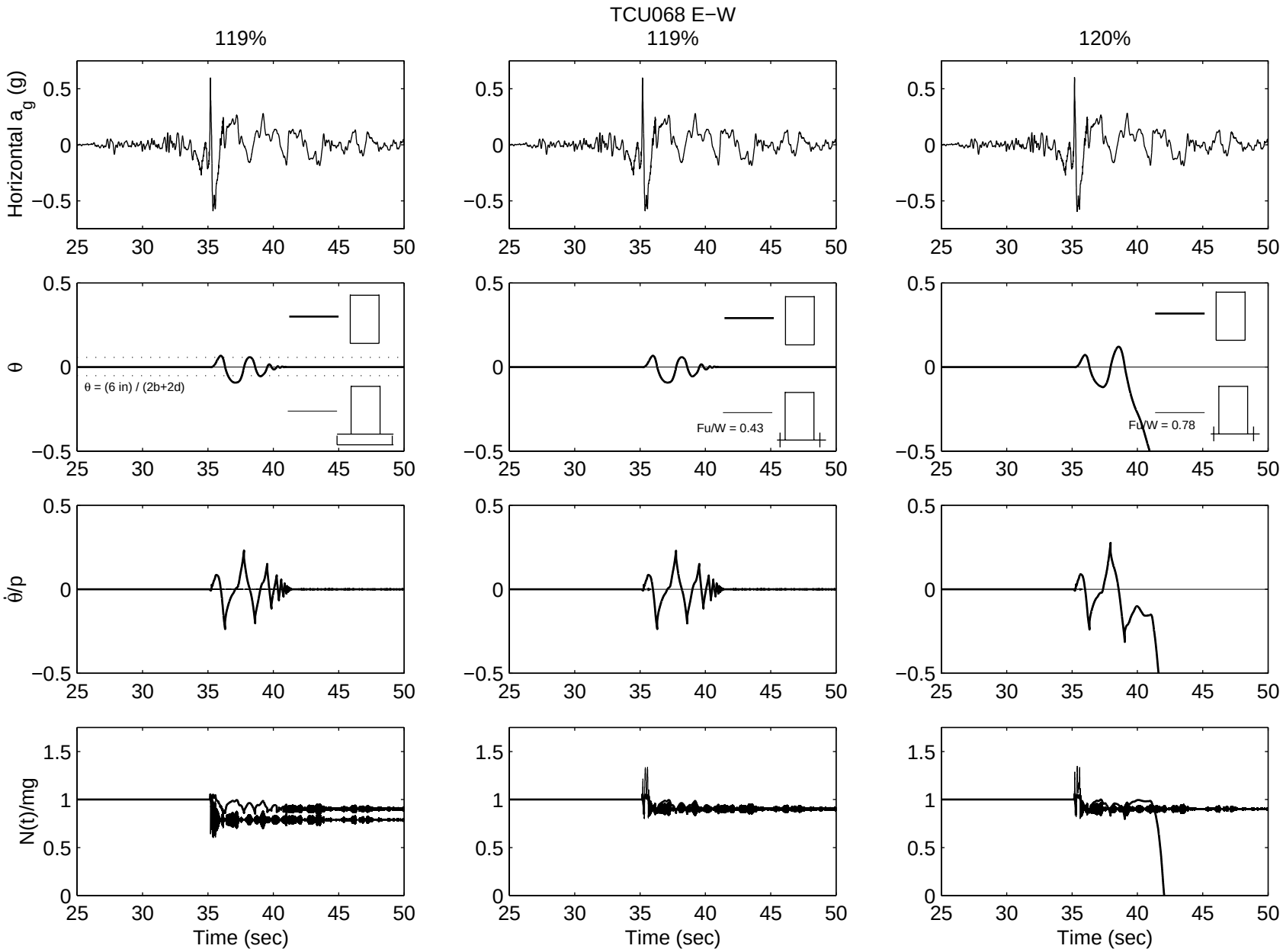

Figure 5.20. Rocking response of the 60 kip equipment to the 1999 Chi-Chi, Taiwan, earthquake — TCU068 EW record at ultimate state.

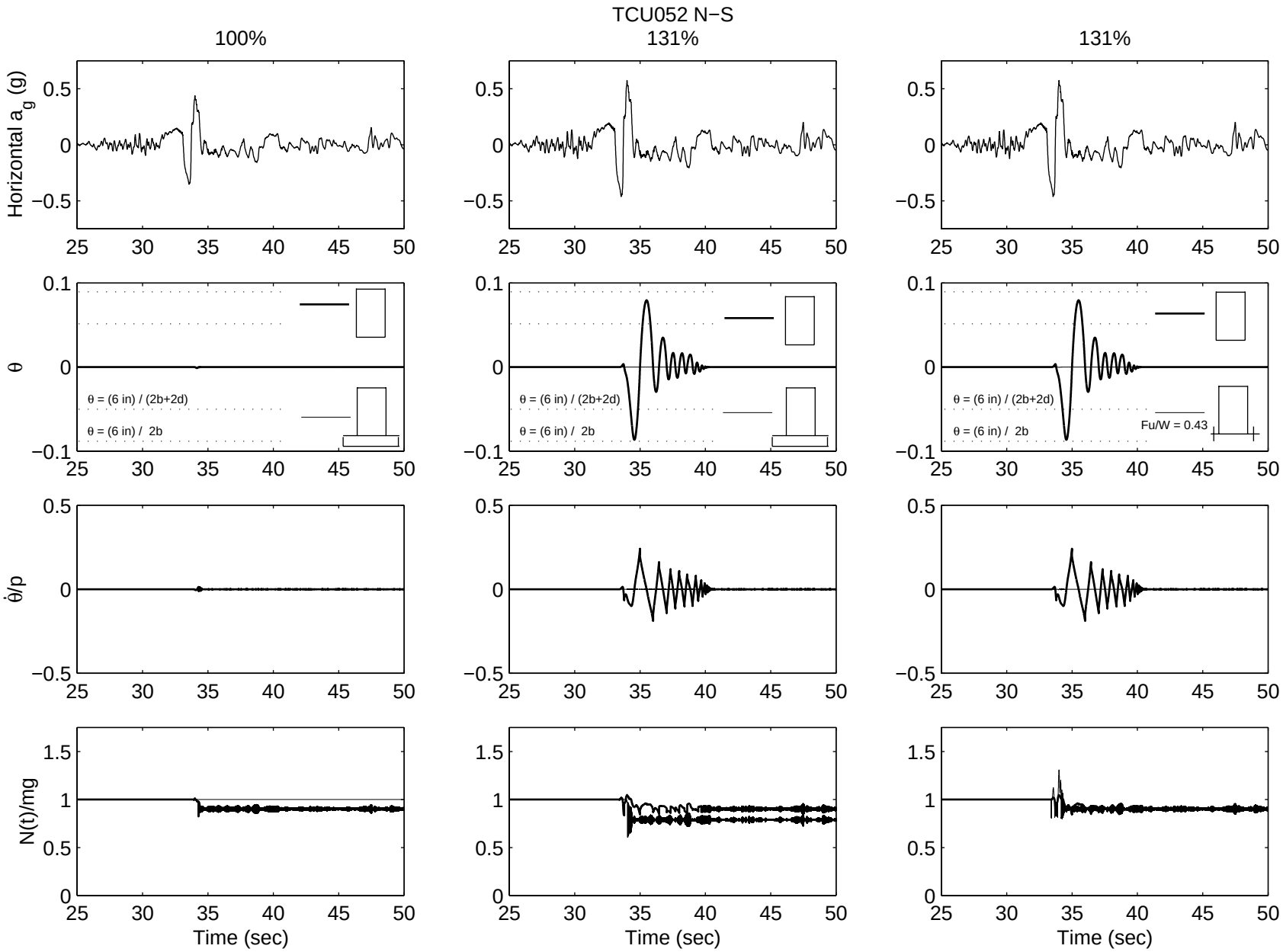

Figure 5.21. Rocking response of the 60 kip equipment to the 1999 Chi-Chi, Taiwan, earthquake — TCU052 NS at serviceability level.

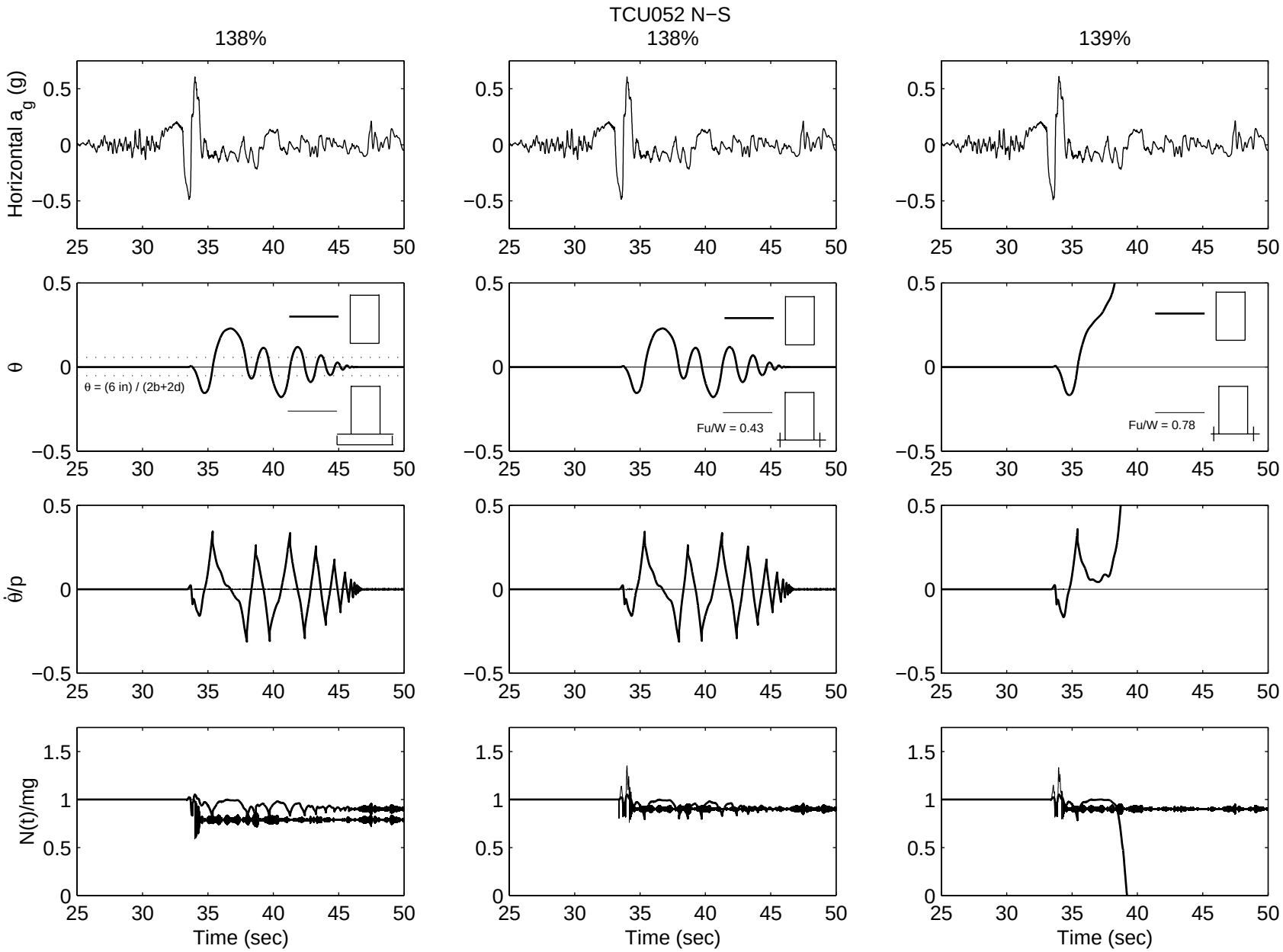

Figure 5.22. Rocking response of the 60 kip equipment to the 1999 Chi-Chi, Taiwan, earthquake — TCU052 NS record at ultimate state.

The results offered by the time history analysis presented in Figures 5.7 through 5.22 are summarized in Figures 5.23 through 5.27 in the form of histograms. The histogram plotted in Figure 5.23 shows the maximum uplift that the 60 kip equipment experiences when subjected to the earthquake records listed in Table 1. The earthquake records have been ordered with increasing peak ground acceleration. It is shown that among these 14 strong records only three records are capable of inducing uplift that exceeds the 6 in. serviceability limit. Each histogram plotted in Figures 5.24 through 5.27 shows the level of the recorded ground motion needed to reach the serviceability limit (6 in. uplift) and the level needed to create overturning. The histograms are plotted as a function of earthquake magnitude, peak ground acceleration, peak ground velocity and $T_p \cdot V_p$ (the product of pulse duration and pulse velocity amplitude of the most dominant pulse of the record) in an effort to identify some correlation between the rocking response and the kinematic characteristics of ground motions.

Figure 5.24 plots the levels of earthquake records needed to reach the serviceability limit (6 in. uplift) and overturning with increasing earthquake magnitude. Interestingly, the Rinaldi, Los Gatos, and Takatori records with respective magnitudes $M_w = 6.7$ and $M_w = 6.9$ can induce 6 in. uplift at a level that is below the level of the $M_w = 7.6$ Taiwan motions. In contrast, the TCU068 E-W motion creates overturning with the lowest percentage raise. When the histograms are plotted with increasing peak ground acceleration (PGA), as in Figure 5.25, one can observe a trend suggesting that less percentage of the recorded motion is needed to generate the 6 in. uplift. However, this order vanishes when looking at the levels needed to overturn the equipment.

Figure 5.26 plots the level of earthquake records needed to reach the serviceability limit (6 in. uplift) and overturning with increasing peak ground velocity. With this arrangement there is more order with respect to the overturning level (i.e., a smaller percentage increase is required to topple the 60 kip transformer for records with higher peak ground velocity). Nevertheless, this order is disturbed by the Pacoima Dam and Cape Mendocino records and vanishes when serviceability uplift is of interest.

Figure 5.27 plots the levels of earthquakes with increasing values of $T_p \cdot V_p$, where T_p = pulse period and V_p = pulse velocity amplitude of the trigonometric pulse that best approximates the recorded motion. With this arrangement, order emerges for toppling but there are no identifiable trends for the serviceability limit. Our study concludes that for estimating the serviceability uplift of the 60 kip (*b = 35", h = 90"*) equipment, the peak ground acceleration should be used as an indicator; whereas for estimating overturning, the product $T_p \cdot V_p$ appears to be the best indicator.

Figure 5.28 shows the minimum restrainer strength required for the restrainer not to fracture. The minimum restrainer strength is strongly correlated with the peak ground acceleration. Of the earthquakes considered, 4 are capable of fracturing the low strength restrainers $F_u/W = 0.43$, and 1 is capable of fracturing the high-strength restrainers $F_u/W = 0.78$.

Finally, Figure 5.29 shows the maximum vertical reaction force at the pivot points. The lowest level corresponds to the reaction force when the block is free standing; whereas, the middle and upper levels correspond to the reaction force for the case when the equipment is anchored with the low- and high-strength restrainers. When the ground motion does not cause uplift the reaction at each edge is taken to be *0.5W*. When the equipment does uplift the reaction force increases appreciably as it opposes not only the full weight of the equipment but also inertia effects and the force in the restrainer opposing uplift. For the Cape Mendocino record the reaction reaches *1.25W* for the freestanding case (*1W* self-weight + *0.25W* dynamic effect) and *1.91W* for the case when the equipment is anchored with the high-strength restrainers. More than half of the earthquakes studied produce a reaction force along the edge that exceeds 1.25 times the weight of the equipment (2.5 times greater than the static edge force *0.5W*).

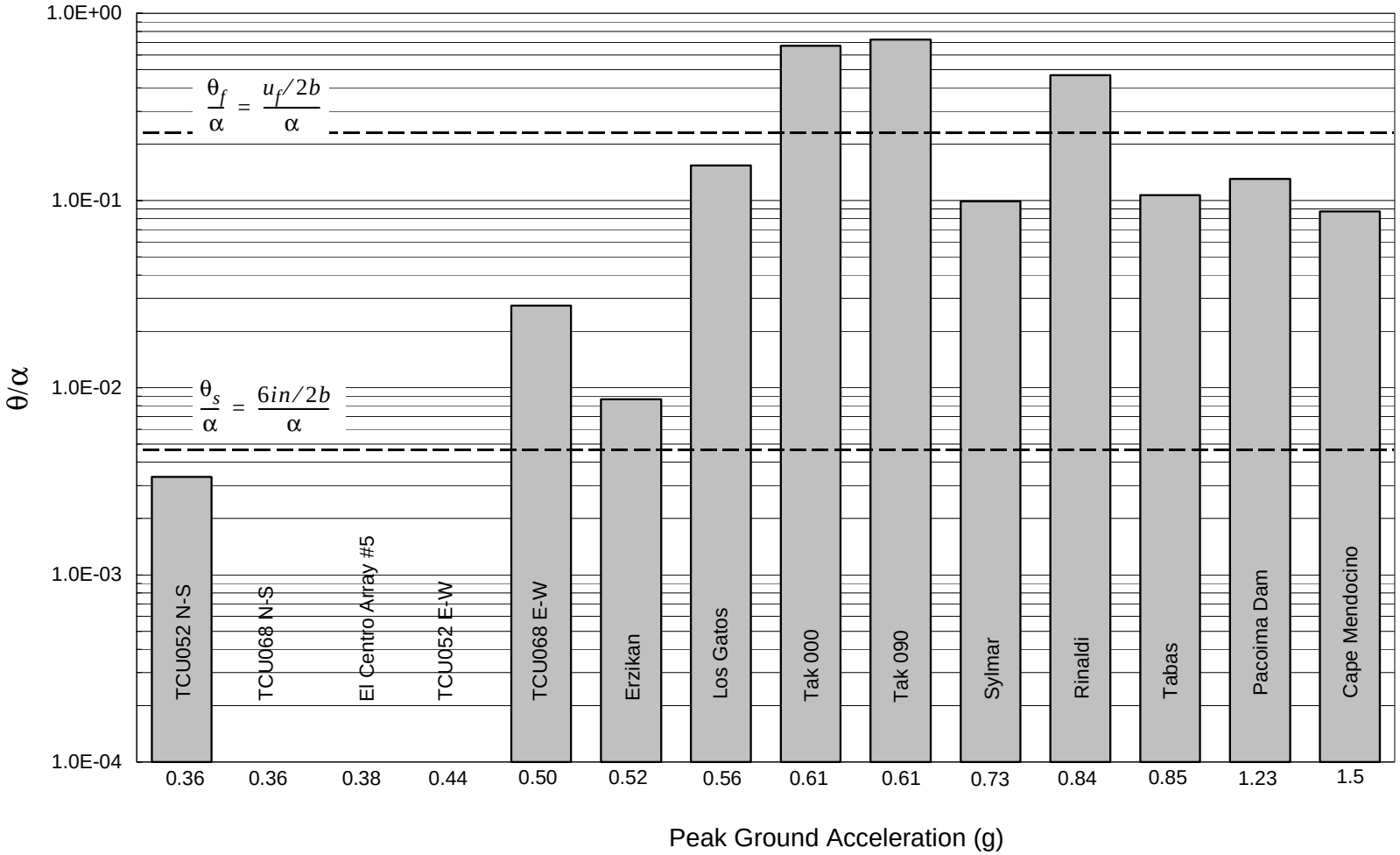

Figure 5.23. Maximum rotation values of the freestanding, 60 kip equipment subjected to earthquake motions. They have been ordered with increasing peak recorded ground acceleration values. The serviceability rotation limit, θ_s, and the rotation, θ_f, where the restrainers of an anchored block fracture, are also shown with dashed lines

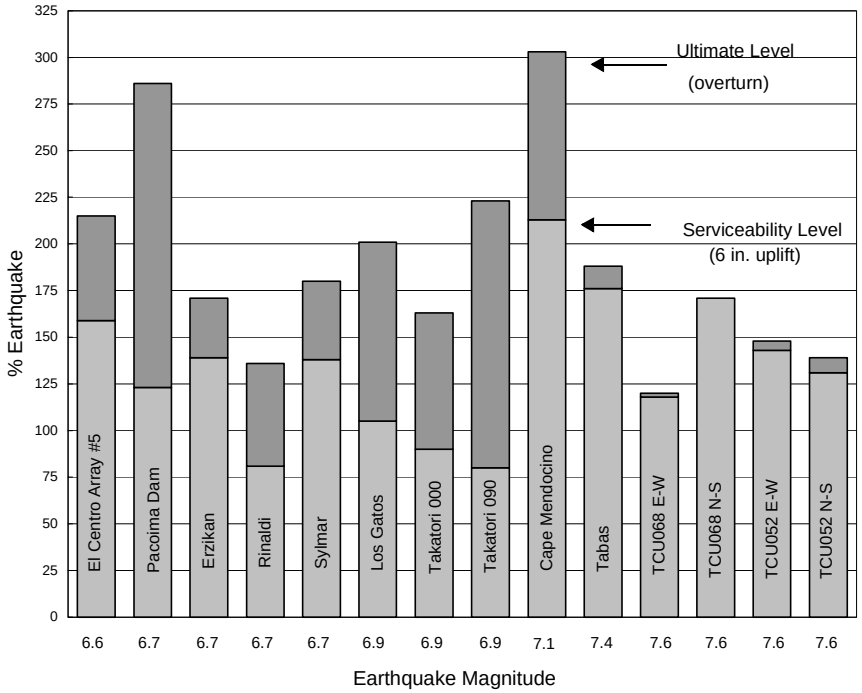

Figure 5.24. Levels of earthquake records required to reach serviceability uplift and overturning of the 60 kip equipment. They have been ordered with increasing earthquake magnitude.

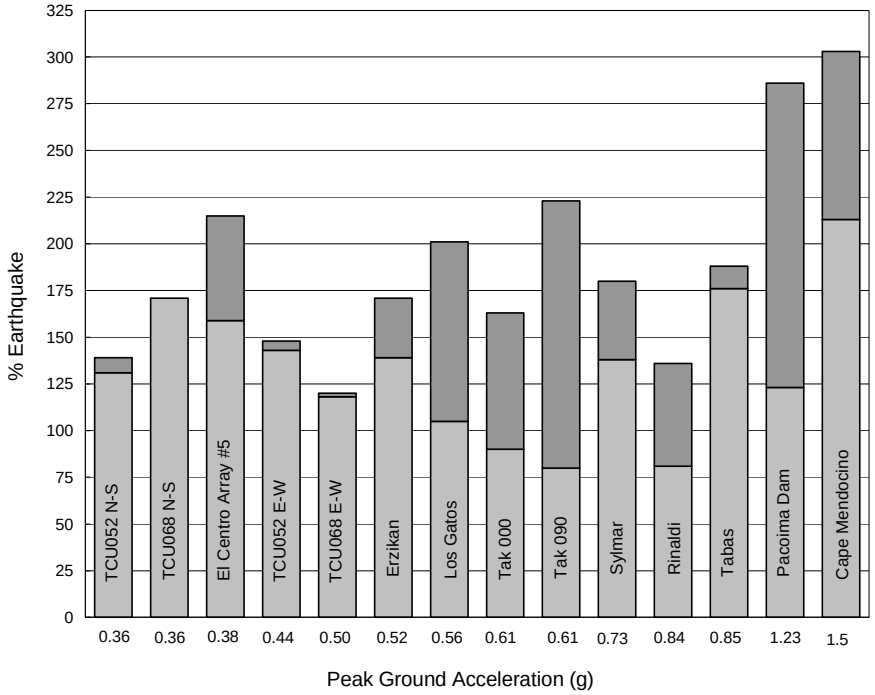

Figure 5.25. Levels of earthquake records required to reach serviceability uplift and overturning of the 60 kip equipment. They have been ordered with increasing peak recorded ground acceleration.

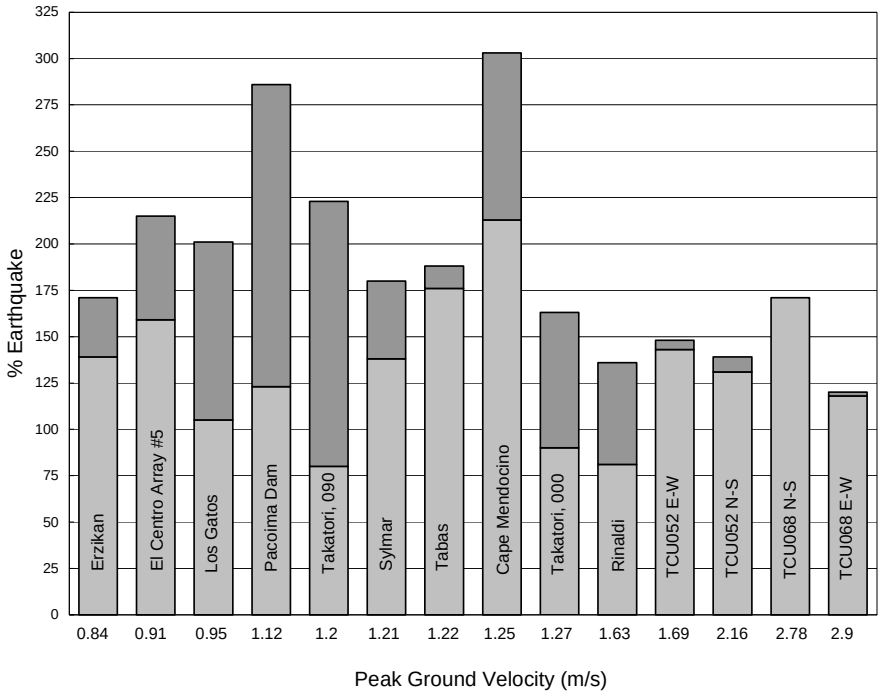

Figure 5.26. Levels of earthquake records required to reach serviceability uplift and overturning of the 60 kip equipment. They have been ordered with increasing peak recorded ground velocity.

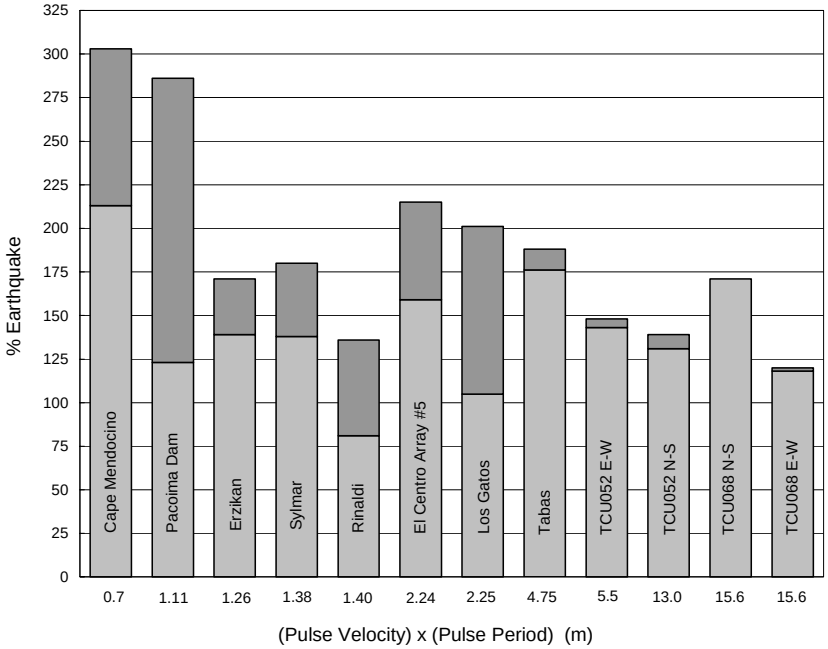

Figure 5.27. Levels of earthquake records required to reach serviceability uplift and overturning of the 60 kip equipment. They have been ordered with increasing $T_p \cdot V_p$ values, where T_p = pulse period and V_p = pulse velocity amplitude of the trigonometric pulse that best approximates the recorded motion.

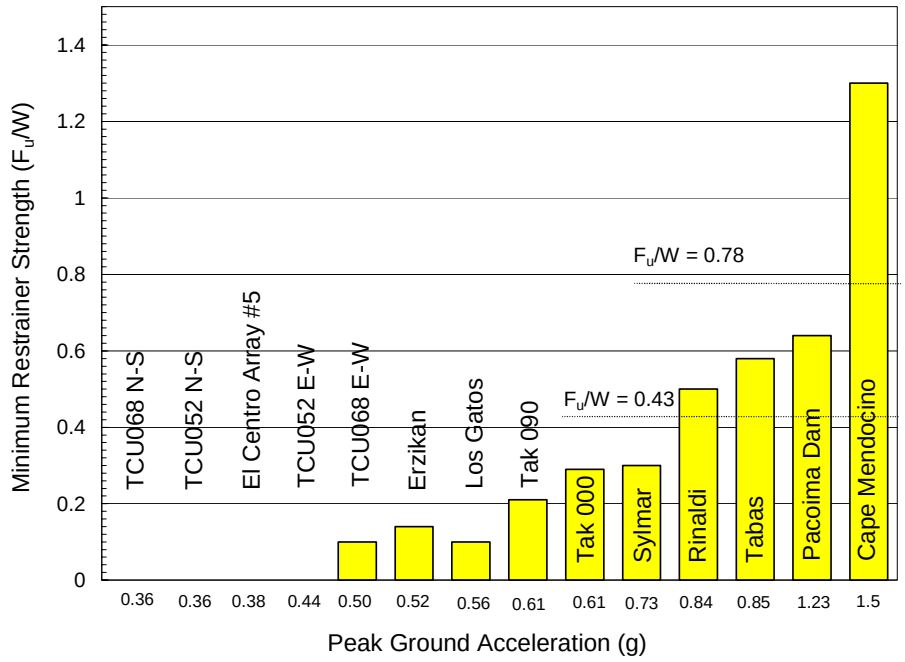

Figure 5.28. Minimum strength needed for the restrainers not to fracture. The records have been ordered with increasing peak recorded ground acceleration.

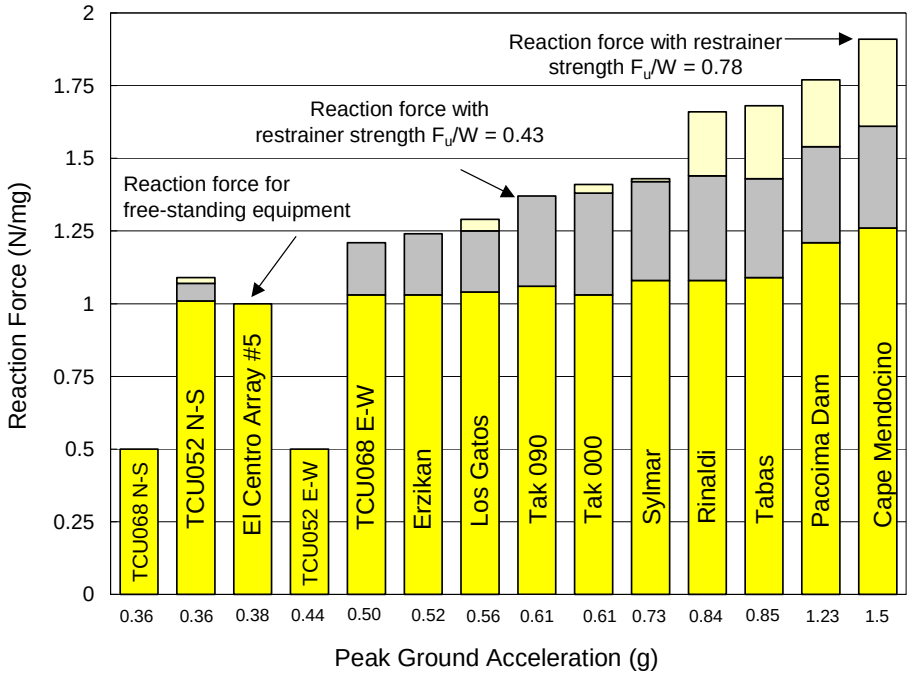

Figure 5.29. Maximum reaction force at pivot points. The records have been ordered with increasing peak recorded ground acceleration.

6 Effect of Base Foundation on Uplift

The time histories of block rotations presented in the previous chapter indicated that the lateral protrusion of the base foundation, *d*, from each side of the equipment with width *2b* might have an appreciable effect on reducing uplift. Figure 6.1 (bottoms) plots the maximum uplift of the 60 kip equipment that engages its foundation in rocking motion as the protrusion of the foundation base, *d*, increases. It is observed that even a small fraction of *d/b* appreciably reduces the uplift induced by certain motions. For instance, Figure 6.1 indicates that when $d = 0.25b = 8.75$ in. the uplift of the equipment-foundation system is below 2 in. for all strong motions considered with the exception of the Rinaldi Station motion. For the existing configuration, *d = 22 in.*, the maximum uplift due to the Rinaldi Station motion is about 1.5 in., whereas all other strong motions induce uplift that is less than 0.3 in. The benefits of the protrusion of the base foundation are of interest provided that the restrainers are capable of engaging the base foundation in the rocking motion. Figure 6.1 (top) indicates the minimum strength of restrainers needed to avoid fracture and thus engage the foundation in rocking when the 60 kip transformer is subjected to the indicated record. It is shown that high-strength restrainers ($F_u/W = 0.78$) survive the shaking from all earthquakes and therefore engage the foundation in rocking motion, while the low-strength restrainers ($F_u/W = 0.43$) fracture when the equipment is subjected to the Pacoima Dam and Rinaldi records. Although the minimum strength was determined from analysis assuming a monolithic foundation, the analysis indicates that the reduced capacity of the low-strength restrainers might govern the response of the equipment-foundation system. That is, if the restrainers fracture, the resulting uplift would likely be larger then the values shown in Figure 6.1 (bottom).

Figure 6.2 (bottom) plots the maximum uplift of the 230 kip equipment, which has the same height as the 60 kip equipment (*h = 90 in.*) but a larger width (*b = 38 in.*). It is clear from the figure that the 230 kip equipment configuration is more conservative than the 60 kip equipment. Figure

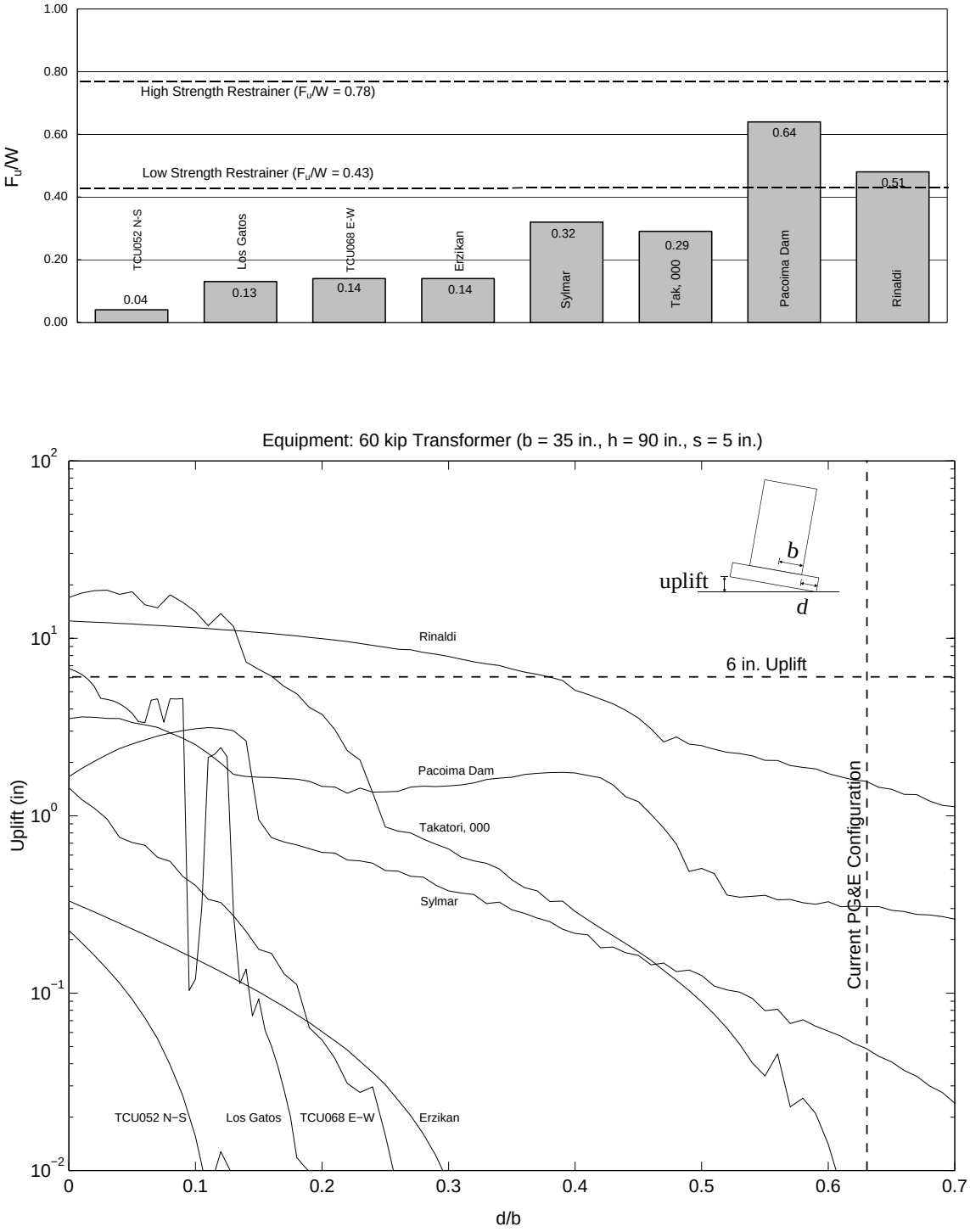

Figure 6.1. Histogram showing the minimum restrainer strength needed to avoid fracture and thus engage the foundation in rocking, when the 60 kip transformer is subjected to the indicated records (top); and the effect of foundation size on the uplift of the 60 kip equipment-foundation system subjected to earthquake motion (bottom).

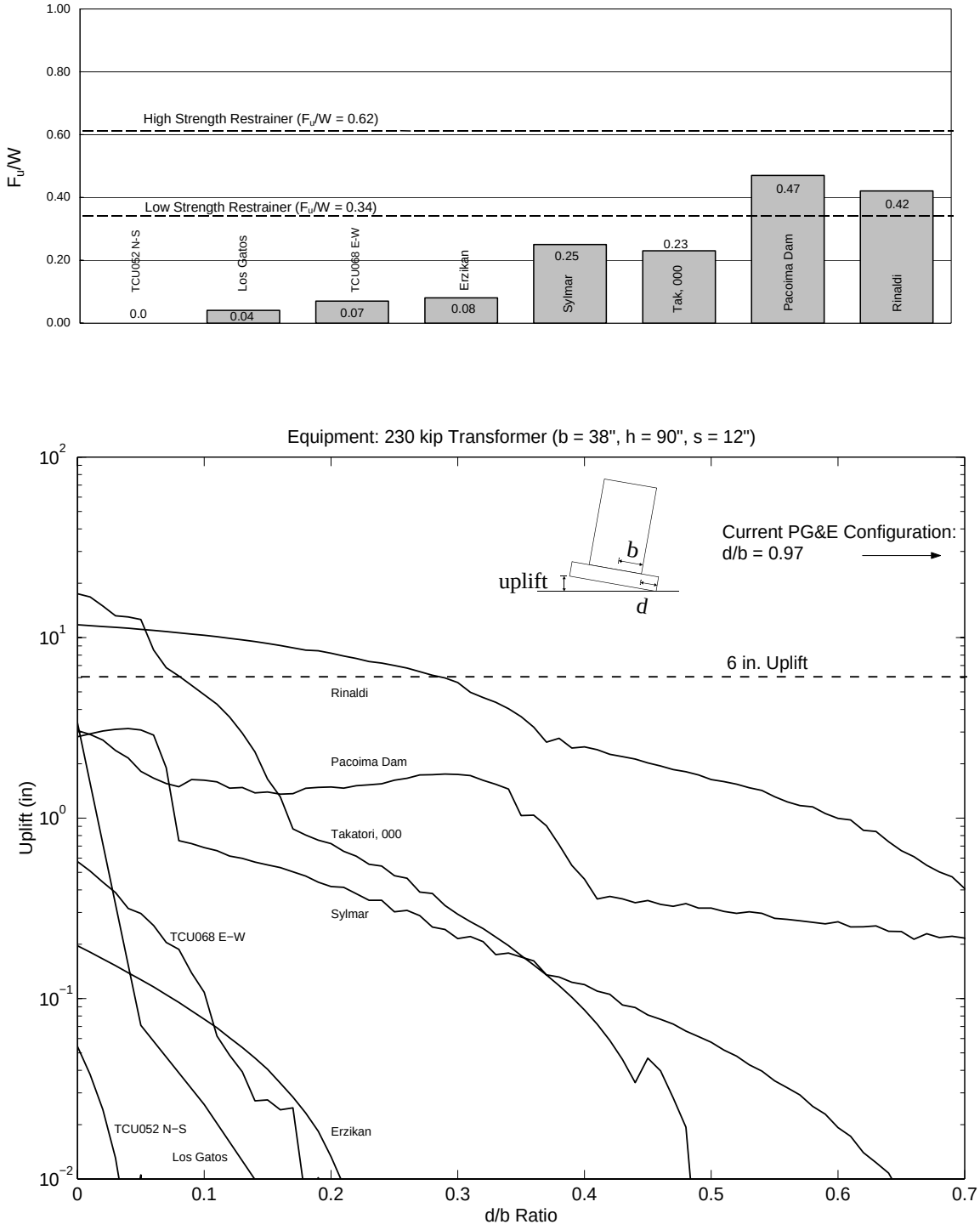

Figure 6.2. Histogram showing the minimum restrainer strength needed to avoid fracture and thus engage the foundation in rocking, when the 230 kip transformer is subjected to the indicated records (top); and the effect of foundation size on the uplift of the 230 kip equipment-foundation system subjected to earthquake motion (bottom).

6.2 (top) shows that the high-strength restrainers ($F_u/W = 0.62$) survive the shaking from all earthquakes; therefore they engage the foundation in rocking.

Figure 6.3 plots the maximum uplift of a rigid block that has the same height as the two previously studied transformers (*h = 90 in.*) but a smaller width (*b = 30 in.*). Interestingly, the TCU068 E-W record, that generated moderate uplift in the other two configurations, is now overturning the more slender block. A small increase in the foundation protrusion, *d*, establishes stability and when $d/b = 0.6$ the uplift is below 6 in. for all records.

One interesting feature of the response curves shown in Figures 6.1, 6.2, and 6.3 is that they do not decrease monotonically as *d/b* increases. The most notable example is the response curve resulting from the Sylmar record which shows that the uplift actually increases as *d/b* increases from 0 to 0.1. This curve has been isolated in Figure 6.4 (top) and has been replotted in a linear scale.

In order to explain this "unexpected" behavior, Figure 6.5 plots the acceleration time history of the Sylmar record (top) and the response of four different configurations: *d/b* = 0, 0.05, 0.1, and 0.15. The Sylmar record contains a violent acceleration pulse ABCDE that initiates at $t = 3\,\text{sec}$ and expires slightly prior to $t = 4\,\text{sec}$. The violent pulse is succeeded by another strong pulse EFGHI, which also exhibits the peak ground acceleration. Indeed, as *d/b* increases (first three plots), the forward rotation of the structure before $t = 4\,\text{sec}$ reduces. It is interesting to note that the first column indicates that at $t = 4\,\text{sec}$, the first forward rotation is at its maximum and some of the action of the following pulse is consumed in re-centering the structure, while the third column indicates that at $t = 4\,\text{sec}$, the first forward rotation has expired and the action of the following pulse is entirely dedicated to induce a new rotation to the system that carries momentum along the same direction. It is this sensitive combination of successive pulses in the record, with the motion of the equipment foundation system, that results in a larger uplift as *d/b* increases from 0 to 0.1. When $d/b = 0.15$ the forward rotation of the structure prior to $t = 4\,\text{sec}$ is totally suppressed and the angular velocity is nearly zero.When the second strong pulse, EFGHI, strikes, the structure is virtually at rest and thus the resulting uplift is substantially smaller than in the previous configurations.

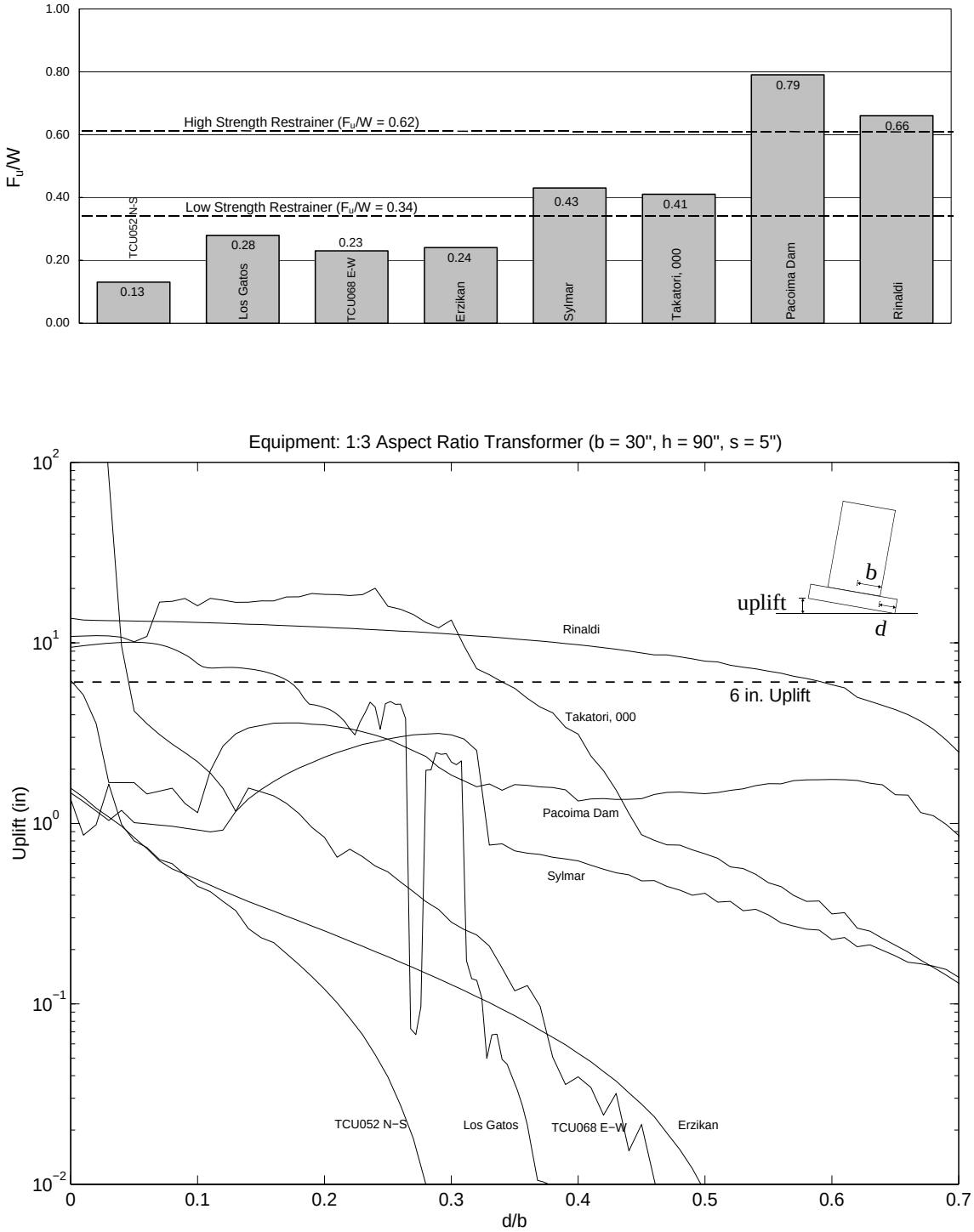

Figure 6.3. Histogram showing the minimum restrainer strength needed to avoid fracture and thus engage the foundation in rocking, when a block with $b = 30in$ and $h = 90in$ is subjected to the indicated records (top); and the effect of foundation size on the uplift of the equipment-foundation system subjected to earthquake motion (bottom).

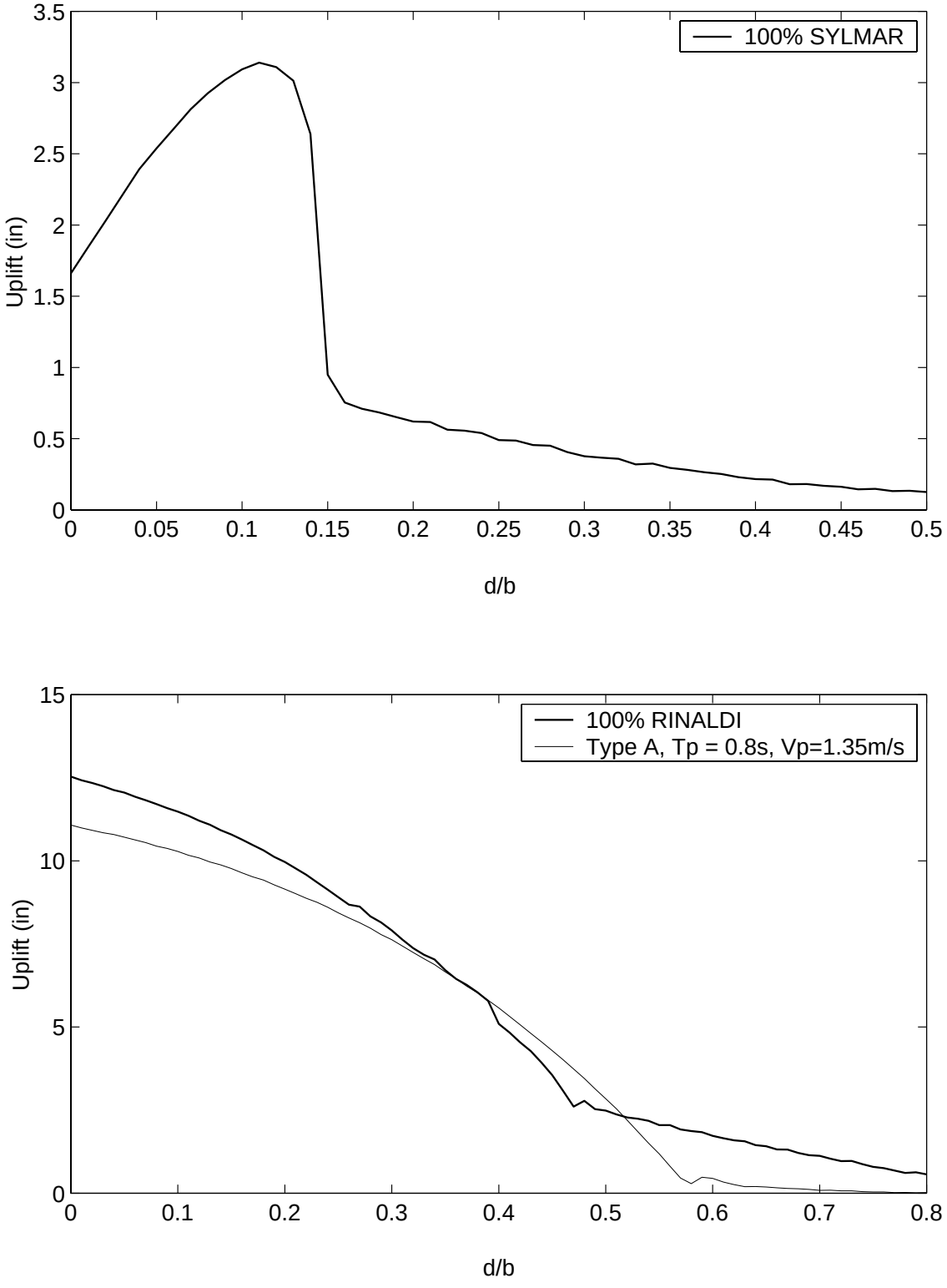

Figure 6.4. Effect of foundation size on the uplift of the 60 kip equipment-foundation system subjected to the Sylmar record (top), and the Rinaldi record (bottom).

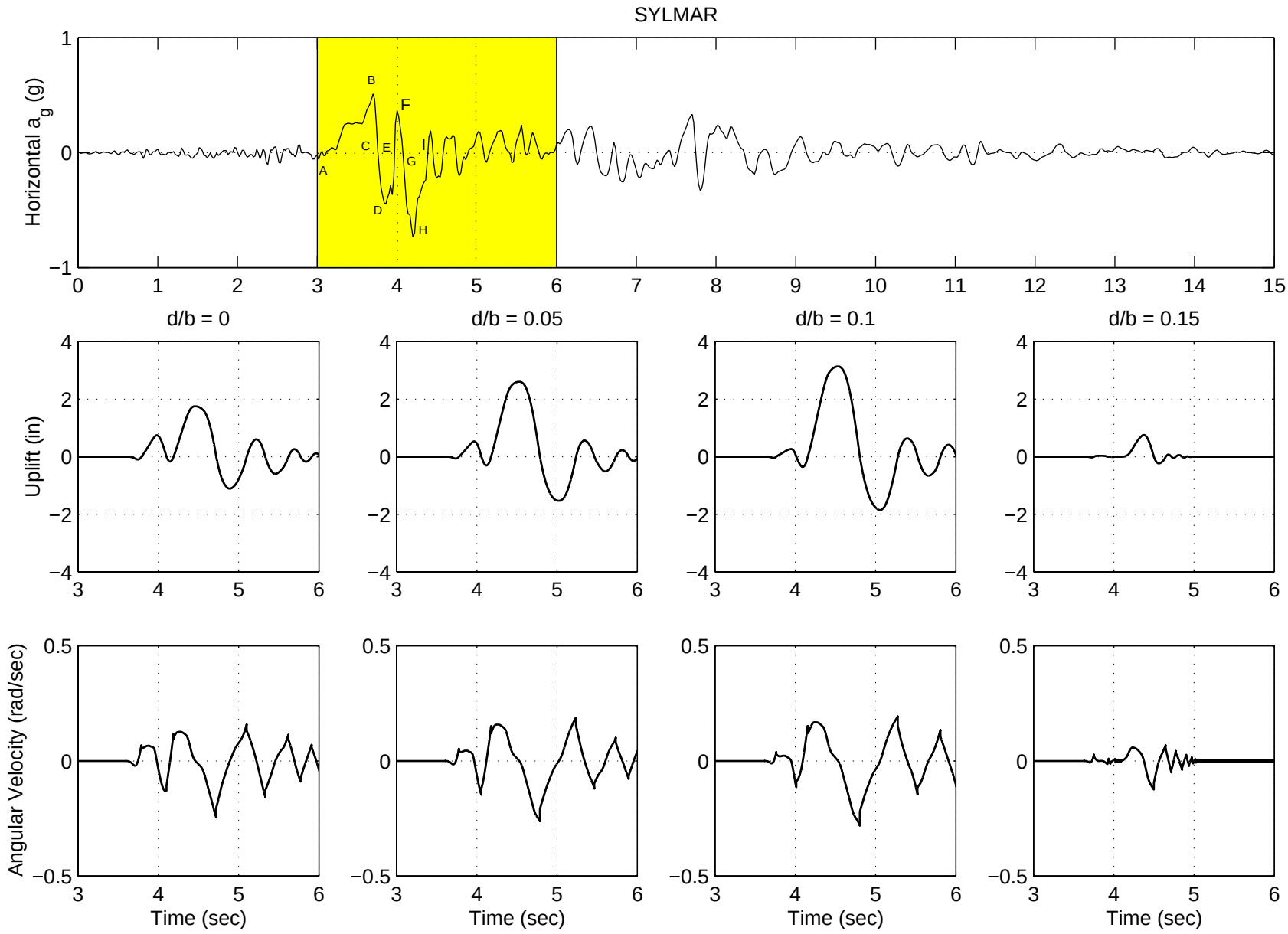

Figure 6.5. Response of the 60 kip equipment-foundation system with increasing values of *d/b* when subjected to the Sylmar record.

In contrast to the response of the equipment-foundation system to the Sylmar record, the response of the 60 kip equipment-foundation system to the Rinaldi motion decreases monotonically as *d/b* increases. This curve has been isolated and is presented in Figure 6.4 (bottom). In addition to this curve, the uplift of the 60 kip equipment-foundation system subjected to the trigonometric pulse approximation of the Rinaldi record is presented for comparison. The fact that these two curves differ only slightly suggests that the pulse approximation of the Rinaldi record captures most of the rocking potential of the actual earthquake. A detailed view of the rocking response of the 60 kip equipment subjected to the Rinaldi record is given in Figure 6.6 for *d/b* ratios: 0, 0.05, 0.1, 0.15. As stated above, the uplift decreases monotonically as *d/b* increases.

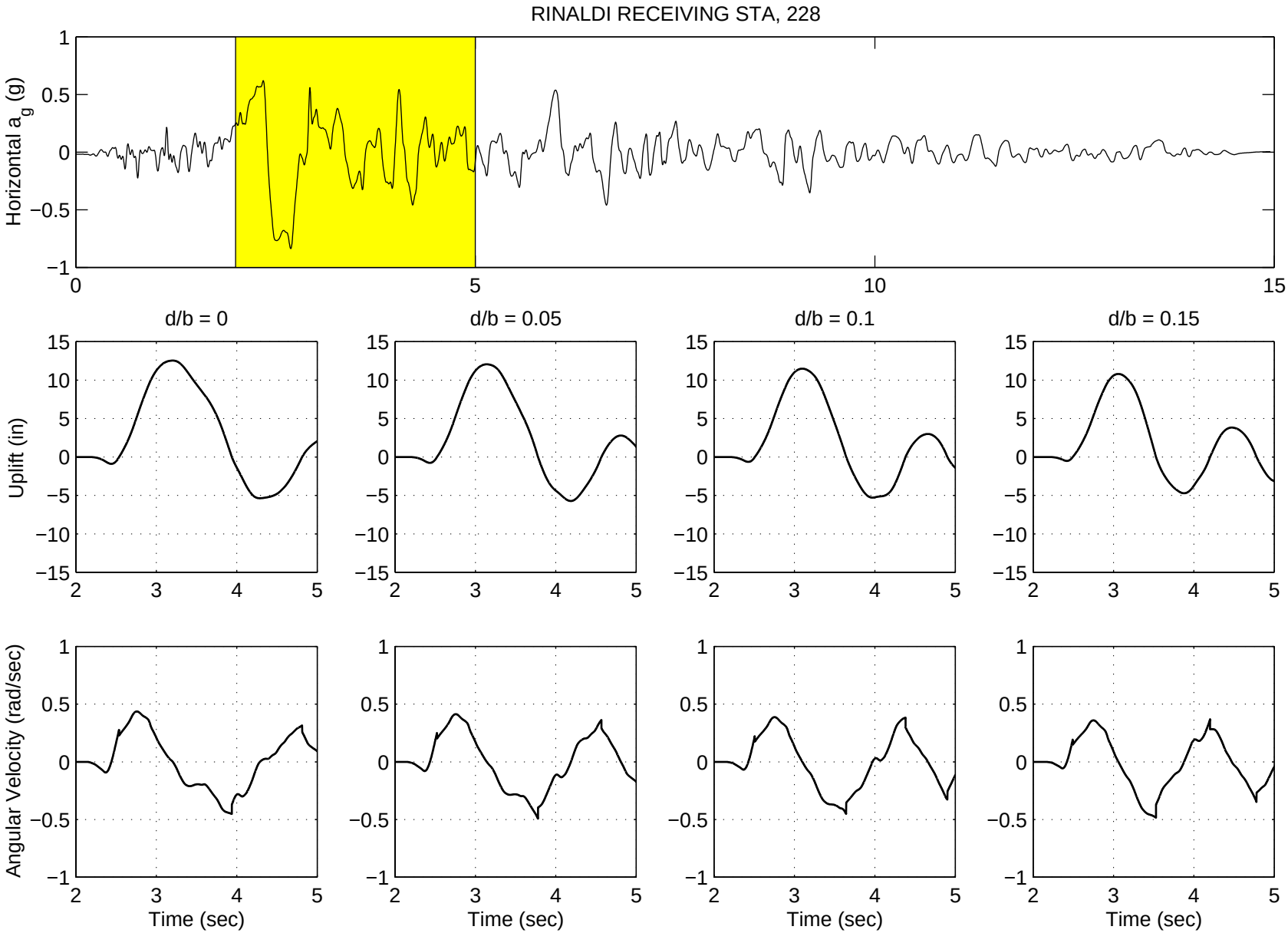

Figure 6.6. Response of the 60 kip equipment-foundation system with increasing values of *d/b* when subjected to the Rinaldi record.

7 Conclusions

In this study we investigated the seismic stability of rigid electrical equipment supported on a base foundation. In most cases the base foundation has plan dimensions that are larger than the footprint of the equipment, which is anchored atop the base with restrainers. With this configuration, the equipment-foundation system exhibits two distinct capacities to resist uplift and eventual overturning: (a) the restrainers are strong enough and the equipment engages the base foundation in rocking motion and (b) the restrainers fracture and the equipment subsequently rocks as a free-standing block atop its foundation.

Initially, the study examined the rocking response of the freestanding transformers and showed that only one of the strong motions considered is capable of fracturing the high-strength restrainers used by PG&E. However, none of the strong motions is capable of overturning the equipment, which is considered the ultimate limit state. The minimum restrainer strength needed to avoid fracture correlates strongly with the peak ground acceleration. Two records (Rinaldi and Takatori) are capable of uplifting the two transformers of interest beyond the serviceability limit (6 in. uplift at equipment edge); however, it is found that small values of foundation protrusion, d, reduce the uplift appreciably. For the most slender of the PG&E configurations studied (width $= 2b = 70$ in. and slenderness $= \alpha = 0.371$ rad), it was found that a ratio of $d/b \approx 0.3$ appears to be adequate to limit uplift.

It was found that for earthquakes with long distinguishable pulses ($T_p > 2.5\,\text{sec}$) the margin between exceeding the serviceability level of uplift and achieving overturning is minimal. Furthermore, the study concludes that the longer the pulse duration, the smaller the acceleration amplitude needed to induce uplifting or overturning.

With the exception of the Cape Mendocino record, which has an unusually high peak ground acceleration, the study concludes that the high-strength restrainers used in practice are sufficient to engage the foundation base in rocking motion and that a restrainer strength of $F_u = mg$ should be sufficient for all practical purposes. When an anchored equipment stretches its restrainers, the reaction at the pivot point includes the weight of the equipment, the force developed in the restrainer opposing uplift, as well as the dynamic effects. The reaction force can be as high as or slightly higher than $mg + F_u = 2mg$ if one follows the recommendation of this paper ($F_u = mg$). This four-fold increase over the static reaction value must be considered in the design of the foundation base.

References

Bouc, R. 1971. “Modèl mathématique d’hysteresis,” *Acustica* 24: 16-25.

Fujisaki. 2001. Personal communication, Pacific Gas and Electric Company, Oakland, CA.

Jacobsen, L.S., and R.S. Ayre. 1958. *Engineering Vibrations*. New York: McGraw-Hill.

Makris, N. 1997. “Rigidity-plasticity-viscosity: Can electrorheological dampers protect base-isolated structures from near-source ground motions?” *Earthq. Engrg. and Struc. Dynamics* 26: 571-91.

Makris, N., and Y. S. Roussos. 1998. “Rocking response and overturning of equipment under horizontal pulse-type motions”. PEER 1998/05. Pacific Earthquake Engineering Research Center, University of California, Berkeley.

Makris, N., and Y. S. Roussos, 2000. “Rocking response of rigid blocks under near-source ground motions,” *Geotechnique*, Vol. 50, No.3, 243-262.

Makris, N., and J. Zhang. 1999. “Rocking response and overturning of anchored equipment under seismic excitations,” PEER 1999/06, Pacific Earthquake Engineering Research Center, University of California, Berkeley.

Makris, N., and S. Chang. 2000. “Effect of viscous, viscoplastic and friction damping on the response of seismic isolated structures,” *Earthq. Engrg. and Struc. Dynamics* 29: 85-107.

Makris, N., and J. Zhang. 2001. “Rocking response and overturning of anchored blocks under pulse-type motions,” *J. Engrg Mech, ASCE*, Vol. 127 No. 5.

MATLAB. 1992. *High-Performance numeric computation and visualization software*. Natick Mass: The Math Works.

Wen, Y-K. 1975. “Approximate method for nonlinear random vibration,” *J. of Engrg. Mech.* 102(EM4): 389-401. ASCE.

Wen, Y-K. 1976. “Method for random vibration of hysteretic systems,” *J. of Engrg. Mech.* 102(EM2): 249-63. ASCE.

Yim, C.K., A.K. Chopra, and J. Penzien. 1980. “Rocking response of rigid blocks to earthquakes,” *Earthq. Engrg. and Struc. Dynamics* 8: 565-87.